UNIVERSITÄT ZU LÜBECK

From the Lübeck Institute of Experimental Dermatology
of the University of Lübeck
Director: Prof. Dr. Ralf Ludwig

"Unravel principles of pemphigus vulgaris pathogenesis"

Dissertation
for Fulfillment of
Requirements
for the Doctoral Degree
of the University of Lübeck

from the Department of Natural Sciences

Submitted by

Veronika Hartmann
from Bad Pyrmont, Germany

Lübeck 2025

First referee: Prof. Dr. med. vet. Jennifer E. Hundt

Second referee: Prof. Dr. rer. nat. Rudolf Manz

Date of oral examination: 30.10.2025

Approved for printing: 03.11.2025

Table of content

1 Summary

Pemphigus vulgaris (PV) is an autoimmune disease affecting the mucosa and the skin. The autoantibodies which are produced in this disease, target desmoglein (Dsg) 3 and Dsg1. These two are adhesion molecules providing intercellular connection between epidermal, hair follicle and mucosal keratinocytes. Once the autoantibodies have bound to these structures, the keratinocytes separate from each other, leading to the formation of blisters in the skin and erosions in the mucosa. The exact molecular mechanism of the pathogenesis is not fully understood yet. This project has the aim to investigate and identify the clinically relevant communication code in the affected tissues.

The human skin organ culture (HSOC) model for PV was used to uncover the early events in basal keratinocytes which were incubated with either the single chain variable fragment PX43 (directed against Dsg3/1) or the murine antibody AK23 (directed against Dsg3). The skin samples were prepared 5, 10, and 24 hours after injection for the quantification of split formation, proliferation, and the basal keratinocytes were isolated for bulk RNA-sequencing. Similarly, further analysis of the proteome was conducted 24 hours after injection and a qualitative staining for the binding of PX43 to Dsg3/1 was done. As another quality control, the distribution of Dsg3/1 in the human skin was visualized by immunofluorescence. As controls, human and murine immunoglobulin G were used, respectively.

As it is evident from hematoxylin and eosin-stained sections, PX43 induced a split in the skin which was increasing with prolonged incubation time. However, AK23 was not able to induce split formation. Further analysis of the proliferation after incubation with PX43 and AK23 shows that the binding of them does not lead to a significant increase in proliferation at the site of basal and suprabasal keratinocytes.

The analysis of the transcriptome used a multi-variate linear model including nuisance factors and reveals prominent upregulation of IFNγ and TNFα pathways in the basal keratinocytes. This coincides with the upregulation of NFkB and JAK-STAT-mediated circuits and increased keratinocyte detachment. In contrast, basal keratinocytes from AK23-injected HSOC models do not show significant differentially regulated genes. These two observations lead to the conclusion that the inflammatory response induced in the basal keratinocytes, does not originate from the binding of PX43 to Dsg3/1 but is a secondary response to the increasing cell detachment.

Analysis of the proteome of basal keratinocytes after 24 hours confirmed the described transcriptomic results showing differentially regulated proteins and pathways of inflammation.

All-together, the cell-wide and long-lasting changes on the transcriptomic and proteomic level originate from the loss of cell-cell adhesion and mechanical stress but are not caused by the binding of PX43 or AK23 to their targets.

2 Zusammenfassung

Pemphigus vulgaris (PV) ist eine Autoimmunerkrankung, die die Schleimhäute und die Haut betrifft. Die Autoantikörper, die bei dieser Krankheit gebildet werden, richten sich gegen Desmoglein (Dsg) 3 und Dsg1. Bei diesen beiden handelt es sich um Adhäsionsmoleküle, die die interzelluläre Verbindung zwischen den Keratinozyten der Epidermis, der Haarfollikel und der Schleimhäute herstellen. Sobald die Autoantikörper an diese Strukturen gebunden haben, trennen sich die Keratinozyten voneinander, was zur Bildung von Blasen auf der Haut und Erosionen auf der Schleimhaut führt. Der genaue molekulare Mechanismus der Pathogenese ist noch nicht vollständig geklärt. Dieses Projekt hat zum Ziel, den klinisch relevanten Kommunikationscode in den betroffenen Geweben zu untersuchen und zu identifizieren.

Das humane Hautorgan-Kulturmodell für PV wurde verwendet, um die frühen Ereignisse in basalen Keratinozyten aufzudecken, die entweder mit dem einkettigen variablen Fragment PX43 (gegen Dsg3/1 gerichtet) oder dem murinen Antikörper AK23 (gegen Dsg3 gerichtet) inkubiert wurden. Die Hautproben wurden 5, 10 und 24 Stunden nach der Injektion für die Quantifizierung der Spaltbildung und der Proliferation präpariert, und die basalen Keratinozyten wurden für die RNA-Sequenzierung isoliert. In gleicher Weise wurde 24 Stunden nach der Injektion eine weitere Analyse des Proteoms durchgeführt und eine qualitative Färbung für die Bindung von PX43 an Dsg3/1 vorgenommen. Als weitere Qualitätskontrolle wurde die Verteilung von Dsg3/1 in der menschlichen Haut durch Immunfluoreszenz sichtbar gemacht. Als Kontrollen wurden humanes bzw. murines Immunglobulin G verwendet.

Wie aus den mit Hämatoxylin und Eosin gefärbten Schnitten ersichtlich ist, führte PX43 zu einer Spaltbildung in der Haut, die mit zunehmender Inkubationszeit größer wird. AK23 war jedoch nicht in der Lage, die Spaltbildung zu induzieren. Eine weitere Analyse der Proliferation nach der Inkubation mit PX43 und AK23 zeigt, dass die Bindung der beiden nicht zu einem signifikanten Anstieg der Proliferation an der Stelle der basalen und suprabasalen Keratinozyten führt.

Bei der Analyse des Transkriptoms wurde ein multivariates lineares Modell verwendet, bei dem Störfaktoren eliminiert werden. Dabei wurde eine deutliche Hochregulierung der IFNγ- und TNFα-Signalwege in den basalen Keratinozyten zeigt. Dies geht einher mit der Hochregulierung von NFkB- und JAK-STAT-vermittelten Signalwege und einer verstärkten Ablösung der Keratinozyten. Im Gegensatz dazu weisen basale Keratinozyten aus AK23-injizierten Hautproben keine signifikant regulierten Gene auf. Diese beiden Beobachtungen lassen den Schluss zu, dass die in den basalen Keratinozyten induzierte Entzündungsreaktion nicht auf die Bindung von PX43 an Dsg3/1 zurückzuführen ist, sondern eine sekundäre Reaktion auf die zunehmende Zellablösung darstellt.

Die Analyse des Proteoms der basalen Keratinozyten nach 24 Stunden bestätigte die beschriebenen transkriptomischen Ergebnisse, die auf unterschiedlich regulierte Proteine und Entzündungswege hinweisen.

Insgesamt sind die zellweiten und langanhaltenden Veränderungen auf der Transkriptom- und Proteomebene auf den Verlust der Zell-Zell-Adhäsion und den mechanischen Stress zurückzuführen, werden aber nicht durch die Bindung von PX43 oder AK23 an ihre Ziele verursacht.

3 Lists

3.1 List of abbreviations

ANOVA	Analysis of variance
Aqua dest.	Distilled water
au	Arbitrary unit
BB	Blocking buffer
BCA	Bicinchonic acid
BSA	Bovine serum albumin
°C	Degree Celsius
Ca^{2+}	Calcium
$CaCl_2$	Calcium chloride
CAND	Cullin associated and neddylation dissociated protein
CO_2	Carbondioxide
CCL	C-C motif chemokine ligand
cm	Centimeter
CXCL	Chemokine (C-X-C motif) ligand
DAG	Dystroglycan
DAPI	4′,6-diamidino-2-phenylindole
DDA	Data dependent acquisition
DDXX58	RNA sensor RIG-1
DEG	Differentially expressed gene
DIA	Data independent acquisition
DIF	Direct immunofluorescence
DMSO	Dimethyl sulfoxide
DNA	Deoxyribonucleic acid
DPBS	Dulbecco's phosphate buffered saline
Dsc	Desmocollin
Dsg	Desmoglein
Dsp	Desmoplakin
EDTA	Ethylenediaminetetraacetic acid
EGF	Epidermal growth factor
EGFR	Epidermal growth factor receptor
ELISA	Enzyme-linked immunosorbent assay
ERK	Extracellular signal-regulated kinases
E. coli	*Escherichia coli*
ETA	Exfoliative toxin A
eV	Electrical volt
Fab	Fragment antigen-binding region
FBS	Fetal bovine serum
Fc	Fragment crystallizable region
FDR	False discovery rate
g	Gramm
GABRB	Gamma-aminobutyric acid receptor subunit
GSVA	Gene set variation analysis
h	Hour
HA	Hemaglutinin
HaCaT cells	Human high calcium immortalized epidermal keratinocytes
HBSS	Hank's balanced salt solution

HDAC	Histone deacetylase
HE	Haematoxylin and eosin
hIgG	Human immunoglobulin G
High $CaCl_2$ CnT-07	CnT-07 medium with supplements and $CaCl_2$ concentration of 1.2 mM
High $CaCl_2$ KGM2	KGM2 medium with supplements and $CaCl_2$ concentration of 1.2 mM
His	Histidine
HLA	Human leukocyte antigen
HS	High solution
HSP	Heat-shock protein
HSOC model	Human skin organ culture model
IF	Immunofluorescence
IFIH	Interferon induced with helicase C domain
IFIT	Interferon induced protein with tetratricopeptide repeats
IFN	Interferon
Ig	Immunoglobulin
IGHV	Immunoglobulin heavy chain variable region
IPTG	Isopropyl-β-d-thioglacatopyranosid
IRF	Interferon regulatory factors
JAK-STAT	Janus kinase – signal transducer and activator of transcription proteins
KCl	Potassium chloride
KDA	Keratinocyte dissociation assay
kDa	Kilo Dalton
KGM2	Keratinocyte growth medium 2
KH_2PO_4	Monopotassium phosphate
KLF5	Kruppel-like factor 5
KLK	Kallikrein
KRT	Keratin
LB	Luria-Bertani
LINC	Long intergenic non-protein coding RNA
LNC	Long non-protein coding RNA
Low $CaCl_2$ CnT-07	CnT-07 medium with supplements and $CaCl_2$ concentration of 0.06 mM
Low $CaCl_2$ KGM2	KGM2 medium with supplements and $CaCl_2$ concentration of 0.06 mM
LS	Low solution
mAb	Monoclonal antibody
MAPK	Mitogen-activated protein kinase
mg	Milligram
mIgG	Murine immunoglobulin G
mIgG1	Murine immunoglobulin G1
min	Minute
$MgCl_2$	Magnesium chloride
MOPS	3-(4-Morpholino)propane sulfonic acid
ms	Millisecond
m/z	Mass to charge ratio
n	Number of replicates
NaCl	Sodium chloride

Na_2HPO_4	Disodium phosphate
NaH_2PO_4	Monosodium phosphate
NFκB	Nuclear factor kappa B
NGS	Normal goat serum
NGSP	Next generation sequencing platform
NMS	Normal mouse serum
NxGS	Next generation sequencing
nL/min	Nanoliter per minute
nm	Nanometer
PASEF	Parallel Acquisition Serial Fragmentation
µl	Mikroliter
µM	Mikromolar
min	Minute
ml	Milliliter
mM	Millimolar
mU	Millivolt
OASL	2'-5'-oligoadenylate synthetase-like protein
OD	Optical density
PBS	Phosphate buffered saline
PCA	Principal component analysis
PF	Pemphigus foliaceus
Pg	Plakoglobin
pH	Potential of hydrogen
pHPEKs	Pooled human primary epidermal keratinocytes
PIP_2	Phosphatidylinositol 4,5-bisphosphate
PKC	Phosphokinase C
Pkp	Plakophilin
PLC	Phospholipase C
PROGENy	Pathway responsive genes for activity interference
PV	Pemphigus vulgaris
PVDF	Polyvinylidene difluoride
RL	Releasing buffer
RNA	Ribonucleic acid
RNAseq	RNA sequencing
rpm	Rounds per minute (used for shakers and stirrers)
RSAD	Radical
RT	Room temperature
SB medium	Super broth medium
scFv	Single chain variable fragment
SDS	Sodiumdodecylsulphate
SDS-PAGE	Sodiumdodecylsulphate-Polyacrylamide gel electrophoresis
sec	Second
Staph. aureus	*Staphylococcus aureus*
T0	Time point zero
TBS	Tris-buffered saline
TBST	Tris-buffered saline with Tween20
TEMED	Tetramethylethylendiamine
TFA	Tri-fluoroacetic acid
TGFb	Transforming growth factor β

timsTOF-HT	Trapped ion mobility-quadrupole-time of flight high throughput
TNF	Tumor necrosis factor
Tris	Tris(hydroxymethyl)aminomethane
Tris-HCl	Tris-hydrogen chloride acid
U	(Enzymatic) units
U/ml	Units per milliliter
V	Volume
VF	Visual field
V_H	Heavy chain
V_L	Light chain
v/v	Volume to volume ratio
WB	Western blot
WDR17	WD repeat domain 17
xg	Times the gravitational force for centrifugation
ZIC2	Zinc finger protein 2

3.2 List of figures and table

4 Introduction

4.1 Structure of the skin and the importance of desmosomes

The skin is a complex structure covering of the human body and is the first line of defence against various dangers: It protects the body from water loss and keeps pathogens away (Fuchs and Raghavan 2002). Despite protecting the body as a physical barrier against the environment in general, it also interacts with its surroundings. Additionally, it helps to regulate the body temperature and it is part of the metabolism (Yannas 2015, Mestrallet *et al.* 2021).

There are three layers which are part of the skin: Deepest is the subcutis, above it is the dermis, and the outer barrier is the epidermis (Fuchs and Raghavan 2002). The subcutis is made from connective tissue and fat cells, which are both responsible to maintain the body's temperature and store energy. Additionally, due to the vascularisation of this layer, it supplies all three skin layers with all necessary supplements (Wierzbicka *et al.* 2017).

The dermis is made from connective fibers like collagen fibers, reticulin fibers, and anchoring fibrils, as well as dermal cells including fibroblasts and mast cells. The fibroblasts make the dermis an important part in the synthesis of the extracellular matrix, while mast cells make the dermis a very important part in immunological processes (Maja M. Suter *et al.* 2009, Yannas 2015, Zou *et al.* 2021). Additionally, sensible and vegetative nerve cells can be found (Abdo, Sopko, and Milner 2020).

The epidermis is constantly renewing itself by proliferation and differentiation of keratinocytes (Maja M. Suter *et al.* 2009). It is made of four different layers (Wierzbicka *et al.* 2017): Starting from the dermal site, the lowest layer is the *stratum basale*, from which basal keratinocytes proliferate, differentiate, and migrate up through the *stratum spinosum* to the *stratum granulosum* and finally into the *stratum corneum* from which they are eventually shed as depicted in **Figure 4.1.**. During this process, the keratinocytes will form cellular junctions between each other, which will provide the mechanical strength to the skin: the desmosomes (Breitkreutz, Mirancea, and Nischt 2009).

Desmosomes are one group of intercellular junctions critical for epithelial cells to connect to each other. The other three groups are adherens junctions, tight junctions, and gap junctions (Miller *et al.* 2013). In brief, adherens junctions connect the actin cytoskeleton to the plasma membrane at the site of cell-cell adhesion, functioning as anchoring junctions. Tight junctions are anchoring junctions, too, but they connect the intermediate filament cytoskeleton to the plasma membrane (Wei and Huang 2013). Further, they can form seals regulating paracellular transport and keeping proteins in their respective compartments in the cell (Green, Jaiganesh, and Broussard 2019). The gap junctions contain connexin and they allow the coupled cells to move small molecules from one to the other (Shigetomi and Ikenouchi 2019). Finally, the desmosomes are essential for the mechanical integrity of the epithelia as cell-cell adhesion complexes (D. Garrod and Chidgey 2008).

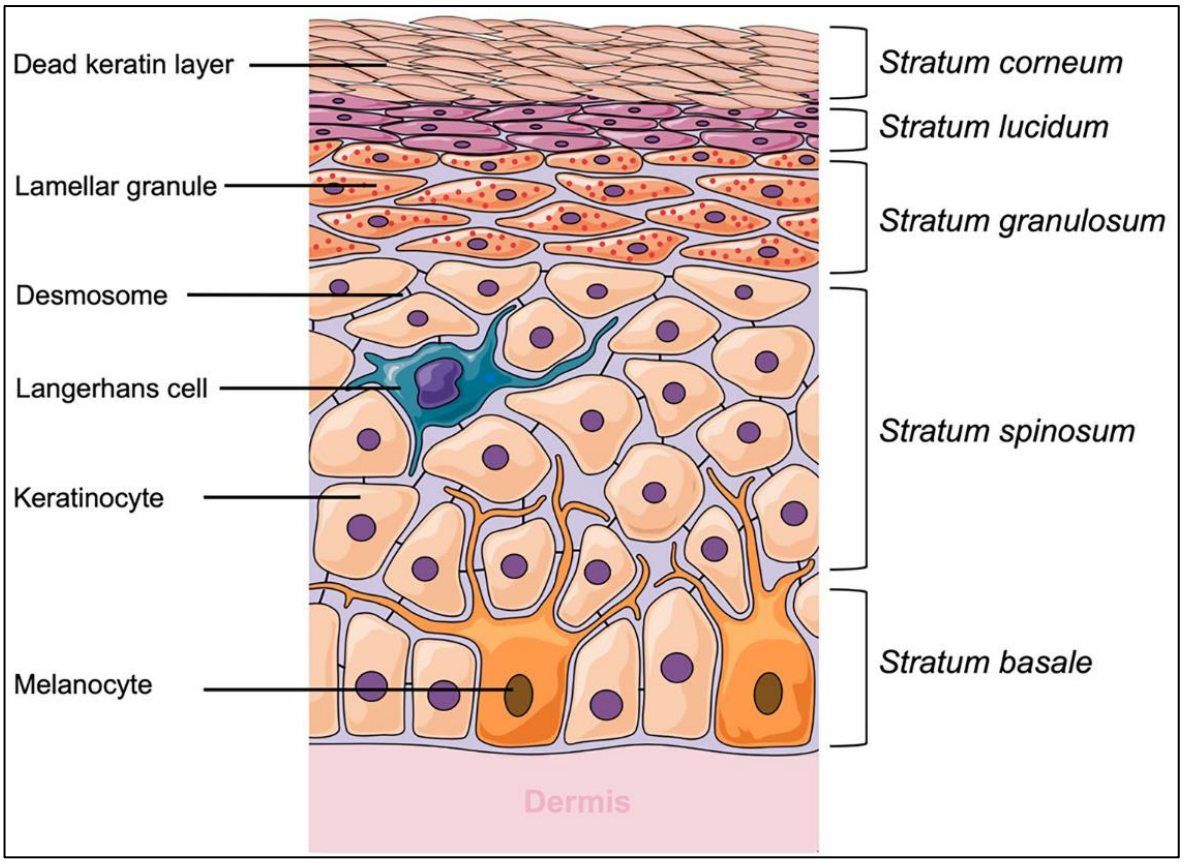

Figure 4.1. Schematic overview of the human epidermis. The epidermis is made of five layers: The *stratum basale* consists of melanocytes and basal keratinocytes. Keratinocytes migrate and proliferate into the *stratum spinosum* and later to the *stratum granulosum* and *stratum lucidum* before these cells are eventually shed off as it forms a dead keratin layer. Figure originally published in (Ramadon *et al.* 2022).

Desmosomes have an intra- and an extracellular domain, latter connecting to the extracellular domain of neighbouring keratinocytes (see **Figure 4.2.**). The intracellular domain is made of desmoplakin (Dsp), connecting the desmosome by intermediate filaments to the cytoskeleton. Towards the cell membrane, Dsp is connected to plakoglobin and plakophilin. Without these, the desmosomal plaque cannot be form in an efficient way, and clustering and segregation cannot take place (Bonné *et al.* 2003). While plakophilin connects several Dsp molecules, plakoglobin is connected to the extracellular desmoglein (Dsg) and desmocollin (Dsc) (Hatzfeld 2007). Dsg can connect to either another Dsg from the neighbouring keratinocyte or to Dsc from the neighbouring keratinocyte. Additionally, Dsc cannot only bind to Dsg, but to another Dsc from the neighbouring cell, too (Calkins *et al.* 2006, Kowalczyk and Green 2013, Green, Jaiganesh, and Broussard 2019).
In contrast to other cellular junctions, desmosomes are in mammalian tissues in a hyperadhesive state. In this state, the desmosomes' connection is calcium-independent and cannot be disrupted by chelating agents. This allows desmosomes to maintain tissue integrity to mechanical stress. This state of hyperadhesion can be disturbed upon wounding, where desmosomes near the wound edge lose hyperadhesion and are calcium-dependent (Garrod *et al.* 2005, Thomason *et al.* 2010).

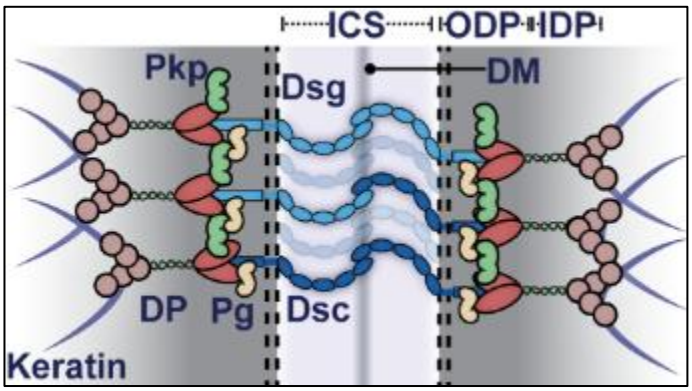

Figure 4.2. Desmosomes make the skin resistant to mechanical stress. Desmosomes mediate adhesion through desmogleins (Dsgs) and desmocollins (Dscs) in the intercellular space (ICS). These are associated with plakoglobins (Pgs) and plakophilins (Pkps) at the dense midline of the outer dense plaque, and desmoplakins (Dps) anchoring keratin-containing intermediate filaments to the membrane of keratinocytes at the inner dense plaque. Figure originally from (Green, Jaiganesh, and Broussard 2019).

4.2 Structure of immunoglobulins and single chain variable fragments

Immunoglobulins (Ig) are molecules produced by plasma cells, mediating the adaptive immune response. They are able to identify virtually every antigen they encounter by somatic recombination processes and develop a high affinity for the antigen by affinity maturation (Schroeder and Cavacini 2010).
Antibodies have a "Y"-shaped structure consisting of four polypeptides. Two of these are heavy chains while the other two are light chains (see **Figure 4.3.**). The core "Y" is formed by the two heavy chains, which are connected by disulfide bonds, while the light chains are attached parallel to the upper arms of the "Y". The idiotype of the antibody is determined by the fragment antigen-binding (Fab) region which has an affinity for the antigen. The immune-related functions like the binding to macrophages or complement as well as the isotype of the antibody are determined by the fragment crystallizable (Fc) region (Janeway, 2001).

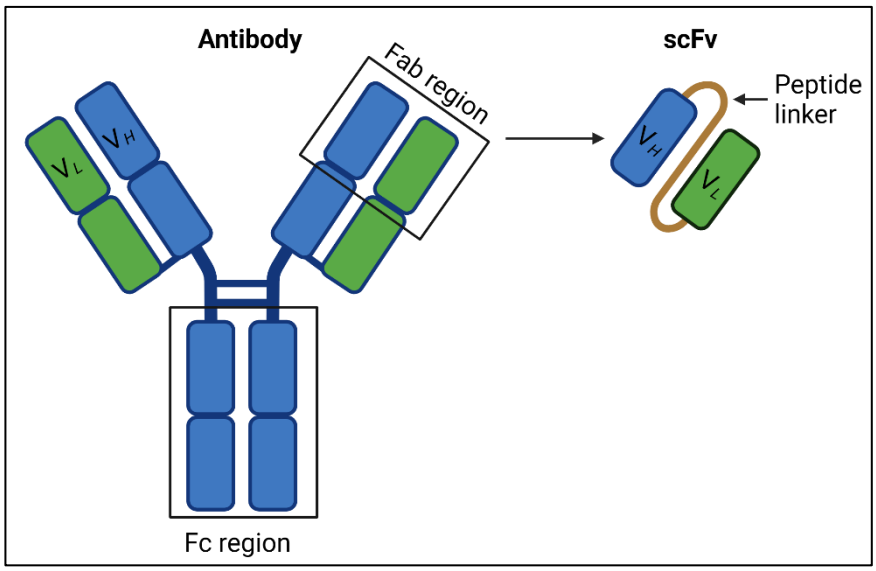

Figure 4.3. Schematic overview of an antibody and a single chain variable fragment. On the left side, a full antibody is depicted. In blue, the heavy chains can be seen while the light chains are depicted in green. Fragment antigen-binding (Fab) region, fragment crystallizable (Fc) region. On the right, a single chain variable fragment (scFv) is shown, composed of one variable heavy (V_H) and one variable light (V_L) chain being linked together by a peptide (yellow). Image created with BioRender.

During their development, lymphocytes undergo a positive selection process in the cortex of the thymus, where those with a potential for self-peptide reactivity are marked and eliminated in the thymic medulla (Ahsan 2023). Afterwards, they can mature and enter the circulation as mature B cells. T cells on the other hand are undergoing the selection process a second time once they leave the thymus. This secondary selection either destroys self-reactive T cells or renders them anergic (L. Wang, Wang, and Gershwin 2015). Immature B cells which express surface immunoglobulin M detecting ubiquitous self-antigen, are deleted by either clonal deletion or clonal anergy. This can be omitted by receptor modification of autoreactive B cells and even healthy people and animals have a small number of these potentially self-reacting lymphocytes without developing any disease (Salinas *et al.* 2013). This physiological autoimmunity is required for the immune system's homeostasis, removing degraded self- and nonself antigens and not causing clinical symptoms (Avrameas and Selmi 2013). Pathological autoimmunity develops when the immune tolerance is broken and the self-reactive lymphocytes as well as the produced autoantibodies are involved in and can cause inflammation (Ahsan 2023). The moment when the physiological autoimmunity switches to pathological autoimmunity can be influenced by genetic predisposition, epigenetic changes, infections, and environmental factors (for example infectious agents, ultraviolet light, chemicals) (Costenbader *et al.* 2012).

The production of recombinant antibodies under laboratory conditions has evolved over the past decades and apart from antibodies, single chain variable fragments (scFvs) are produced, too. The scFv is composed of the smallest unit of an immunoglobulin, the variable fragment which is part of the Fab region (Muñoz-López *et al.* 2022). In the format of an scFv, one variable fragment of the heavy chain and one variable of the light chain are linked by a flexible peptide. The variable fragments are still able to bind to their designated target, thereby allowing research on the effect of their binding to their antigen without the involvement of immune cells (Ahmad *et al.* 2012).

4.3 Pemphigus vulgaris

Pemphigus comprises a group of chronic, rare, and life-threatening autoimmune bullous diseases affecting the mucosa and the skin (Hammers and Stanley 2016). Pemphigus foliaceus (PF) is caused by the binding of autoantibodies to Dsg1, thereby manifesting only in the skin (Ishii *et al.* 2020). On the other hand, pemphigus vulgaris (PV) can present in two clinical manifestations: In the mucosal-dominant PV, autoantibodies target Dsg3 only, leading to erosions in mucous membranes (Udey 1999) as depicted in **Figure 4.4.a**. First symptoms are painful, non-healing ulcerations in the mucosa (Bystryn and Rudolph 2005). Once the autoantibodies target Dsg1 in addition, mucocutaneous PV leads to blister formation on the skin (**Figure 4.4.a**) can be observed (Di Zenzo *et al.* 2016, Hammers and Stanley 2016). This correlation of the observed antibody profile and the clinical phenotype can be explained by the Dsg compensation hypothesis (Mahoney *et al.* 1999): According to the hypothesis, there are different expression patterns of Dsg3 and Dsg1 in the mucous membranes and the cutaneous epidermis. In the mucosa, mostly Dsg3 but only very little to none Dsg1 is expressed. Binding of the autoantibody to Dsg3 leads to erosions, since there is no other molecule to compensate for the loss of function of Dsg3. In the epidermis on the other hand, Dsg1 is expressed throughout the different layers, while Dsg3 can be found in the lower layers only. Once the Dsg3 is bound by autoantibodies, Dsg1 can compensate here for the loss in function of Dsg3, but as soon as autoantibodies bind to Dsg1 blister formation in the skin will occur (see **Figure 4.5.**) (Chernyavsky *et al.* 2019, Kalantari-Dehaghi *et al.* 2013, Lotti *et al.* 2019). The observed suprabasal acantholysis is a histopathologic hallmark in PV, presenting with shrinked basal cells which then appear as 'tombstones' (Grando *et al.* 2009).

a) Pemphigus vulgaris manifestation in the mucous membrane	**b)** Pemphigus vulgaris manifestation in the skin
	

Figure 4.4. Clinical manifestation of pemphigus vulgaris in patients. a) Pemphigus vulgaris manifestation on mucous membranes of the mouth of a patient. **b)** Skin with pemphigus vulgaris manifestation in a patient. Picture originally from (Didona *et al.* 2019).

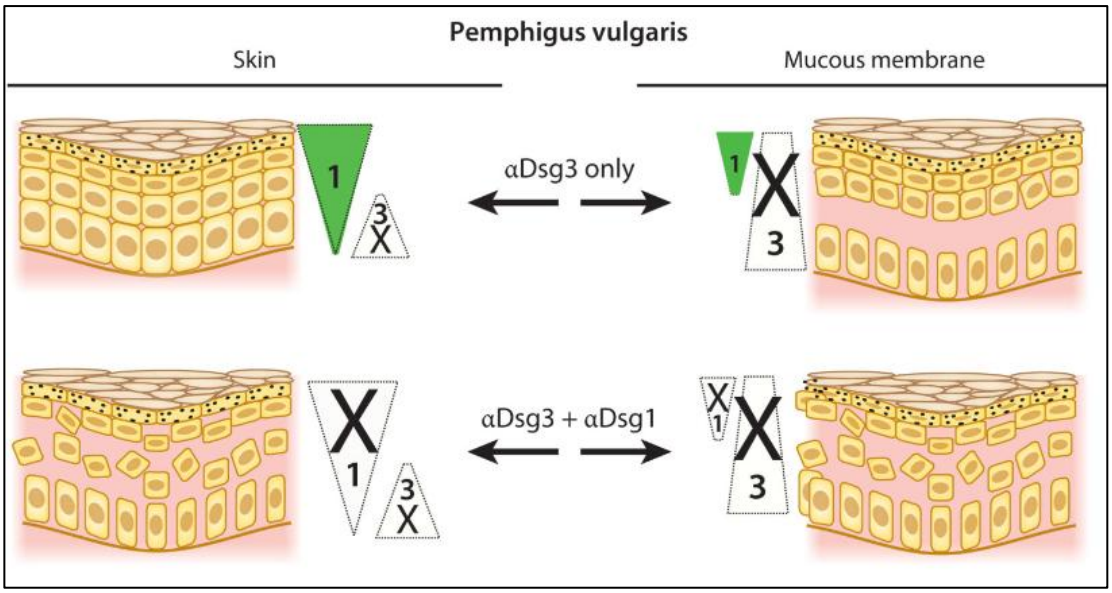

Figure 4.5. Desmoglein distribution in skin and mucous membranes. In mucosal pemphigus vulgaris (PV), autoantibodies target desmoglein 3 (αDsg3) cause blisters in the mucous membranes, where desmoglein 1 is expressed in the upper layers only. Since the skin expresses desmoglein 1 throughout all skin layers, the tissue integrity remains preserved. Autoantibodies targeting desmoglein 1 (αDsg1) together with αDsg3 cause blisters on the skin, too. Figure originally from (Hammers and Stanley 2016).

It is established that the autoantibodies in pemphigus are pathogenic themselves and do not require any other immune reaction by the immune system to cause disease (Kasperkiewicz *et al.* 2017). The discussed mechanism of how these autoantibodies can cause acantholysis are explained in section 4.3.1.
PV has an incidence of 0.1 – 0.5 per 100,000 persons without a sex preference (Shimanovich *et al.* 2020). The affected people are usually between 40 to 60 years old. It is known that there is a significant association of PV with the human leukocyte antigen (HLA) II HLA-DBR1*0402, which is found in the Jewish population, as well as HLA-DQBI*0503 in the non-Jewish population. Other factors in favour for the disease are suspected to be environmental agents, infections, drugs, and tumors (Pollmann *et al.* 2018).
If PV is not treated, it leads to death of the patients due to the disturbed skin barrier leading to water loss and infections. So far, the first-line therapy consists of systemic corticosteroids, sometimes in combination with immunosuppressive therapies (Murrell *et al.* 2020). Additionally, the chimeric monoclonal anti-CD20 antibody rituximab is used as an adjuvant (Tovanabutra *et al.* 2022). Plasmapheresis is another option which removes the autoantibody from the patient's plasma which can also be achieved by immunoadsorption which works by passing the patient's blood through an adsorption column with a high affinity towards IgGs (Lotti *et al.* 2022).

4.3.1 Pathogenesis

Although the pathological picture of PV is clear, it is a complex disease and the exact mechanism of pathogenesis is not fully understood yet, while the immune pathogenesis is well characterized nowadays (Pollmann *et al.* 2018).
The disease initiation and progression rely on a dysregulated immune response. Autoreactive T cells are activated by antigen presenting cells through HLA class II and further connection with B cells leads to the production of autoantibodies (Hertl 2006). T cells are the main initiator to PV, while B cells are maintaining the disease by autoantibody production (Yuan, Yang, and Zhang 2023). The autoantibody then binds to Dsg3/1, causing acantholysis and in this regard erosions in the mucosa and blisters in the skin (Bystryn and Rudolph 2005).
There are three major theories on how exactly the binding of the autoantibody to Dsg3/1 leads to the formation of the blisters in the patients. All three theories are supported by different studies, each of them having their arguments favouring and contradicting them. So far, none of them could be ruled out and it is also possible that the explanation of the pathogenesis is a combination of the three.
These theories shall be explained in the following three sections.

4.3.1.1 Steric hindrance

The binding of autoantibodies to Dsg1 and Dsg3 causes an uncoupling of trans-adhesion between neighbouring cells and an uncoupling of cis-adhesion between molecules on the same cell (see **Figure 4.6.**). This disruption of the cell-cell contact ultimately leads to acantholysis (Kasperkiewicz *et al.* 2017). Evidence for this theory comes from epitope mapping studies which were done with PV and PF autoantibodies from patients sera: It was shown that the epitopes bound by the autoantibodies were critical for the adhesion (Sekiguchi *et al.* 2001). It was also shown that the majority of the pathogenic anti-Dsg3/1 autoantibodies targets domains in the mature Dsgs which are not present in precursor molecules of Dsgs (Yokouchi *et al.* 2009). Finally, there are also monovalent Fab antibodies from pemphigus patients as well as scFvs which are not able to cross-link Dsgs and are still able to cause pemphigus in mice and the skin organ culture model (Payne *et al.* 2005, Ishii *et al.* 2008).

4.3.1.2 Desmoglein internalization

As described in 4.3., the Dsg compensation hypothesis states that at least Dsg1 can compensate for the loss of function of Dsg3. The binding of the autoantibodies inhibits desmosome assembly and will cause clustering of the Dsg molecules (see **Figure 4.6.**). After the crosslinking, the Dsgs are internalized without being incorporated into the desmosome, which will lead to the inhibition of desmosome assembly and ultimately weakened cell-cell adhesion (Hammers and Stanley 2016). Only the unbound Dsg is left on the cell surface, unable to provide the same mechanical strength like a desmosome (Kasperkiewicz *et al.* 2017). This theory is supported by patients' and cell culture data, showing clustering of Dsg3/1 by autoantibodies at the cell membrane (Oktarina *et al.* 2011, Van Der Wier *et al.* 2014, Aoyama and Kitajima 1999, Jennings *et al.* 2011).

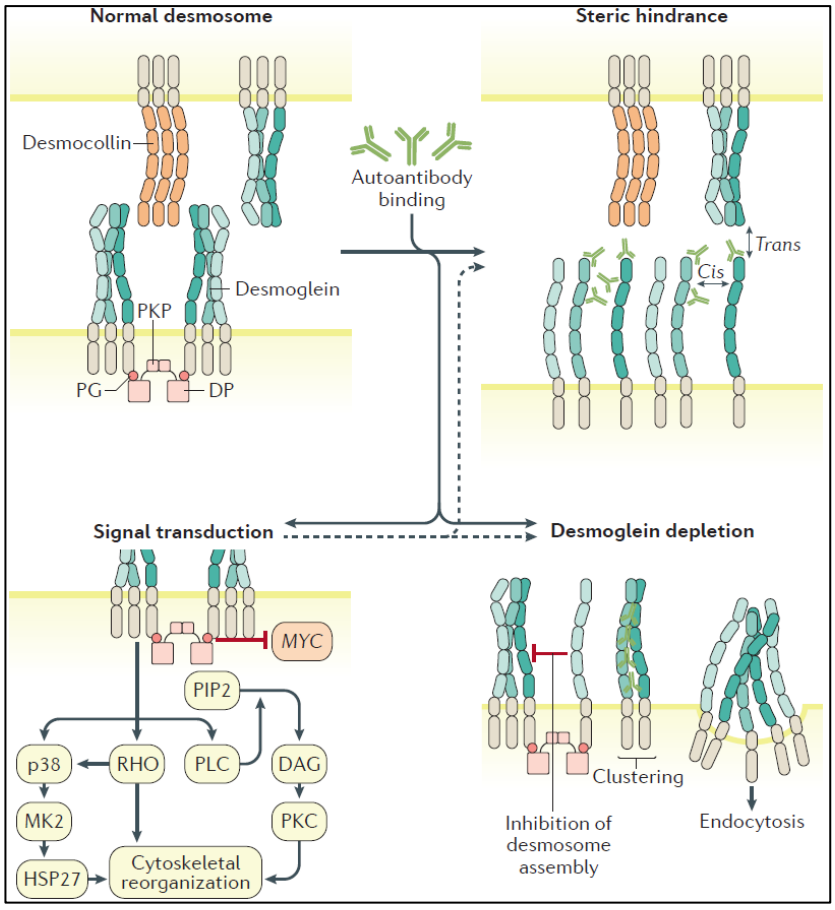

Figure 4.6. Autoantibody binding to desmoglein 1 and desmoglein 3 is theorized to cause acantholysis in the skin and mucous membranes by either steric hindrance, desmoglein depletion or signal transduction. Before autoantibody binding, desmosomes connect neighbouring cells by binding of desmoglein and desmocollin to either one (upper left). After autoantibody binding, they cause either steric hindrance leading to disruption of trans-adhesion between neighbouring cells or disruption of cis-adhesion between molecules of the same cell (upper right), or the desmosome assembly is inhibited leading to endocytosis (lower right) or a signalling pathway is activated which ultimately leads to cytoskeletal reorganization (lower left). Figure originally from Kasperkiewicz *et al.* 2017.

4.3.1.3 Outside-in signalling

The signalling in PV is caused by the binding of the autoantibodies to Dsg3 which leads to the phosphorylation of the same and dissociation from plakoglobin with subsequent endocytosis and degradation. Furthermore, it was shown in cultured human keratinocytes that protein kinase C (PKC) α which is usually in the cytoplasmic fraction can be found in the membrane. The proposed signalling pathway involves phosphatidylinositol-4,5-bisphosphate (PIP_2) and phosphoinositide-specific phospholipase C (PLC) which influence diacylglycerol (DAG) which in turn influences PKC leading to cytoskeletal reorganization (see **Figure 4.6.**). There are two more possibilities leading to blister formation by cytoskeletal reorganization: First one proposes direct signalling by Rho GTPases (Waschke *et al.* 2006). The second one suggests that either Rho GTPase activation by autoantibody binding to Dsg3 or the autoantibody binding itself leads to an activation of p38 mitogen-activated protein kinases (MAPK) (Berkowitz *et al.* 2006; Mavropoulos *et al.* 2013), which

activate heat shock protein (HSP) 27, leading to cytoskeletal reorganization (Hammers and Stanley 2016, Kasperkiewicz *et al.* 2017).

4.4 Experimental methods exploit in pemphigus vulgaris research

4.4.1 Cell culture model for keratinocyte dissociation

Keratinocyte cell culture is used to investigate the molecular mechanism of PV pathogenesis since 1982 (Watt and Green 1982). The keratinocytes originate from the skin of humans, mice, and other mammals, and can form a monolayer. Since these primary epidermal keratinocytes are a mixture of stem cells and progenitor cells, the early differentiation processes can be observed once the calcium concentration of the cell culture medium is set to 1.2 mM (Barrandon and Green 1987, Watt and Green 1982). The analysis of these cell cultures revealed several hallmarks which are defining PV: The cellular spaces are widened upon binding of the PV IgG to its target and the PV IgG is even internalized into sub-membranous vesicles, while the disruption of the desmosomes ultimately leads to acantholysis (Woo *et al.* 1983, Jones *et al.* 1984, Patel *et al.* 1984). It was first thought that the target of the PV IgG is a cell adhesion molecule of the desmosomes and it was later established that PV IgG binds to a target outside of the desmosomal structure, too (Jones, Yokoo, and Goldman 1986, Patel *et al.* 1984, Jones, Yokoo, and Goldman 1986, Suter *et al.* 1990). Over the past decades, it could be shown that desmosomes cluster upon using only the Fab fragment on murine keratinocytes (de Bruin *et al.* 2007). Further discoveries are the endocytosis of Dsg3 leading to desmosome disassembly (Calkins *et al.* 2006) and keratin retraction (Kitajima, Inoue, and Yaoita 1986, Wilgram, Caulfield, and Lever 1961).
Since 2001, the keratinocyte dissociation assay (KDA) is the main tool to study acantholysis induced by antibodies as seen in PV. In addition to the cell culture as described above, the cells are detached after the incubation with PV IgG from the cell culture dish with the help of dispase and disrupted by mechanical stress (Caldelari *et al.* 2001). The resulting fragments are then counted and analysed. In combination with pre-incubation of the keratinocytes before application of PV IgG, the KDA is a powerful *in vitro* assay allowing screening of substance libraries in search for new treatment options in PV patients, as well as investigation of the effect of autoantibody binding on the strength of cell-cell contact (Schmidt *et al.* 2022).

4.4.2 The human skin organ culture model for pemphigus vulgaris

In 1977, the first skin organ culture model was established by (Michel and Ko 1977). They used skin which was removed under local anaesthesia from healthy volunteers and placed it on lens paper. The lens paper then floated on the surface of culture medium containing fetal calf serum and human pemphigus serum. The PV IgG from the patients bound to the keratinocyte surface could be detected by direct immunofluorescence microscopy. Conventional histology showed split formation in the skin after 24 hours of incubation (Michel and Ko 1977). Since the serum was heat treated to deactivate complement, these findings suggested that the acantholysis is independent from the immune system. In the following years, this set up of the human skin organ culture (HSOC) model for PV was used to study morphological and ultrastructural changes in the presence of either serum, plasma, or purified IgG not only from PV, but also from PF patients (Hu, Michel, and Schiltz 1978, Schiltz, Michel, and Papay 1979, Morioka, Naito, and Ogawa 1981, Swanson and Dahl 1983, Jeffes, Kaplan, and Ahmed 1984, Schuh *et al.* 2003). Pas and Jonkman modified the

HSOC model further by placing the skin in a transwell at an air-liquid interface (van der Wier, Pas, and Jonkman 2010). By this modification, only the subcutis of the skin was in contact with the medium containing patient IgG.
The HSOC model was developed further by Waschke *et al.* (D. T. Egu *et al.* 2017) who use skin from cadavers of the human body donor programme. The biopsies are taken from donors without a history of skin diseases within 24 hours *post mortem* and the PV IgG is injected into the epidermis instead of adding it to the medium. This has the advantage to expose the keratinocytes to the antibody in a more synchronized way. Additionally, to mimic the patients' situation, shear stress was applied to the skin samples. This version of the HSOC model was the first one where the murine monoclonal antibody AK23 was used which targets Dsg3 (Schulze *et al.* 2012). Using a monoclonal antibody instead of polyclonal PV IgG made the experiments more reproducible (Tsunoda *et al.* 2003). Also, while PV IgG from one patient is very limited in its amount and varies in specificity from patient to patient, the monoclonal antibody can be produced in unlimited amounts and always has the same well-characterized specificity. However, AK23 on its own cannot achieve acantholysis, so a co-injection of exfoliative toxin A (ETA) is required because it cleaves Dsg1 (Amagai *et al.* 2000, Saito *et al.* 2012).
The HSOC model for PV became even more robust and reliable by two major modifications introduced in 2019 by Burmester *et al.* (Burmester *et al.* 2019). Firstly, instead of using AK23 and ETA or PV IgG to induce acantholysis, a cloned, bi-specific anti-Dsg3 and -Dsg1 scFv called PX43 (also known as (D31)2/29 (Payne *et al.* 2005)) was used. This scFv originates from an active pemphigus patient and was cloned by antibody phage display and does not require the addition of ETA to cause acantholysis in the HSOC model (Payne *et al.* 2005, Burmester *et al.* 2019, Hammers *et al.* 2015). The scFv is well-defined and -characterized and can be produced with a standardized procedure in high amounts with high quality. As it was already introduced by Waschke *et al.*, the scFv is injected into the skin (Burmester *et al.* 2019) (see **Figure 5.4.**). The second modification is the use of fresh human skin which comes from plastic surgeries instead of using the skin from cadavers.
The HSOC model for PV has been used for pre-clinical compound testing, which allows to analyse the effects of substances when being either pre- or co-injected with the scFv or being applied topically (Varani 2012, Burmester *et al.* 2020, Neil, Brown, and Williams 2020). The analysis of the potential therapeutic effect is determined by comparison of the split formation along the length of the epidermis by conventional histology. This approach has the advantage that the effect of the substances to test does not have to be known; in case a desired effect namely the reduction in split formation is observed, it can be assumed that the affected pathway has a functional relevance for PV and treatment of it (Burmester *et al.* 2020). The substances are not limited to be tested by injection into the skin organ culture model but can also be mixing with a cream and applied to the skin.
The HSOC model for PV has been valuable to the research community allowing the investigation of the pathomechanism leading to acantholysis (Burmester *et al.* 2019, Michel and Ko 1977). It is possible to test already established therapeutic drugs from other diseases and discover new ones before these are tested in mouse models (Burmester *et al.* 2020).

4.5 Research objectives

So far, the underlying mechanism of PV is not resolved and remains a highly discussed topic within the research community.
In this project, I want to shed light on the early events of autoantibody fragment binding to Dsg3/1 and clarify whether steric hindrance, Dsg internalization or a specific outside-in signalling pathway is the source of PV pathogenesis. The project aims to answer the question of, if and what signal exactly is given to the cell once Dsg3 and Dsg3/1 is bound by AK23 and PX43, respectively. What signals are detectable in the HSOC model for PV over the course of time and how they react in terms of increasing split formation or no split formation at all. What happens on the transcriptome level and what proteins are influenced by the binding of Dsg3/1.

5 Material and methods

5.1 Reagents, substances, and kits

Name	Catalogue-No.	Company
Acetic acid	2234.1000	ChemSolute
Acetone	5025.5	Roth
Acetonitrile	100665	Merck
Acrylamide mix	1610156	BioRad
Ammonia water	221228	Merck
Ammonium persulfate	A3678-25G	Sigma Aldrich
Antibiotic-Antimycotic mix (100x)	15240-062	Gibco
Bicinchonic acid reagent A	23228	Thermo Fisher
Bicinchonic acid reagent B	23224	Thermo Fisher
Bovine serum albumin (BSA)	A8806-5G	Sigma
Calcium chloride ($CaCl_2$) solution	34005	PromoCell
Calcium chloride solution (2 M)	349610025	Acros Organics
Carbenicillin	6344.1	Th. Geyer
CnT-07 medium	CnT-07	CELLnTEC
Cryomatrix	6769006	Epredia
Crystal violet	V5265-250ML	Sigma Aldrich
4′,6-diamidino-2-phenylindole (DAPI) Fluoromount-G	0100-20	Southern Biotech
Dispase II	07913	StemCell
DNase I	EN0521	Thermo Scientific
DPBS	14190-094	Gibco
Eosin	230251-25G	Merck
Ethanol	2246.1000	ChemSolute
Eukitt	03989	Fluka
Exfoliative toxin A (ETA)	ST101	Toxin Technology
Fastbreak lysis buffer (10x)	V857C	Promega
Fetal bovine serum (FBS)	FBS-GP-0500	BioSell
Formic acid	9820	J.T. Baker
Gel marker	161-0374	BioRad
Gentamycin and amphotericin B mix	CnT-GAB-10	CELLnTEC
L-Glutamine	59202C	Sigma Life Science
β-Glycerophosphate	14405	Cayman Chemical Company
Haematoxylin	H3136	Merck
Histofix®	P087.3	Roth
Histol	6640.4	Roth
Hoechst	62249	Thermo Fisher Scientific
Imidazole	56750-100G	Sigma-Aldrich
innuPREP RNA Mini Kit 2.0	845-KS-2040050	Analytik Jena
innuSPEED Lysis Tube P	845-CS-1020050	Analytik Jena
Insulin (human)	12643-250MG	Merck
Isopropyl-β-d-thioglacatopyranosid (IPTG)	2316	Roth
Keratinocyte growth medium (KGM2)	C-20011	PromoCell

Laemmli buffer (4x)	1610732	BioRad
Magnesium chloride ($MgCl_2$)	A537.4	Roth
β-mercaptoethanol	M3148-100ML	Sigma
Methanol		
3-(4-Morpholino)propane sulfonic acid (MOPS)	BP308-500	Fisher Bioreagens
Normal goat serum (NGS)	X0907	DAKO
Normal mouse serum (NMS)	M5905	Sigma
Paraffin	CN48.1	Roth
Penicillin and streptomycin mix	15140-122	Gibco
Phenylmethylsulphonylsulphonyl fluoride	36978	Thermo Scientific
Protease inhibitor cocktail	11873580001	Roche
RNAprotect	1017980	Qiagen
RNase Away	7003	Molecular BioProducts
Simple blue staining	LC6060	BioRad
Sodium chloride (NaCl)	BP358-10	Fisher Bioreagents
Sodium-dodecylsulphate (SDS) (powder)	10593335	Fisher Scientific
SDS-gel	4561093	Sigma
Sodium citrate	PHR3875	Merck
Sodium-fluoride	2618.1	Roth
Sodium-orthovanadate	Sigma Aldrich	450243
Supplement mix	C-39016	PromoCell
Talon beads	635506	TaKaRa
Tetramethylethylendiamine (TEMED)	1107320100	Merck
Tri-fluoroacetic acid (TFA)	T6508-1AMP	Merck
Tris buffered saline (TBS) (10x)	170-6435	BioRad
Tris/Glycine/SDS buffer (10x)	1610732	BioRad
TrisHCl	15567-027	Invitrogen
Triton™X-100	X100-500ML	Sigma Aldrich
Trypan blue	93595-2.5L	Honey Well
Trypsin	C-41010	PromoCell
Tryptone	6681.2	Roth
Tween®20	437082Q	VWR
William's E-medium	BS.F1115	BIO Sell
Yeast extract	BP1422-500	Fisher Bioreagens

5.2 Antibodies

Name	**Catalogue-Nr.**	**Company**
AK23	Produced by William Hariton	
Donkey anti-mouse IgG Red IRDye 680	926-68072	Licor
Goat anti-rat IgG Green IRDye 800	926-32219	Licor
Goat anti-rat IgG (H+L)	A11007	Lifetechnologies

Goat anti-mouse IgG CyTM3-conjugated AffiniPure	115-165-146	JIR
Goat anti-mouse IgG (H+L) Alexa Fluor 488	A11029	Invitrogen
Human immunoglobulin G	624 101	Origene
Murine anti-γ-catenin	610254	BD Transduction
Murine anti-human desmoglein 1	AM26377PU-N, Clone: 27B2	Origene
Murine anti-human desmoglein 3	TA309631	Origene
Murine immunoglobulin G	Produced by William Hariton	
Murine anti-β-tubulin	T7816-0.2ML	Merck
PX43	Produced by Laura Tomaschewski	
Rabbit monoclonal anti-e-cadherin	3195S	Cell Signaling Technologiy
Rabbit monoclonal anti-Ki-67	275R-14	CellMarqueAntibodies
Rabbit monoclonal anti-β-tubulin	Ab6046	Abcam
Rat anti-HA monoclonal antibody (mAb)	11867423001	Roche

5.3 Buffers and media

Name	**Content**
Bacteria lysis buffer	1x Fastbreak lysis buffer, 20 Kunitz/mL DNase I in distilled water (Aqua dest.)
Blocking buffer (fluorescence staining)	1 % bovine albumin in washing buffer (WaB)
High calcium chloride ($CaCl_2$) CnT-07 medium with supplements (high $CaCl_2$ CnT-07)	CnT-07 medium containing 10 µg/mL gentamycin, 0.25 µg/mL amphotericin B, and 1.2 mM $CaCl_2$
High $CaCl_2$ keratinocyte growth medium 2 (KGM2) with supplements (high $CaCl_2$ KGM2)	KGM2 containing supplement mix and 1.2 mM $CaCl_2$
Isolation medium	100 Units (U)/mL penicillin, 100 µg/mL streptomycin, and 0.025 µg/mL amphotericin B in William's E-medium
Low $CaCl_2$ CnT-07 medium with supplements (low $CaCl_2$ CnT-07)	CnT-07 containing 10 µg/mL gentamycin, 0.25 µg/mL amphotericin B, and 0.06 mM $CaCl_2$
Low $CaCl_2$ KGM2 with supplements (low $CaCl_2$ KGM2)	KGM2 containing supplement mix and 0.06 mM $CaCl_2$
Odysee blocking buffer	Tris-buffered saline (TBS) containing additionally 0.1 % Tween®20, and 0.1 % sodium-dodecyl sulphate (SDS)
Phosphate buffered saline (PBS)	155 mM sodium chloride (NaCl), 12.3 mM Disodium phosphate (Na_2HPO_4), and 1.68 mM Monosodium phosphate (NaH_2PO_4) in Aqua dest. pH 7.2
PBS+	137 mM NaCl, 2.62 mM potassium chloride (KCl), 1.47 mM monopotassium phosphate (KH_2PO_4), 4.01 mM Na_2HPO_4,

	2.1 mM magnesium chloride ($MgCl_2$), and 1.19 mM $CaCl_2$ in Aqua dest. pH 7.3
Protein lysis buffer	1 % Triton™X-100, 150 mM NaCl, 20 mM Tris-hydrogen chloride acid (Tris-HCl), 15 mM Sodium-Orthovanadate, 15 mM β-glycerophosphate, 15 mM Sodium fluoride, 1.5 mM Phenylmethylsulphonyl fluoride, 1x Protease inhibitor cocktail in Aqua dest
SDS running buffer	1x Tris/Glycine/SDS buffer in Aqua dest.
Separating gel	8 % Acrylamide mix, 380 mM Tris, 0.1 % SDS, 0.1 % ammonium persulfate, and 0.06 % Tetramethylethylendiamine (TEMED) in Aqua dest.
Sodium citrate buffer	Sodium citrate ($C_6H_5Na_3O_7$) in Aqua dest. pH 6.0
Stacking gel	5 % acrylamide mix, 127 mM Tris, 0.1 % SDS, 0.1 % ammonium persulfate, and 0.01 % TEMED in Aqua dest.
Super Broth (SB)-medium	30 g/L tryptone, 20 g/L yeast extract, 10 g/L MOPS, 20 mM magnesium chloride, 100 µg/mL carbenicillin in Aqua dest.
Tris-buffered saline (TBS)	1 M Tris base and 155 mM NaCl in Aqua dest.
TBS with Tween®20 (TBST)	TBS with 0.5 % Tween®20
Transfer buffer	24.8 mM TRIS base, 19.2 M glycine, and 20 % methanol in Aqua dest. pH 8.3
WaB (fluorescence staining)	1x TBS, 2 mM $CaCl_2$, 0.5 % Tween20 in Aqua dest.
William's E-medium with supplements	2 mM L-glutamine, 100 U/mL penicillin, and 100 µg/mL streptomycin, 0.01 µg/mL hydrocortisone, and 1 µg/mL human recombinant insulin

5.4 Consumables

Name	**Catalogue-No.**	**Company**
ActivFlow routine I Amicon Ultra centrifugal filter units	UFC901024	Millipore
Aluminum foil	1770.1	Roth
BCA plate (96 wells, U bottom, crystal clear)	10625821	Fisher Scientific
Cell culture flask	83.3911.002	Thermo Fisher Scientific
Chromatography column	732-1010	BioRad
Cover slide	7695 031	TH Geyer
Cryomold	4557	TissueTek
Cryostat blade	14035838382	Leica
Falcon tube (15 mL)	62.554.502	Sarstedt
Falcon tube (50 mL)	62.547.254	Sarstedt
Fat pan marker	S2002	DAKO

Insulin syringe	324827	BD Microfine
Low protein binding tube	0030 108 442	Eppendorf
Microtome blade	220611	Micros Austria
PepSep column (C18 10-cm column 100 x 0.075 mm, 1.9 µm)		ThermoFisher
Pipet tip (0.1 – 10 µL)	7699840	Labsolute
Pipet tip (20 – 200 µL)	70.3030.020	Sarstedt
Pipet tip (100 – 1000 µL)	70.3050.020	Sarstedt
Polyvinylidene difluoride (PVDF) membrane	1620177	BioRad
Pre-column (C18 PepMap 100, 5µm, 100A, 300µm i.d. x 5mm length)		ThermoFisher
Superfrost glass slide	J1800AMNZ	Epredia
Tissue disruptor attachment	21-30750H	Omni TH biolab products
Transwell	83.3930.041	Sarstedt
Vivaspin 15R columns	VS15RH01	Satorius
6-well plate	83.3920500	Sarstedt

5.5 Devices

Name	**Company**
Bacteria incubator	Axon Labortechnik
CaptiveSpray source	Bruker Daltonics
Cell culture sterile bench	Nuaire Biological Safety Cabinets
Centrifuge 5415 R	Eppendorf
Cooling plate	Reichert-Jung
Cryostat CM3050S	Leica
Electrophoretic chamber	BioRad
GloMax	Promega
Heating block	Eppendorf
BioZero 9000 fluorescence microscope	Keyence
Microtome	Reichert-Jung
Nanodrop	Thermo Fisher
Nano Elute2	Bruker Daltonics
Neubauer counting chamber	Blaubrand
Nikon Eclipse Ti fluorescence microscope	Nikon
Odyssey imaging system	Licor
Pipets	Eppendorf
Speed Mill	Analytik Jena
Stereomicroscope	Olympus
Superspeed Centrifuge RC5C Plus	Sorvall
timsTOF HT	Bruker Daltonics
Tissue Disruptor Ultra Tarax T25	IKA-Werke
Water bath (small)	Medax
Water bath (cell culture)	GFL

5.6 Cells and bacteria

Name	Catalogue-No.	Company
Escherichia coli K12 TOPF‘ (*E. coli*)	Provided by Dr. Dr. Christoph M. Hammers	
HaCaT cells	Provided by Betjije Naumann	
Pooled human primary epidermal keratinocytes (pHPEKs)		CellnTec

5.7 Bacterial culture

5.7.1 Production of the single chain variable fragment PX43

The scFv PX43 was produced by Laura Tomascheswki in the lab of Prof. Dr. med. Dr. rer. nat. Christoph M. Hammers. Instead of culturing the safety strain *Escherichia coli* (*E. coli*) K12 during the scFv production in the Erlenmeyer flasks, the bacterial growth, and scFv production took place in a bioreactor located in the lab of Prof. Dr. rer. nat. Dagmar Willkomm from the Technische Hochschule Lübeck. The *E. coli* K12 contain the pComb3XSS vector encoding the single chain variable fragment PX43 (see **Figure 5.1.**) (Payne *et al.* 2005, Hammers and Stanley 2014, Burmester *et al.* 2019).
The safety strain *E. coli* K12 is a well-known Gram-negative, facultative anaerobe bacterium, that genome is sequenced completely, and it cannot survive outside the laboratory (Blattner *et al.* 1997). Due to the simplicity of its culturing conditions and the possibility of molecular and genetic manipulation, it is used frequently in biotechnological processes which includes the production of antibodies (Russo 2003).
The scFv producing bacteria were grown first in 25 mL Super Broth (SB)-medium as pre-culture at 30 °C, 350 rpm overnight (see **Figure 5.2.**).
On the next day, the grown pre-culture was added to 2 L of SB-medium. During the following incubation at 37 °C at 500 rpm the optical density (OD) was measured at 600 nm wavelength repeatedly until it reached 0.8 – 1.0. Once this was achieved, isopropyl-β-d-thioglacatopyranosid (IPTG) was added to a final concentration of 1 mM, which starts the expression of the scFv in the bacteria. The temperature was set to 30 °C and the fermentation ran for up to 12 hours (h).

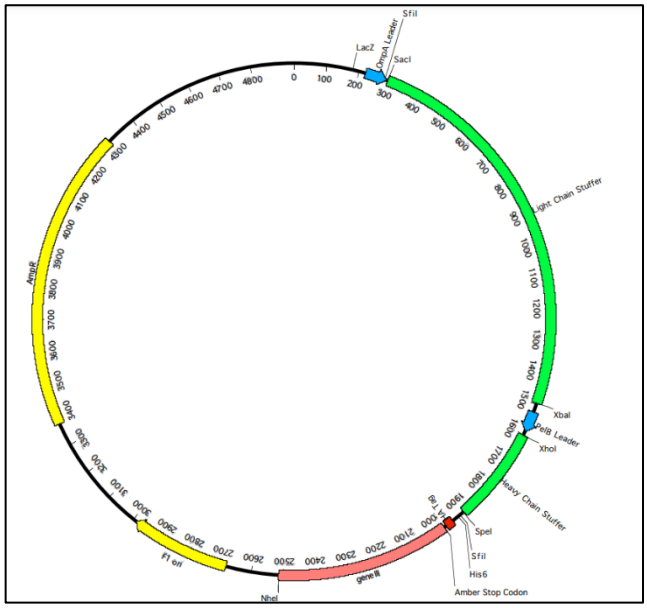

Figure 5.1.: The single chain variable fragment PX43 is encoded on the vector pComb3XSS. Vector map of the vector pComb3XSS which encodes the single chain variable fragment (scFv) PX43 and carbenicillin-resistance gene.

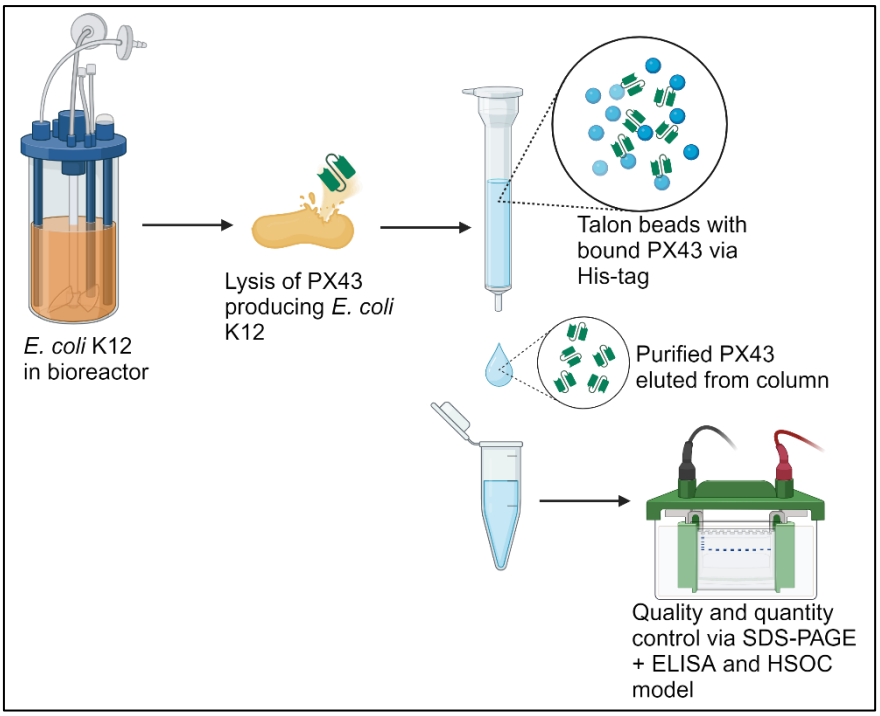

Figure 5.2.: PX43 production in a bioreactor and procedure of isolation and purification. PX43 is produced by *Escherichia coli* (*E. coli*) K12 in a bioreactor in which large amounts of the single chain variable fragment (scFv) can be produced. After production overnight, the cells were lysed and the PX43 bound to Talon® beads via its histidine (His-) tag. The purified PX43 was eluted from the beads on a column and the quality as well as the quantity was assessed by sodium-dodecylsulphate polyacrylamide gel electrophoresis (SDS-PAGE), as well as enzyme-linked immunosorbent assay (ELISA) and the human skin organ culture (HSOC) model for pemphigus vulgaris.

5.7.2 Isolation of the single chain variable fragment PX43

After collection of the culture, it was centrifugated at 8,000 times the gravitational force (xg) for 35 minutes (min) and stored at -80 °C until the isolation and purification of the scFv was started. For isolation, bacteria lysis buffer was prepared. The thawn bacterial culture was mixed with the lysis buffer and incubated for 1 h at RT on a shaker at 50 rpm. Afterwards, the culture was centrifugated at 15,000 xg for 15 min at 4 °C. The supernatant containing the scFv was mixed with Talon® beads in the ratio 1:15 (Talon® beads:supernatant), which were washed previously by addition of PBS and centrifugation at 800 xg for 2 min at RT for a total of three times. After the addition of imidazole to a final concentration of 10 mM, the supernatant/beads mix was incubated on a rotator at 50 rpm at RT for 1 h. The supernatant/beads mixture was loaded onto a chromatography column, which was washed with PBS buffer once. The flowthrough of the supernatant/beads mixture was added once more onto the column and then washed three times with 4 °C cold PBS buffer. The flowthroughs were collected on ice. For the elution of the scFv bound to the Talon® beads, PBS with 300 mM imidazole was added onto the column stepwise, so 9 fractions of 1 mL volume each were collected.
For visualization of the fractions containing the scFv, 5 µL of each fraction was mixed with 15 µL 4x Laemmli buffer containing 10 % β-mercaptoethanol and heated at 95 °C for 5 min in a heating block. Afterwards, the samples were placed on ice and a sodium-

dodecylsulphate gel (SDS-gel) was placed in an electrophoretic chamber. Once the SDS running buffer was added to the electrophoretic chamber, a gel marker was loaded as well as the prepared fraction samples. The gel was run first at 80 V for 20 min, and once the samples were run through the separating gel, the voltage was increased to 180 V for 45 min. After the electrophoretic run, the gel was washed with water and simple blue staining was used to stain the gel for 1 h at RT on a shaker; destaining was done with distilled water (Aqua dest.) overnight at RT on a shaker. The eluates containing the highest yield of protein were pooled and loaded onto Vivaspin 15R columns which were prepared with Dulbecco's phosphate buffered saline (DPBS) and centrifugated at 3220 xg for 10 min at 4 °C. The eluates loaded onto the column were centrifugated at 3220 xg for 30 min at 4 °C and then washed with DPBS for a total of two times. Another SDS-gel was prepared and additionally to the purified scFv, standards containing a known amount of bovine serum albumin (BSA) were prepared as described above. The electrophoretic run and gel staining were performed under the same conditions as described previously. Finally, the band intensity of the BSA standards was compared to the band intensity of the scFv and the concentration of the purified PX43 was calculated accordingly. The scFv was stored at -80 °C until further use. For further validation experiments, Prof. Dr. rer. nat. Matthias Peipp provided us with PX43 and a corresponding control as well as AK23 and its control produced in a hamster ovary cell line.

5.8 Cell culture

5.8.1 Cultivation of HaCaT cells

The spontaneously immortalized human keratinocyte cell line HaCaT originates from adult skin and is a widely used cell line in dermatological research. It is a monoclonal cell line, which can differentiate from its basal state upon calcium stimulation (Colombo *et al.* 2017). HaCaT cells were obtained from cryoconservation and thawn at RT for 5 min. The cells were transferred into cold low calcium chloride keratinocyte growth medium 2 with supplements (low $CaCl_2$ KGM2) and centrifugated at 220 xg for 5 min at RT. Afterwards, the supernatant was discarded and the cell pellet re-suspended in warm low $CaCl_2$ KGM2. The cells were then transferred into a cell culture flask and placed into a cell culture incubator under standard cell culture conditions (37 °C, 5 % CO_2) for 24 h. The medium was replaced once more and then changed on a regular basis of 2-3 days.
Once cells reached 80 - 90 % confluency, the medium was aspirated and the HaCaT cells washed with pre-warmed DPBS two times. After addition of the appropriate amount of trypsin, the cells were placed back for 10 min into the incubator and once they detached completely, fetal bovine serum (FBS) was added. The detached cells were transferred into a Falcon tube and centrifugated at 220 xg at RT for 6 min. Afterwards, the supernatant was aspirated, and the cell pellet resuspended in 1 mL pre-heated low $CaCl_2$ KGM2. The cell count was determined by counting with a Neubauer counting chamber and afterwards, 500,000 cells were placed in a new cell culture flask with fresh pre-heated low $CaCl_2$ KGM2 and into the cell culture incubator.

5.8.2 Cultivation of pooled normal human primary epidermal keratinocytes cultivation

The pooled normal human primary epidermal keratinocytes (pHPEKs), those cells originate from at least three donors and are all together in one culture (Wierzbicka *et al.* 2017).
pHPEKs were obtained from cryoconservation and thawn in a 37 °C water bath. The thawn cells were added to pre-warmed low $CaCl_2$ CnT-07 with supplements (low $CaCl_2$ CnT-07) and the pHPEKs counted with the help of a Neubauer counting chamber. The cells are then centrifugated at 300 xg for 5 min at RT, the supernatant aspirated, and the cells resuspended in 1 mL fresh low $CaCl_2$ CnT-07. Into a cell culture flask, pre-warmed low $CaCl_2$ CnT-07 is added before adding the resuspended cells. The first medium change is performed after 24 h by aspirating the old one and adding fresh, pre-warmed low $CaCl_2$ CnT-07. Afterwards, the medium is changed every 2 to 3 days.
There was no additional passaging performed on pHPEKs before the keratinocyte dissociation assay (KDA) was performed.

5.8.3 Antibody titration by keratinocyte dissociation assay

While the experiment for HaCaT cells was performed with low and high $CaCl_2$ KGM2 medium with supplements, for pHPEKs low and high $CaCl_2$ CnT-07 medium with supplements was used.
The murine anti-Dsg3-antibody AK23 and murine immunoglobulin G1 (mIgG1) for all following experiments were provided by the laboratory of Prof. Dr. phil. nat. Eliane Müller (Bern). The quality and quantity controls were done by the Müller lab, too.

For the titration of AK23 and PX43, 74,500 cells were seeded into the wells of a 24-well plate and grown until 100 % confluency was reached. Once this was achieved, the calcium concentration was increased to 1.2 mM for 6 h. AK23, PX43, murine immunoglobulin G1 (mIgG1) and human immunoglobulin G (hIgG) were added to the cells in concentrations of 1, 10, 20, 50, and 100 µg/mL.
The cells were incubated for 24 h in the cell culture incubator under standard cell culture conditions. Once the incubation time was over, the medium was discarded and to each well 400 µL of 2.5 U/mL dispase II were added. After 40 min incubation under standard cell culture conditions, mechanical stress was applied by pipetting the cell sheet up and down ten times with pipet tips which were coated in 1 % BSA for at least 30 min previously.
The cell fragments were fixed by adding Histofix® and stained by adding 0.1 % of crystal violet. After 24 h, pictures were taken, and the number of fragments was counted with the help of a plugin developed by Siavash Rahimi in ImageJ.

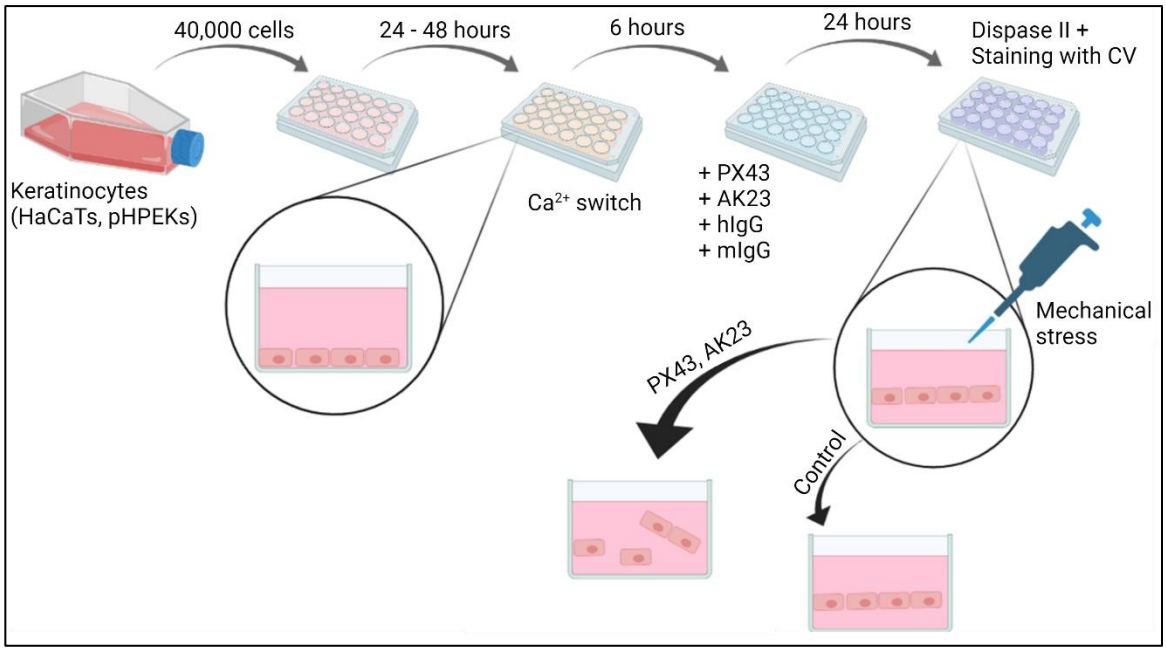

Figure 5.3.: Keratinocyte dissociation workflow with PX43 and AK23 for titration. HaCaTs and pooled human primary epidermal keratinocytes (pHPEKs) were grown under standard cell culture conditions in low calcium medium until there were enough cells to give 40,000 cells into each well of a 24-well plate. The keratinocytes were grown between 24 and 48 hours until confluency of 100 % was reached and the medium was switched from low to high calcium for 6 hours. Afterwards, PX43 and human immunoglobulin G (hIgG) as well as AK23 and murine immunoglobulin G (mIgG) were added to the cells in the concentration of 1, 10, 20, 50, and 100 µg/mL. After an incubation for 24 hours, the cell monolayers were detached by the addition of dispase II for 40 minutes and the cells underwent mechanical stress by pipetting. Once the fragments were stained with crystal violet (CV) and fixed with Histofix®, pictures were taken and the number of fragments counted.

5.9 Human skin organ culture model for pemphigus vulgaris

5.9.1 Ethical approval

The Ethical Committee of the Medical Faculty of the University of Lübeck reviewed all experiments with human samples (reference numbers: 12-178 and 06-109), which were performed following the Declaration of Helsinki. All patients gave their written informed consent for the use of the serum or skin for research purposes.

5.9.2 Experimental set up for the titration confirmation of AK23 with exfoliative toxin A

To verify the titration results from the KDA described above, AK23 was titrated additionally together with exfoliative toxin A (ETA) in HSOC model for PV. AK23 on its own cannot cause a split in healthy skin, due to the compensation of Dsg1 for the lack of function of bound Dsg3 by AK23. The addition of ETA from *Staphylococcus aureus* (*S. aureus*), which cuts Dsg1, was used to verify that the amount of AK23 injected, was added in the same effective amount as PX43.
The received skin from plastic surgery was obtained not later than 16 h post-surgery and the sex, age, and localisation of the donors are listed in **Table 5.1.**. It was placed in isolation medium, and the fat was trimmed so that only one layer of fat cells was remaining under the dermis. Afterwards, the skin was cut into 1 cm x 1 cm square pieces and placed at 4 °C until use.

Table 5.1.: Overview of received skin from healthy donors after plastic surgery and experiments in which them were used.

No.	Sex	Age [years]	Localisation	Experiment
HS22-005	Female	53	Abdomen	AK23/ETA Titration, Transcriptomics
HS22-006	Female	55	Abdomen	AK23/ETA Titration, Transcriptomics
HS22-007	Female	41	Abdomen	AK23/ETA Titration, Transcriptomics
HS22-009	Female	40	Abdomen	AK23/ETA Titration, Transcriptomics
HS22-010	Female	30	Abdomen	AK23/ETA Titration, Transcriptomics
HS22-018	Female	37	Abdomen	AK23/ETA Titration, Transcriptomics
HS22-025	Female	47	Abdomen	Proteomics
HS22-026	Female	42	Abdomen	Proteomics
HS22-027	Female	45	Abdomen	Proteomics
HS22-032	Female	39	Abdomen	Proteomics
HS23-010	Female	41	Abdomen	Proteomics
HS23-015	Female	33	Breast	Proteomics

The final injection volume of 50 µL contained either 0.08 µg of ETA and 34 µg of AK23 in DPBS, 34 µg of AK23 in DPBS, 85 µg of PX43 in DPBS, 34 µg of mIgG1 or 85 µg of hIgG (see **Figure 5.4.**). The different injections were performed with an insulin syringe, placing the needle parallel to the dermis and inserting the needle between epidermis and dermis; the contents were then injected into the middle of the skin piece. The injected skin piece was then transferred epidermis site up into a transwell sitting in a well of a 6-well plate containing William's E-medium with supplements. The plates were transferred into a cell culture incubated and incubated under normal cell culture conditions (37 °C, 5 % CO_2) for 24 h.
Once incubation time was over, the skin pieces were taken out of the incubator and prepared for different analyses: The skin was bisected and one half placed in RNAprotect, while the other half was placed in Histofix®. The samples in RNAprotect were placed at 4 °C for 48 h and then stored at -20 °C until microdissection followed by RNA isolation. Samples in Histofix® were given after at least 3 days to the routine laboratory of the Department of Dermatology, Allergology and Venerology for dehydration. After incubation in Histofix®, the tissue samples are submerged in 70 % ethanol for 30 min, then for 1 h in 80 % ethanol and twice in 96 % ethanol for 1 h each. Afterwards, the samples are submerged for 1 h in 100 % ethanol followed by two more baths in fresh 100 % ethanol for 30 min each. Finally, the tissue is incubated three times in fresh xylol for 1 h before embedded in paraffin and stored at RT until use.

5.9.3 Experimental set up for the transcriptome analysis

For transcriptome analysis of the HSOC model for PV, human abdominal skin from plastic surgery was obtained not later than 16 h post-surgery. The sex, localisation, and age of the donors are listed in **Table 5.1.**.
The received skin was prepared as described in 5.9.2. and seen in **Figure 5.4.**.
For injection, four different injections were prepared: In 50 µL, either 85 µg of PX43, 85 µg of hIgG, 34 µg of AK23 or 34 µg of mIgG1; necessary dilutions from stock solutions were made with DPBS. The injection solutions were injected into the prepared skin pieces with the needle attached to an insulin syringe inserted parallel to the dermis between epidermis and dermis. Once the opening of the needle is in the middle of the skin, the prepared solution was injected, and the skin piece transferred epidermis site up into a transwell sitting in a well of a 6-well plate containing supplemented medium made from William's E-medium with supplements. The plates were transferred into a cell culture incubator and incubated under normal cell culture conditions (37 °C, 5 % CO_2) for either 5, 10, or 24 h; in addition, right before injections took place, another sample was taken as time point zero (T0) and prepared as described in the following part.
After each incubation period, one skin piece from each injection condition was taken out of the incubator and prepared as described before.

5.9.4 Experimental set up for the proteome analysis

The experimental set up for proteome analysis is the same as described in 5.9.3 with the following changes:
Additionally, to 5, 10, and 24 h, samples are also taken at 1 h post injection. For harvesting, the skin pieces are first bisected and one half placed in a cryomold, wrapped in aluminium foil and snap-frozen in liquid nitrogen. These samples for proteome analysis were then stored at -80 °C until further preparation. The remaining half was bisected again, so that one quarter

could be fixed in TissueTek, and frozen at -20 °C, while the other quarter was placed in Histofix® until preparation for embedding in paraffin.

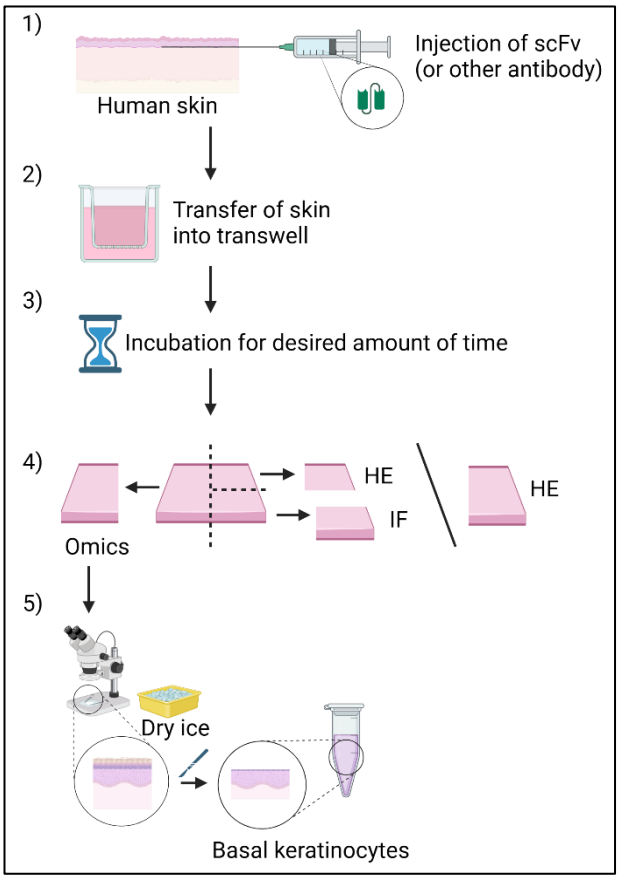

Figure 5.4.: Human skin organ culture model for pemphigus vulgaris workflow. 1) After the skin from healthy donors is cut into 1 x 1 cm pieces, the single chain variable fragment (scFv) PX43 or the murine antibody AK23 is injected into the skin between epidermis and dermis. 2) The injected skin pieces are transferred into a transwell sitting in a well with medium. 3) The skin pieces are incubated for the desired amount of time, in this case 1, 5, 10, and 24 hours depending on the setting. 4) Once the incubation time is over, one half of the skin piece is prepared for either haematoxylin/eosin (HE) staining or additionally for immunofluorescence (IF) as well. The remaining half is prepared for the omics analysis and 5) the basal keratinocytes are isolated by microdissection under a stereomicroscope on dry ice and analysed for transcriptome and proteome changes. Image made with BioRender.

5.9.5 Haematoxylin/eosin staining

For the quantitative analysis of the split formation, paraffin sections were prepared from the paraffin blocks containing skin samples of the previously described HSOC model.
The paraffin blocks were cooled to -20 °C before cutting with a blade at the microtome. Firstly, the paraffin was trimmed off until the epidermis, dermis, and subcutis were exposed completely. Then, at 4 µm thickness, the tissue sections were taken, placed onto water at 45 °C and transferred onto a Superfrost glass slide. The sections were dried overnight at 37 °C and stored at RT until staining.

Haematoxylin and eosin staining was performed as follows: The tissue slides were placed at 60 °C for 20 min before placed in Histol® for another 20 min and changed two more times. The slides were then placed shortly in 100 % ethanol two times and then into 96 % ethanol following 70 % ethanol and finally Aqua dest..
The slides were then placed in haematoxylin for 5 min, then washed shortly under tap water, followed by two short dips in an acetic acid/ethanol and again a rinse in running water until there is no more foaming. The slides are dipped two times in ammonia water and rinsed under tap water followed by a rinse in Aqua dest. The counterstain with eosin was performed for 30 – 90 seconds (sec).
Finally, the slides were placed in 96 % ethanol shortly, then two times in 100 % ethanol. After three short placements in Xylol, the slides were embedded with Eukitt and covered with a cover slide. The finished slides were stored at RT.

5.9.6 Direct immunofluorescence staining of PX43

For the staining of the bound PX43 in the human tissue, a direct immunofluorescence (DIF) staining for the hemagglutinin-part (HA) of the PX43 was done. This staining was only performed on skin samples injected with PX43 and as a control skin samples injected with hIgG.
The tissue sections were prepared from the skin samples embedded in TissueTek with the cryostat. After setting the chamber temperature to -22 °C and the objective table temperature to -20 °C, the skin samples were glued to the holder with a drop of TissueTek and cut at 6 µm with the help of a razor blade. Then, the sections were placed on a Superfrost slide. The final sections were stored at -20 °C until the fluorescence staining was performed. The remaining sample was stored at -80 °C.
Tissue sections were prepared from tissue samples prepared in 3.9.3. The tissue sections were dried at RT for 5 min and the sections encircled with a fat pan marker before washing twice with 50 µL of washing buffer (WaB). The blocking was done in a humid chamber by adding 50 µL of blocking buffer (BB) to each tissue section. Then an incubation with a rat anti-HA monoclonal antibody (mAb) diluted 1:100 in BB at RT for 60 min followed. Afterwards, the sections were washed 3 times with 50 µL WaB and a goat anti-rat IgG diluted 1:200 in BB is added and incubated at RT for 30 min. Once the incubation time was over, the antibody was dropped and the sections washed 3 times with 50 µL WaB. The tissue sections were embedded with 4′,6-diamidino-2-phenylindole (DAPI) Fluoromount-G and dried protected from light for at RT for 1 h. Until the pictures were taken at the BioZero 9000 fluorescence microscope, the slides were stored at -20 °C.

5.9.7 Immunofluorescence staining of desmoglein1/3

For the staining of human skin samples for the qualitative analysis of the distribution of Dsg1/3, tissue sections of 6 µm thickness were prepared from tissue samples prepared in 3.3.4. The tissue sections were dried at RT for 5 min and fixed in acetone at -20 °C for 10 min. Afterwards, the sections were encircled with a fat pan marker to ensure that during the incubation with primary antibodies the negative control had not been in contact with those. From here on, the sections were kept in a humid chamber. The sections were washed with PBS 3 times and blocked with 10 % normal goat serum (NGS) in PBS at RT for 20 minutes. After dropping the serum, one half of the sections was incubated with 50 µL of a mouse anti-human Dsg1 antibody diluted 1:100 in PBS containing 2 % NGS at RT for 3 h; the other half of the tissue sections (negative control) received only 2 % NGS in PBS. After washing

with PBS for 3 times, the secondary antibody CyTM3-conjugated AffiniPure goat anti-mouse IgG was diluted 1:200 in PBS with 2 % NGS and 50 µL added to all tissue sections. The incubation was done at RT for 45 min and the sections washed afterwards 3 times with PBS. Afterwards the sections were blocked again with 10 % NGS in PBS at RT for 20 min and dropped. Then 50 µL of a mouse anti-human Dsg3 antibody diluted 1:50 in PBS with 2 % NGS was added to all sections which received the mouse anti-human Dsg1 antibody and incubated at 4 °C until the next day; the other half of the sections was incubated with 2 % NGS in PBS as a negative control. After washing with PBS, 50 µL of a goat anti-mouse IgG (H+L) Alexa Fluor 488 diluted 1:200 in PBS with 2 % NGS were added to all sections and incubated at RT for 45 min. Once the incubation time was over, the sections were washed 3 times with PBS and embedded with DAPI Fluoromount-G. The objective slides were then dried at RT for 1 h and stored at -20 °C until pictures are taken at the BioZero 9000 fluorescence microscope.

5.9.8 Immunofluorescence staining of Ki-67

Slides with paraffin sections from HSOC models done for transcriptomic analysis were deparaffinized two times for 5 min in Histol and then rehydrated with decreasing concentrations of ethanol; for this, the slides were placed after the Histol in 100 % ethanol for 5 min, then in 95 % ethanol for 5 min, then in 70 % ethanol for 5 min and finally in Aqua dest. for 5 min. Afterwards, the slides were placed in PBS+ for 10 min. For the heat mediated antigen retrieval, the slides were placed in a cuvette with sodium citrate buffer. The cuvette was placed in a waterbath, then put in a microwave and processed at 720 W for 5 min three times with 2 min pause. Once it was cool enough to handle, the slides were taken out of the citrate buffer, wiped as dry as possible without touching the tissue and then placed in a wet chamber. The tissue sections were washed three times for 5 min with PBS+. After surrounding the sections with a fat pen marker, 100 µL of blocking buffer containing PBS+ and 10 % FBS per section were added for 1 h at RT. The blocking buffer was poured off after the required incubation time and 100 µL of Ki-67 rabbit monoclonal antibody diluted 1:100 in blocking buffer were added to the sections. After incubation overnight at 4 °C in the wet chamber, the primary antibody was poured off, the sections washed with PBS+ buffer for 3 times and then 100 µL of the secondary antibody diluted 1:200 in blocking buffer was added to the sections. Once incubation of 1.5 h at RT in the dark were over, 100 µL of 1:1,000 diluted Hoechst was added to each section. After 3 min, the solutions were poured off and the sections washed 3 times for 5 min with PBS+. The slides were dried, mounting medium was applied and the objective slides covered with cover slips.
Pictures were taken with Nikon Eclipse Ti fluorescence microscope. For analysis, tissue sections from AK23, mIgG, and T0, the basal and suprabasal cells in the middle of the tissue section were counted and then the Ki-67 positive cells were counted separately. For analysis of HSOC model tissue sections injected with PX43 and hIgG, the basal and suprabasal cells outside of the split were counted and then the Ki-67 positive cells counted separately.

5.10 Ribonucleic acid isolation and sequencing

5.10.1 Procedure of ribonucleic acid isolation

The isolation of basal keratinocytes for ribonucleic acid (RNA) isolation and sequencing was done with the help of the Olympus stereomicroscope by microdissection. For this, a Petri dish was filled with dry ice and the lid placed on top. On the lid, two glass slides were placed and let to cool down. Forceps, scalpels, and razor blades were kept on dry ice, too. Between the different skin pieces, everything was cleaned with RNase Away. The skin samples for microdissection were kept on dry ice throughout the procedure, as well as the isolated basal layers.
The skin piece was placed on one of the cooled glass slides with the epidermis facing up and cut into 0.5 to 1 mm thin slices with the help of the cooled razor blade; the skin piece was held by cooled forceps and the slices pulled away from the razor blade with a cooled scalpel. Then, one skin slice at a time was placed on the second glass slide and as much of the epidermis was removed as possible. Then, the dermis was cut off and the remaining basal layer was transferred with the help of the cooled forceps into an empty Eppendorf tube on dry ice. This procedure was repeated until all basal keratinocytes were microdissected from the skin sample.
After microdissection of the basal keratinocytes, the samples were kept on dry ice until further processing. The releasing (RL), high solution (HS), and low solution (LS) buffers were prepared according to the instruction for the innuPREP RNA Mini Kit 2.0. Once a set of samples was prepared, 200 µL of RL buffer were added to each sample and the keratinocytes transferred with the buffer into the innuSPEED Lysis Tube P. The homogenization was done with the help of the Speed Mill for once 20 sec. After the addition of 250 µL of RL buffer to the homogenized samples and shaking at 1,000 rpm for 10 min at RT, the samples were centrifugated for 1 min at 13,500 xg. The liquid above the beads was pipetted into the blue column from the kit, sitting on the receiver tube. The blue filter unit binds all genomic DNA, while the RNA is collected in the receiver tube. After centrifugation at 12,000 xg for 2 min at RT, the RNA in the receiver tube was mixed with the same volume of 70 % and then added to the pink column from the kit, sitting on a receiver tube. The filter binds the RNA, while the impurities will be in the receiver tube after centrifugation.
Once another round of centrifugation at 12,000 xg for 2 min at RT was over, the flow through was thrown away and 350 µL of HS buffer added onto the filter column. After centrifugation at 12,000 xg for 1 min at RT, DNase was added to the filter and incubated for 15 min at RT. Then, the filter columns were centrifugated for another 1 min at 12,000 xg at RT, the flow through discarded afterwards and the filter washed with another 350 µL of HS buffer. Centrifugation at 12,000 xg for 1 min at RT was followed by the addition of 500 µL LS buffer and another round of centrifugation as described previously. Once the column was on a new receiver tube, 700 µL of 80 % ethanol were added and the samples centrifugated at 13,500 xg for 1 min at RT. Changing the receiver tube again was followed by another round of centrifugation at 11,000 xg for 2 min at RT. For the final centrifugation and elution of the RNA from the filter column, the filter column was placed on a sterile, RNase-free tube and 20 µL of ddH_2O were added. Then, centrifugation at 12,000 xg for 1 min at RT followed and the samples were stored directly on ice. For quality control, 1 µL of the RNA was measured via the Nanodrop and the remaining RNA was stored at -80 °C until sent for RNA sequencing to the next generation sequencing platform (NGSP) of the university of Bern.

5.10.2 Ribonucleic acid sequencing

For the library prep protocol, the Illumina TruSeq Stranded Total RNA Library Prep Kit with RiboZero Plus rRNA depletion was used. The sequencing was performed on an Illumina Novaseq6000 with 2x 150 base pair read-length. For analysis, the data was de-multiplexed at the NGSP and further analysis performed by Sen Guo.
In brief, the raw reads were processes via FastQ, Kalisto and DeSeq2. The next step, dimension reduction, was achieved by principal component analysis (PCA) and generation of a differentially expressed genes (DEGs) list. By gene pathway analysis, functions were annotated and finally upstream transcription factors were identified.

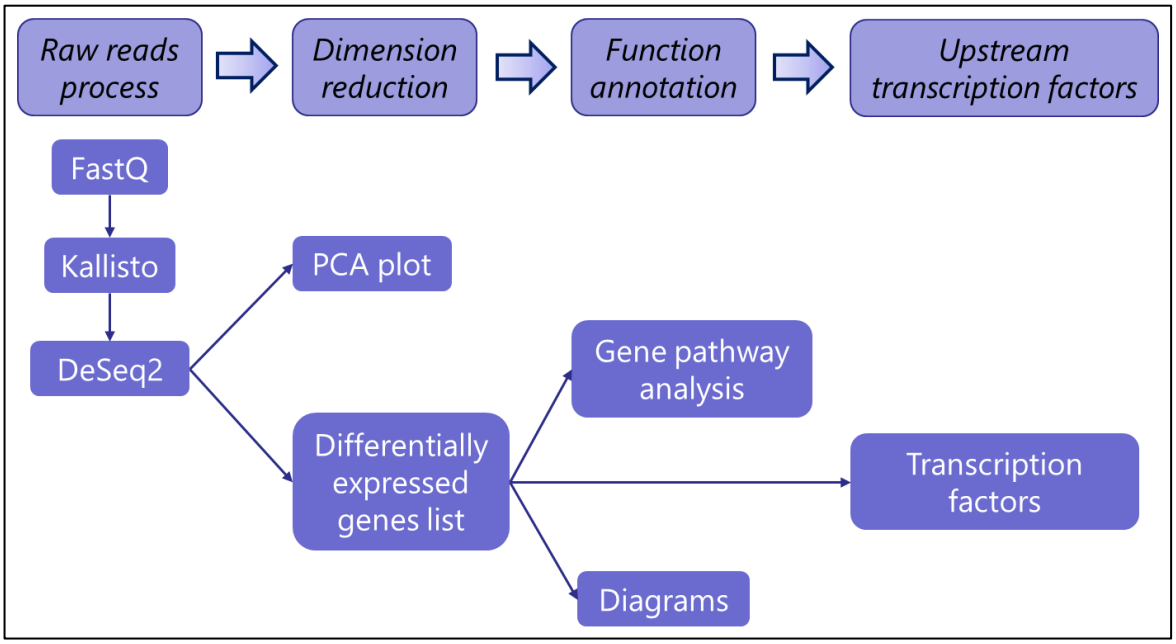

Figure 5.5.: Overview of data analysis from transcriptome analysis. The raw reads acquired after ribonucleic acid sequencing were processed via FastQ, followed by Kallisto and DeSeq2. For the reduction of dimensions, principal component analysis (PCA) plots and differentially expressed genes (DEGs) lists were created. Latest was used to annotate the functions by gene pathway analysis and creation of diagrams (for example, heat maps) to get an overview of the data. Finally, the upstream transcription factors were analysed and aligned with the data.

5.11 Triton™X-100 soluble and insoluble protein fraction isolation and mass spectrometry

5.11.1 Triton™X-100 soluble and insoluble protein fractions

Triton™X-100 soluble fraction contains all membrane associated proteins, while the insoluble fraction contains all cytoskeletal associated proteins (Aoyama and Kitajima 1999).

5.11.2 Procedure of protein isolation

The microdissection for the isolation of basal keratinocytes was performed as described in 5.10.1..
For protein isolation, the microdissected basal keratinocytes were placed into 2 mL of protein lysis buffer, vortexed briefly and kept on ice. The samples were homogenized on ice with the help of tissue disruptor attachments fixed on the tissue disruptor. For every sample, a fresh tissue disruptor attachment was used. After disruption, the samples were kept on ice for 30 min and vortexed once after 15 min. Once the incubation time was over, the samples were centrifugated at 200 xg for 1 min at 4 °C. The supernatant was transferred into a new, low protein binding tube, vortexed, divided upon five tubes and snap frozen with liquid nitrogen. The pellet was washed with 1 mL protein lysis buffer, centrifugated at 15,000 xg for 10 min at 4 °C and after discarding the supernatant, snap frozen on liquid nitrogen, too. All samples were stored at -80 °C until quality and quantity control were performed, as well as mass spectrometry analysis.

5.11.3 Quantity control: Bicinchonic acid assay

The quantity of protein isolated from the microdissected keratinocytes was determined via the bicinchonic acid (BCA) assay. For this, 5 µL from the isolated Triton™X-soluble fraction were added to a BCA plate and mixed with 95 µl of a 50:1 mixture of BCA reagent A and BCA reagent B, respectively. After incubation for 25 min at 37 °C, the absorbance of the samples was measured at 562 nm with the GloMax and compared to a concentration standard curve made from BSA to determine the protein concentration.

5.11.4 Quality control: Western blot

For the qualitative control of the isolated Triton™X-soluble fraction, SDS-PAGE was performed with following Western blotting.
For separation, an 8 % separating gel was prepared. After polymerization of the separating gel, the 5 % stacking gel was added.
The protein samples were diluted with Aqua dest. so that a maximum of 30 µg of protein was loaded to the gel. After the addition of 5 x Laemmli buffer, the samples were incubated for 10 min at 98 °C, then allowed to cool to RT.
Once the samples and the protein marker were loaded onto the polyacrylamide gels in the electrophoresis chamber with SDS running buffer, the electrophoretic run was started at 50 V for 40 min and the voltage then increased to 120 V for 60 min. After the electrophoretic run, the gel chamber was disassembled and the gel used for following Western blotting.
The proteins from the SDS-PAGE were transferred on a polyvinylidene difluoride (PVDF) membrane by the wet transfer method. The PVDF membrane was soaked in 100 % methanol

for a few sec before transferred into transfer buffer until use. The SDS-gel was equilibrated in transfer buffer for 10 min before assembly of the transfer sandwich: On the black frame, foam, Whatman paper, the gel, PVDF membrane, a second Whatman paper and finally another foam were stacked in the named order before closed with the white frame. The closed cage was then transferred into a tank containing transfer buffer, surrounded by ice. After connecting the transfer tank to a voltmeter, the wet transfer was done at 120 V for 90 min in a cold room.
After the transfer and disassembly of the transfer sandwich, the membrane was blocked with 5 % BSA in TBS with Tween®20 (TBST). After blocking for 1 h at RT at 50 rpm, the membrane was washed in cold TBST three times for 5 min at RT at 32 rpm. As primary antibodies rabbit e-cadherin and murine anti-γ-catenin (plakoglobin) were added to blocking buffer and incubated overnight at 4 °C at 30 rpm.
Before addition of the secondary antibody, the membrane was washed three times for 5 min with TBST at RT at 32 rpm. The secondary antibodies directed against murine Fc-region coupled to IRDye 680 (red) for detection of plakoglobin and against rabbit Fc-region coupled to IRDye 800 (green) for detection of e-cadherin were diluted 1:10,000 in Odysee blocking buffer. The membrane was incubated for 90 min at RT in the dark at 50 rpm.
After washing the membrane with TBST for two times for 5 min at RT at 32 rpm and one last time in TBS under the same conditions, the membrane got scanned on the Odysse scan machine.
Detection of β-tubulin as a loading control was done by using the primary murine antibody anti-β-tubulin and the secondary antibodies directed against murine Fc-region coupled to IRDye 680 (red) for detection.

5.11.5 Mass spectrometry analysis of Triton™X-100 soluble fraction

The Triton™X-soluble fractions from T0, PX43 injection after 24 h and hIgG injection after 24 h were used for the mass spectrometry analysis. This was done by the Core Facility Proteomics & Mass Spectrometry at the university of Bern.
The samples were precipitated with 5 volumes of cold acetone overnight at -20 °C and pelleted afterwards via centrifugation at 16,000 xg for 10 min at 4 °C. After the discard of the supernatant, the pellets were air dried at RT for 15 min and stored at -20 °C until use.
Before evaluation of the protein concentration via BCA assay, the proteins were re-dissolved in 100 µL 8 M urea in 50 mM Tris-HCl, pH 8. The protein reduction and alkylation was done as described by (Braga-Lagache *et al.* 2016). The urea was diluted to 1.6 M with 20 mM Tris-HCl in 2 mM calcium chloride and the samples mixed with trypsin in a 1:100 ratio. After an initial incubation for 2 h at 37 °C, more trypsin was added for an overnight incubation at RT. The digestion was stopped by the addition of 20 % TFA in a 1:20 ratio (v/v).
Using a Nano Elute2 which was connected to a timsTOF HT, via a CaptiveSpray source, the digests underwent nano-liquid chromatography analysis.
For the analysis, an endplate offset of 500 V, a drying temperature of 200 °C, and the capillary voltage fixed at 1.6 kV were set. For the following chromatographic separation, 500 ng protein digest was loaded onto a pre-column followed by the elution in back flush mode onto a PepSep column by applying a 30-minute gradient of 5 % acetonitrile to 30 % in water with 0.1 % formic acid at a flow rate of 400 nL/min.
Using the Parallel Acquisition Serial Fragmentation (PASEF) mode, the timsTOF HT was operated either in DDA or DIA mode. For the DDA method, the mass range was set between 100 and 1700 m/z, with 8 PASEF scans between 0.75 and 1.35 V s/cm2. The accumulation and ramp time were set to 100 ms. Fragmentation was triggered at 15,000 arbitrary units

(au), and peptides (up to charge 5) were fragmented using collision induced dissociation with a spread between 20 and 75 eV.
The dia-PASEF acquisition method was set with 47 isolation windows of 26 m/z width, including an overlap of 1 m/z. The isolation windows were associated with ion mobility range between 0.7 to 1.45V s/cm2. TIMS accumulation and separation were both set at 100 ms.
The DDA data were used to produce a spectral library with fragpipe (Yu *et al.* 2020) version 20.0 and the following parameters: database was SwissProt Homo Sapiens (version 2023_04), to which common contaminants were added; precursor and fragment mass tolerances were set to ±20 ppm and ±0.05 Da, respectively. The protein digestion was set to trypsin, with a maximum of 3 missed cleavages. The variable modifications allowed were oxidation on methionine and protein N-terminal acetylation. The carbamidomethylation of cysteines was given as fixed modification.The the minimum number of matched fragments was set to 5 and the validation was done with Percolator (MSBooster enabled). The filtering was done at 1 % FDR for protein level. DIA data was analyzed by DIA-NN 1.1.8.2 integrated in the fragpipe suit using the spectral library.
Potential contaminants were then removed for further analysis. Missing DIA protein intensity values were imputed as follows: If there was at most 1 detection in a replicate group, then the remaining missing values were imputed by a random draw from a Gaussian distribution of width 0.3 x sample standard deviation and shifted left from the sample mean mu by 2.5 x sample standard deviation. All other missing values were replaced by the Maximum Likelihood Estimation method (Silver, Ritchie, and Smyth 2009) for differential expression tests using the paired moderated t-test (Kammers *et al.* 2015). For multiple test correction, the R tool fdrtool (Strimmer 2008) was applied. Significance criteria using 20 imputation cycles were applied as described in (Uldry *et al.* 2022), imposing a minimum log2 fold change of 1 in absolute value, and a maximum adjusted p-value of 0.05 (the latter value reachable at asymptotically high log2 fold changes).

5.12 Statistics and other programs

In addition to the already mentioned programs, ImageJ was used to assess the fragmentation in the KDA and to quantify the split formation in the HSOC model. GraphPad Prism was used to make the graphical representations, as well as the included statistics. The individual statistical tests used for the different analysis are described below the graphs.
The analyses of the RNA sequencing, shot-gun proteomics mass spectrometry and spatial transcriptomics were performed by Prof. Dr. rer. nat. Hauke Busch and Sen Guo.

6 Results

6.1 The titration of AK23 and PX43 by the keratinocyte dissociation assay and the validation by the human skin organ culture model for pemphigus vulgaris give contradicting results

For the determination of the amount of AK23, corresponding to the amount of 85 µg PX43 used in the HSOC model for PV, the KDA was used. In brief, HaCaT cells were grown in a monolayer and mechanically stressed to assess the binding of the Dsgs. Counting the fragments, for AK23 the highest fragmentation was detected at 20 µg/mL and for PX43 at 50 µg/mL, as depicted in **Figure 4.1.**. There is a clear drop in fragmentation between 20 µg/mL and 50 µg/mL of AK23. For the different concentrations tested for PX43 only tendencies, but no significancies are visible (**Figure 4.1.a**). Exemplary pictures of the disrupted monolayers are shown in **Figure 4.1.b**. This could also be validated by the same approach done on pHPEK cells (**Figure 4.2.**): Again, there is a significant drop between 20 µg/mL and 50 µg/mL AK23. For PX43, the drop between 50 µg/mL and 100 µg/mL, which was only a tendency when tested on HaCaT cells, is now clearly visible and significant (**Figure 4.2.a**). Calculating the concentration of AK23 for the HSOC model, it was determined that 34 µg of AK23 will bind to Dsg3 in the same manner as 85 µg of PX43. An observation made during the experiment is that the controls exhibit unusual fragmentation when the KDA is performed on HaCaT cells (**Figure 4.2.a**); this could not be seen for the KDA performed on pHPEK cells (**Figure 4.2.b**).
The calculated amount of AK23 for the HSOC model was tested further in the HSOC model for PV. In brief, 34 µg AK23 was injected together with 0.08 µg ETA from *Staph. aureus* in a total injection volume of 50 µL. Simultaneously, 85 µg PX43 in 50 µL was injected to see if the split caused by them is similar in superbasal split formation and split length. After 24 hours incubation, the injected skin pieces were prepared for embedding in paraffin and cut for H&E staining. As it is evident by the H&E stainings in **Figure 4.3.b**, the split caused by both injections is superbasal and similar to the split formation in PV patients. On the other hand, the split caused by PX43 is larger than the one by AK23 with ETA (**Figure 4.3.a**). Although the differences are not significant when comparing the time points, a tendency is clearly visible.

(a)

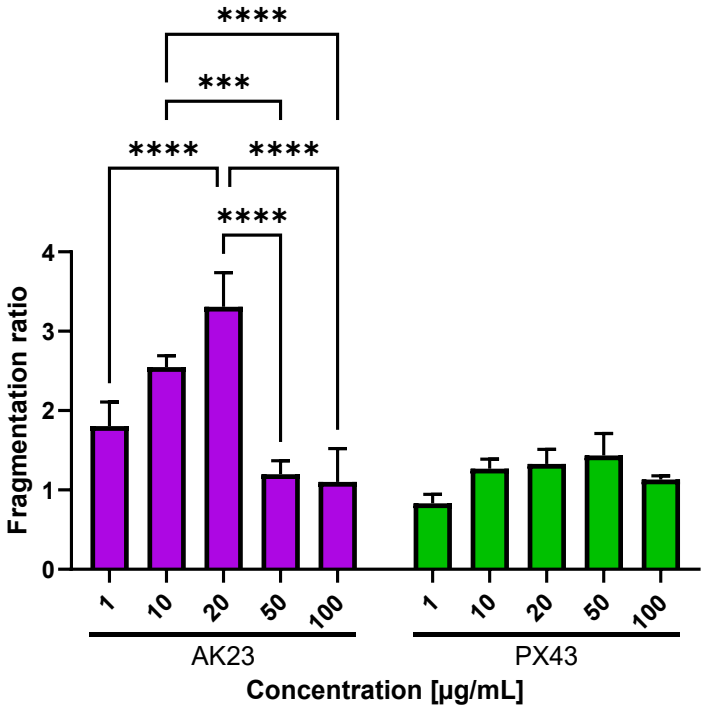

(b)

Antibody	Concentration [µg/mL]				
	1	10	20	50	100
AK23	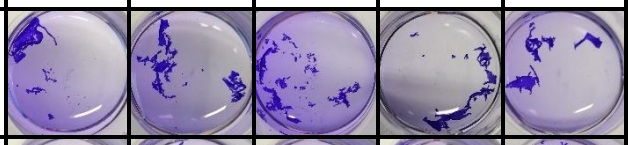				
mIgG	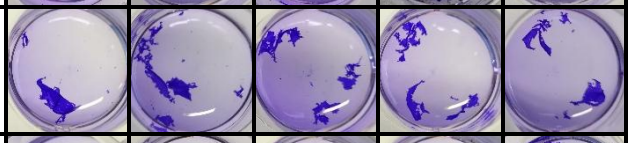				
PX43	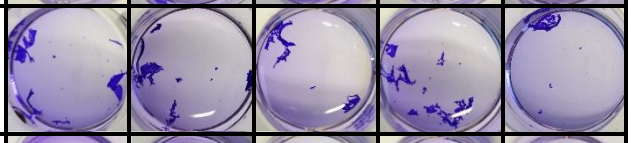				
hIgG	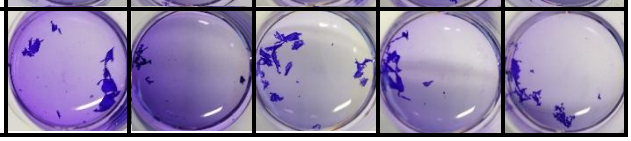				

Figure 6.1.: In the keratinocyte dissociation assay performed on HaCaT cells, 20 µg/mL of AK23 and 50 µg/mL of PX43 cause the highest fragmentation. (a) Graphical representation of the fragmentation ratio of human high calcium immortalized epidermal keratinocytes (HaCaT cells) incubated with 1, 10, 20, 50, and 100 µg/mL AK23 (violet) and PX43 (green) for 24 hours in comparison to murine immunoglobulin G (mIgG) and human immunoglobulin G (hIgG), respectively. n (technical) = 3. Two-way ANOVA was performed and p value < 0.0004 [***] and p value < 0.0001 [****] are shown. More significant differences are depicted in **Figure 10.1.** in the appendix. **(b)** Representative pictures of the HaCaT cells monolayer after fragmentation by mechanical stress stained with crystal violet and fixed with Histofix® after application of mechanical stress.

(a)

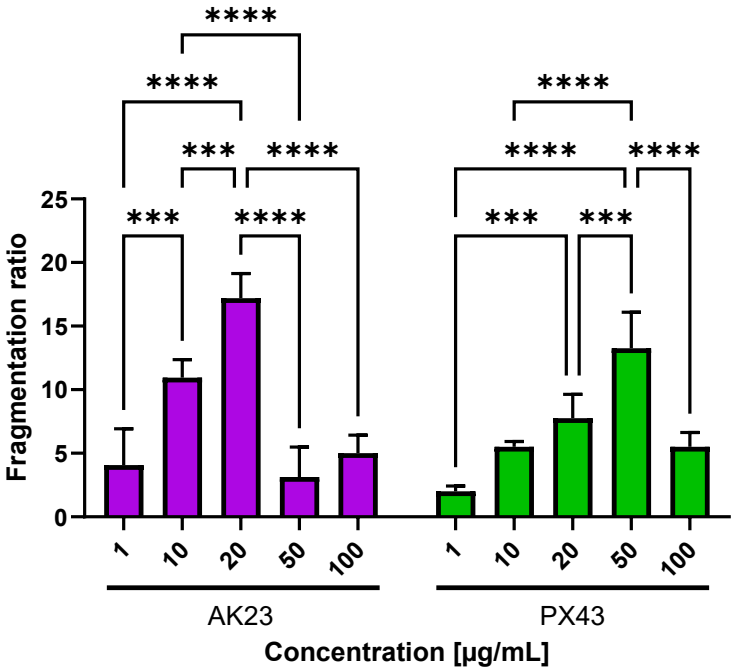

(b)

Antibody	Concentration [µg/mL]				
	1	10	20	50	100
AK23	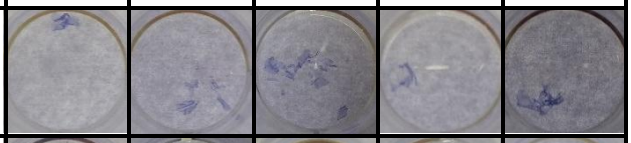				
mIgG					
PX43	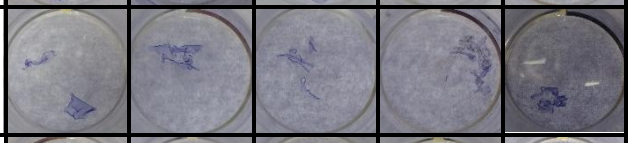				
hIgG	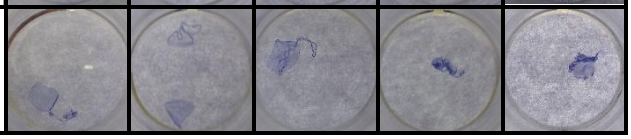				

Figure 6.2.: In the keratinocyte dissociation assay performed on pooled normal human primary epidermal keratinocytes cells, 20 µg/mL of AK23 and 50 µg/mL of PX43 cause the highest fragmentation. (a) Graphical representation of the fragmentation ratio of pooled normal human primary epidermal keratinocytes (pHPEKs) incubated with 1, 10, 20, 50, and 100 µg/mL AK23 (violet) and PX43 (green) for 24 hours in comparison to murine immunoglobulin G (mIgG) and human immunoglobulin G (hIgG), respectively. n (technical) = 3. Two-way ANOVA was performed and p value < 0.0004 [***] and p value < 0.0001 [****] are shown. More significant differences are depicted in **Figure 10.2.** in the appendix. **(b)** Representative pictures of the pHPEK monolayer after fragmentation by mechanical stress stained with crystal violet and fixed with Histofix® after application of mechanical stress.

(a)

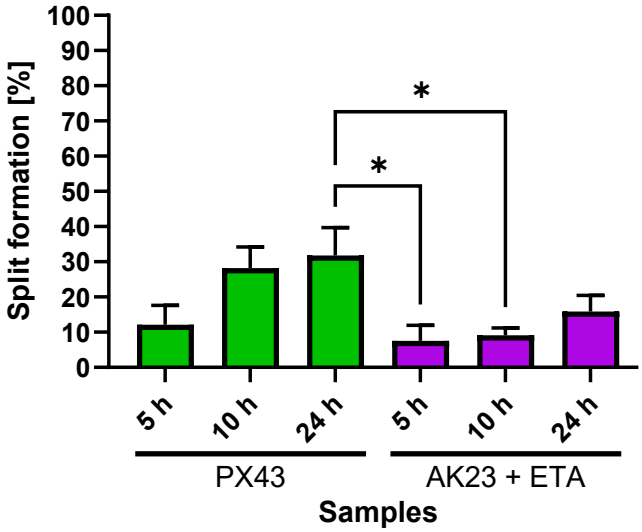

(b)

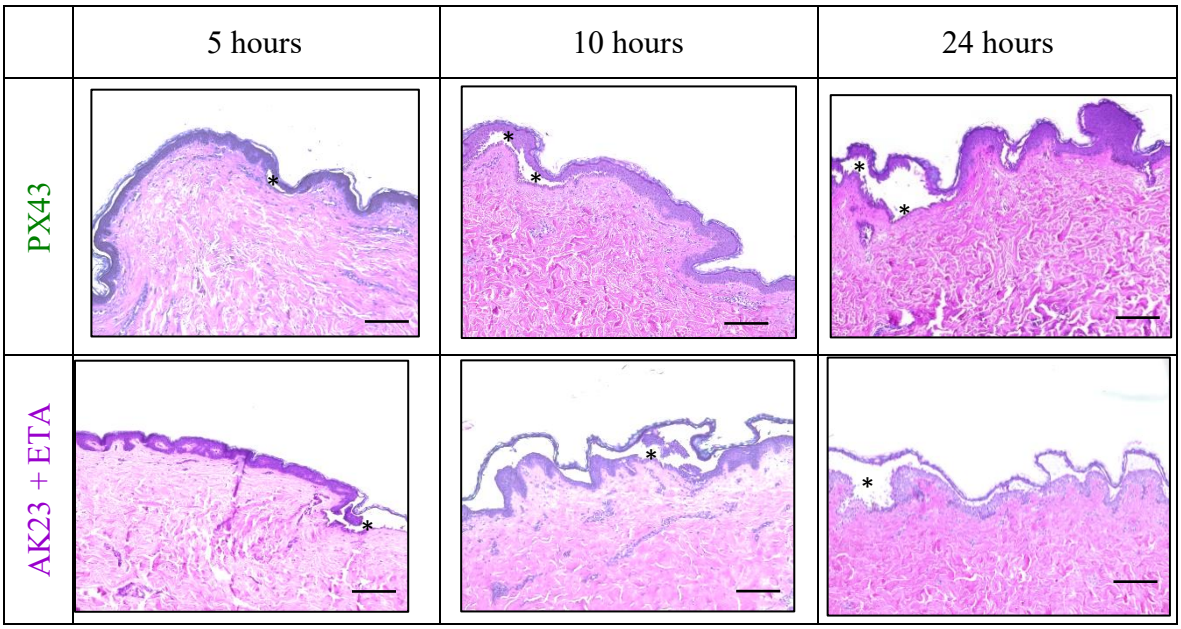

Figure 6.3.: 34 µg AK23 and 0.08 µg of exfoliative toxin A cause a similar split to 85 µg PX43, but the split is smaller. (a) Graphical representation of the split formation [%] in the human skin organ culture (HSOC) model for pemphigus vulgaris (PV) with skin samples injected with 50 µL of either 85 µg PX43 (green) or 34 µg AK23 with 0.08 µg exfoliative toxin A (ETA) (violet) for 5, 10, and 24 hours. n (biological) = 5, number of visual fields (VFs) = 5 – 9. Two-way ANOVA was performed and p value < 0.05 [*] is shown. **(b)** Representative pictures of haematoxylin-and eosin-stained tissue sections from the HSOC model for PV injected with either PX43 or AK23 with ETA. * = split formation. Scale bars = 100 µm.

6.2 No specific autoantibody signalling is detectable in the human skin organ culture model for pemphigus vulgaris on the transcriptomic level

The goal of the transcriptomic analysis was to see whether there is a signalling on RNA level specific for the binding of PX43 and AK23 to Dsg1/3 and Dsg3, respectively.
The analysis of the HSOC model performed on the skin from six different donors (further information in **Table 5.1.** for the transcriptome evaluation after 5, 10, and 24 hours of incubation with PX43 and AK23 revealed differences between the two injections. Since the production of PX43, AK23 and mIgG does not lead to endotoxin-free preparations, the genes responding to endotoxins were excluded based on the recalculation via a gene set variation analysis (GSVA)-based time series analysis.
On a microscopic level, it is evident that AK23 alone is indeed not able to cause a split in the human skin on its own (**Figure 4.4.**). For PX43, an increase in split formation over the course of time is visible. A small proportion of the split caused by the scFv is comparable to a split caused by autoantibodies directed against Dsg1 only, replicating the clinical picture of PF, but the vast majority of the formed split is replicating the split formation seen in PV.
To address the question if the injection of either AK23 or PX43 causes an increase in the number of proliferating cells, paraffin sections from the HSOC model from three different patients were stained for Ki-67 positive cells. As it can be seen in **Figure 4.5.**, there are no significant differences in AK23 and mIgG injected skin pieces after 5 **(Figure 4.5.a)**, 10 **(Figure 4.5.b)** and 24 hours **(Figure 4.5.c)**. The only significant difference reported here is a significant increase in Ki-67-positive suprabasal keratinocytes after 10 hours of incubation in comparison to the basal keratinocytes **(Figure 4.5.c)**. When comparing PX43 injected skin after 24 hours to the other conditions, the only significant difference is in the relative number of Ki-67-positive basal keratinocytes which is higher in skin sections from T0 **(Figure 4.5.c)**. This is also seen in the exemplary pictures (**Figure 4.5.d**).

(a)

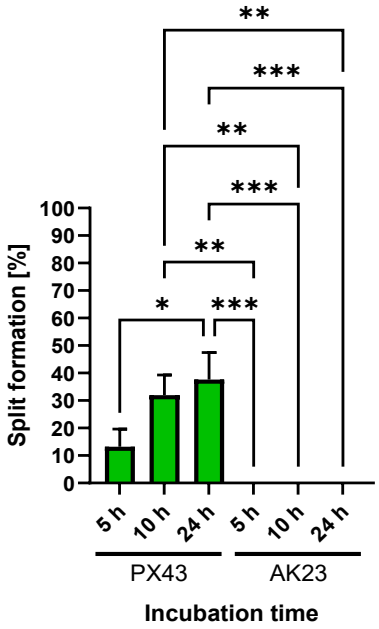

(b)

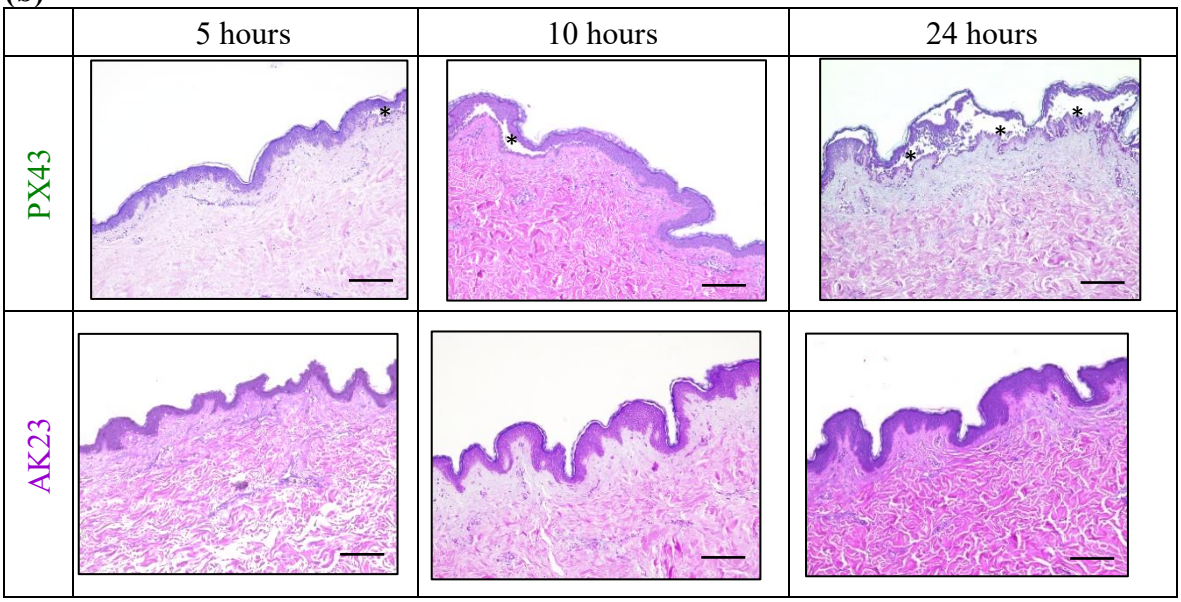

Figure 6.4.: Injection of PX43 leads to an increase in split size over time in the human skin organ culture model for pemphigus vulgaris, while AK23 alone cannot cause a split. (a) Split formation [%] in the human skin organ culture (HSOC) model injected with 85 µg PX43 and incubated for 5, 10, and 24 hours [h]. Two-way ANOVA was performed and p value < 0.05 [*], p value < 0.005 [**] and p value < 0.0005 [***] are shown. n (biological) = 6, visual fields per biological replicate of the HSOC model = 5 – 8. **(b)** Representative pictures of haematoxylin-and eosin-stained tissue sections from the HSOC model for PV injected with either PX43 or AK23 after 5, 10, and 24 hours. * = split formation. Scale bars = 100 µm.

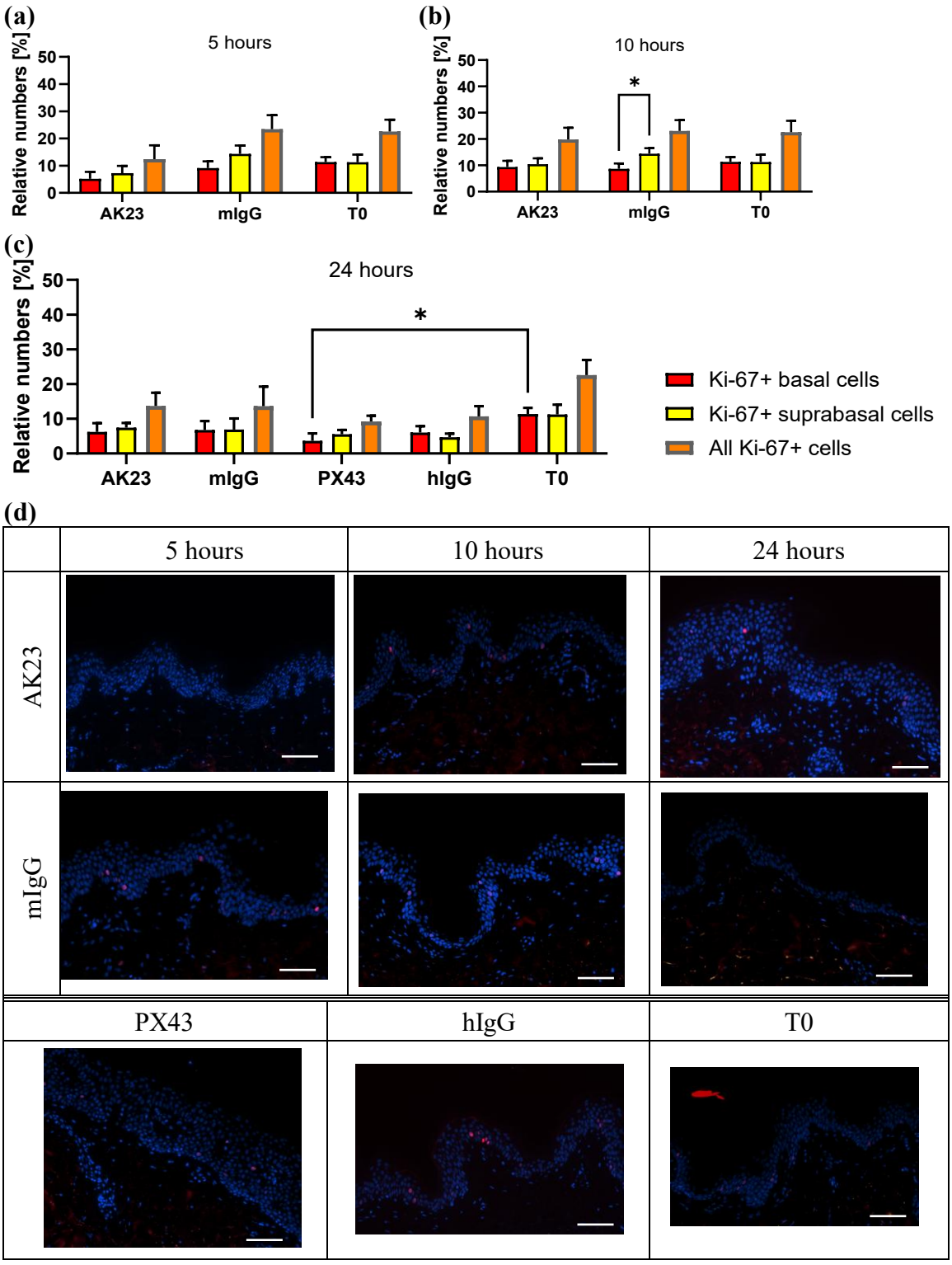

Figure 6.5.: There is no significant difference in proliferating cells after AK23 / mIgG injection or PX43 / hIgG injection in the human skin organ culture model for pemphigus vulgaris. (a) – **(b)** Relative number [%] of Ki-67 positive cells in the basal (red) and suprabasal (yellow) layer as well as all Ki-67 positive cells combined (orange) in paraffin sections of the human skin organ culture (HSOC) model for pemphigus vulgaris injected with AK23 and murine immunoglobulin G (mIgG) after 5 **(a)**, 10 **(b)** and 24 hours **(c)** of incubation, as well as HSOC model injected with PX43 and human immunoglobulin G (hIgG) incubated for 24 hours **(c)** and time point zero (T0). Two-way ANOVA was

performed and p value < 0.05 [*] is shown. n (biological) = 3. **(d)** Representative pictures of Ki-67-stained tissue sections. Nuclear staining 4′,6-diamidino-2-phenylindole (DAPI) is depicted in blue, while Ki-67 positive cells are stained in red. Scale bar = 200 µm.

As seen in **Figure 6.6.**, the principal component analysis (PCA) reveals biological differences for PX43 compared to hIgG, while AK23 injected skin is similar to the skin injection with mIgG. The injection of AK23 into human skin does not cause a suprabasal split (**Figure 6.4. and 6.6.**), same is true for the injection with mIgG; this absence of a phenotype after 5, 10, and 24 hours of incubation is also visible in the similarity of the PCA plots in which AK23-injected skin (violet) shows only minimal biological difference to skin injected with mIgG (yellow). In contrast, skin injected with PX43 (green) shows a phenotype (suprabasal split) after 5 hours, but clear biological differences to hIgG-injected skin (control) are visible after 10 hours. After 24 hours of incubation, the PX43 and hIgG treated skin show a small overlap but are still two distinct groups.

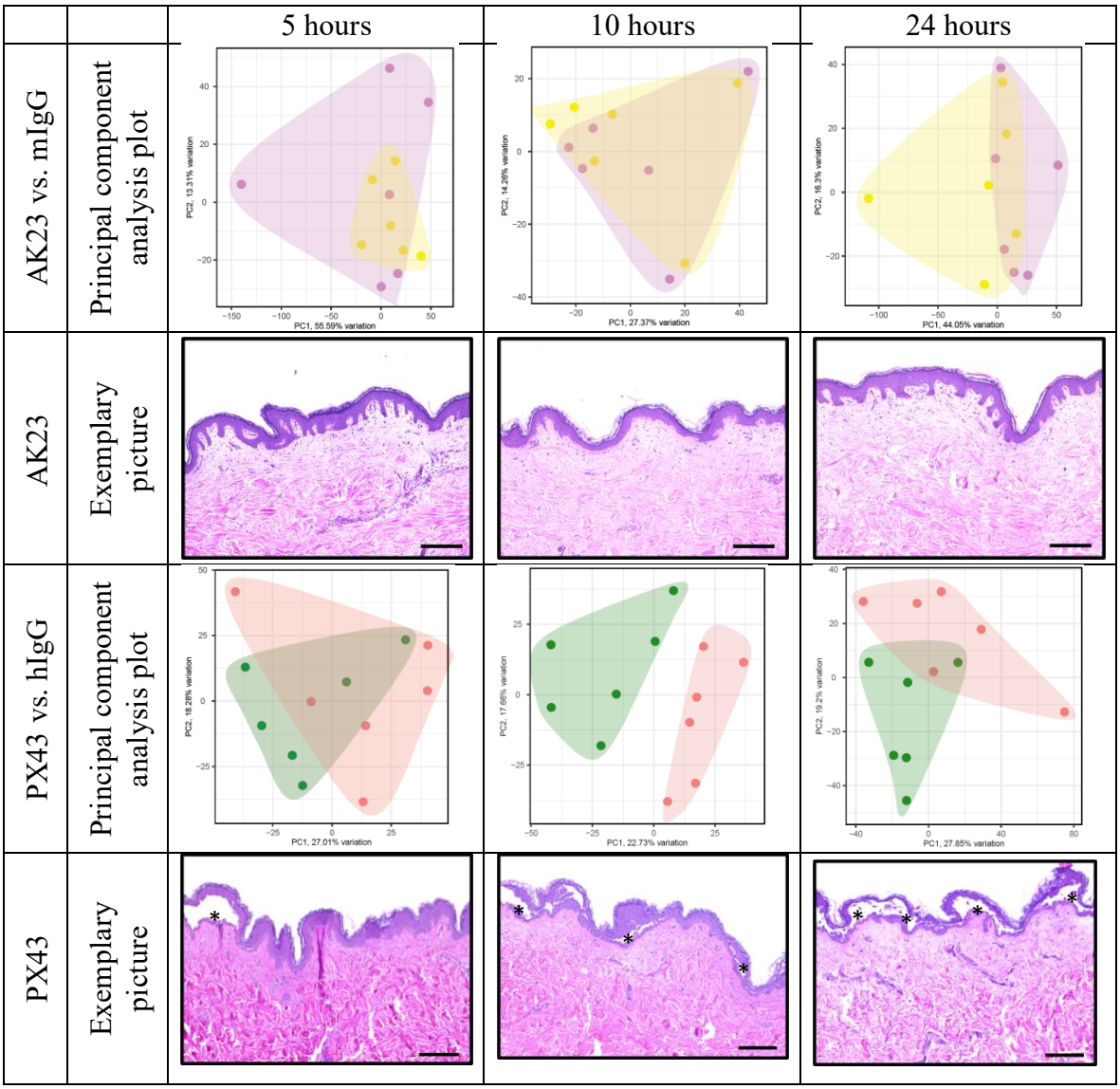

Figure 6.6.: AK23 and mIgG injected skin samples show minimal biological differences after 5, 10, and 24 hours, while PX43 and hIgG injected skin samples show clear biological differences after 10 hours of incubation. Principal component analysis (PCA) plot of the human skin organ culture (HSOC) model injected with 34 µg AK23 (violet) (first row), murine immunoglobulin G (mIgG) (yellow) (second row), 85 µg PX43 (green) (third row) and human immunoglobulin G (hIgG) (red) (fourth row) after 5, 10, and 24 hours (from left to right) incubation with corresponding exemplary pictures of haematoxylin-and-eosin-stained paraffin sections. * = split formation. Scale bars = 100 µm. n (biological) = 6.

As seen in the volcano plots (**Figure 6.7.**) for AK23 compared to mIgG at 5, 10, and 24 hours post injection, only a small number of differentially regulated genes is upregulated significantly. After 5 hours, PEDS1-UBE2V1, kallikrein related peptidase (KLK) 6, and ERICHE-AS1 are significantly upregulated, while radical S-adenosyl methionine domain containing (RSAD) 2, c-c motif chemokine (CCL) 4, interferon (IFN) induced protein with tetratricopeptide repeats (IFIT) 1, 2'-5'-oligoadenylate synthetase like (OASL), and γ-aminobutyric acid type A receptor subunit β (GABRB) 3 are downregulated. After 10 hours, only two genes are significantly upregulated (Cullin associated and neddylation dissociated (CAND) 2 and immunoglobulin heavy variable (IGHV) 3-33) while there are no significantly downregulated genes. After 24 hours, most genes are downregulated (the majority being CXCL-genes) and only two genes (WDR17 and ZIC2) are upregulated. Looking at the volcano plots after PX43 injection, there is a larger number of genes upregulated after all time points, as well as downregulated. Throughout all time points, CXCLs and CCLs are upregulated, as well as NFκBs. Most significantly upregulated genes include RNA sensor RIG-1 (DDXX58), OASL, IFN-induced with helicase c domain (IFIH) 1, IFIT 1, ISG15 upiquitin like modifier (ISG15), and long intergenic non-protein coding RNA (LINC) 02605 after 5 hours, GBP5, TNIP3, LCN2, CD38, CCL5, and LNC02605 after 10 hours, and finally IFI44L, CFB, GBP1, IFI44, and OAS2 after 24 hours after PX43 injection compared to hIgG injected after the respective time points. Downregulated genes 5 hours after injection of PX43 include ADORA3, SASH3, SIRPB2, and FZD2, after 10 hours RNASE6, P2RY14, CLEC10A, and CHP2 and after 24 hours FLGs, LORICRIN, IL37, and SLC46A2.

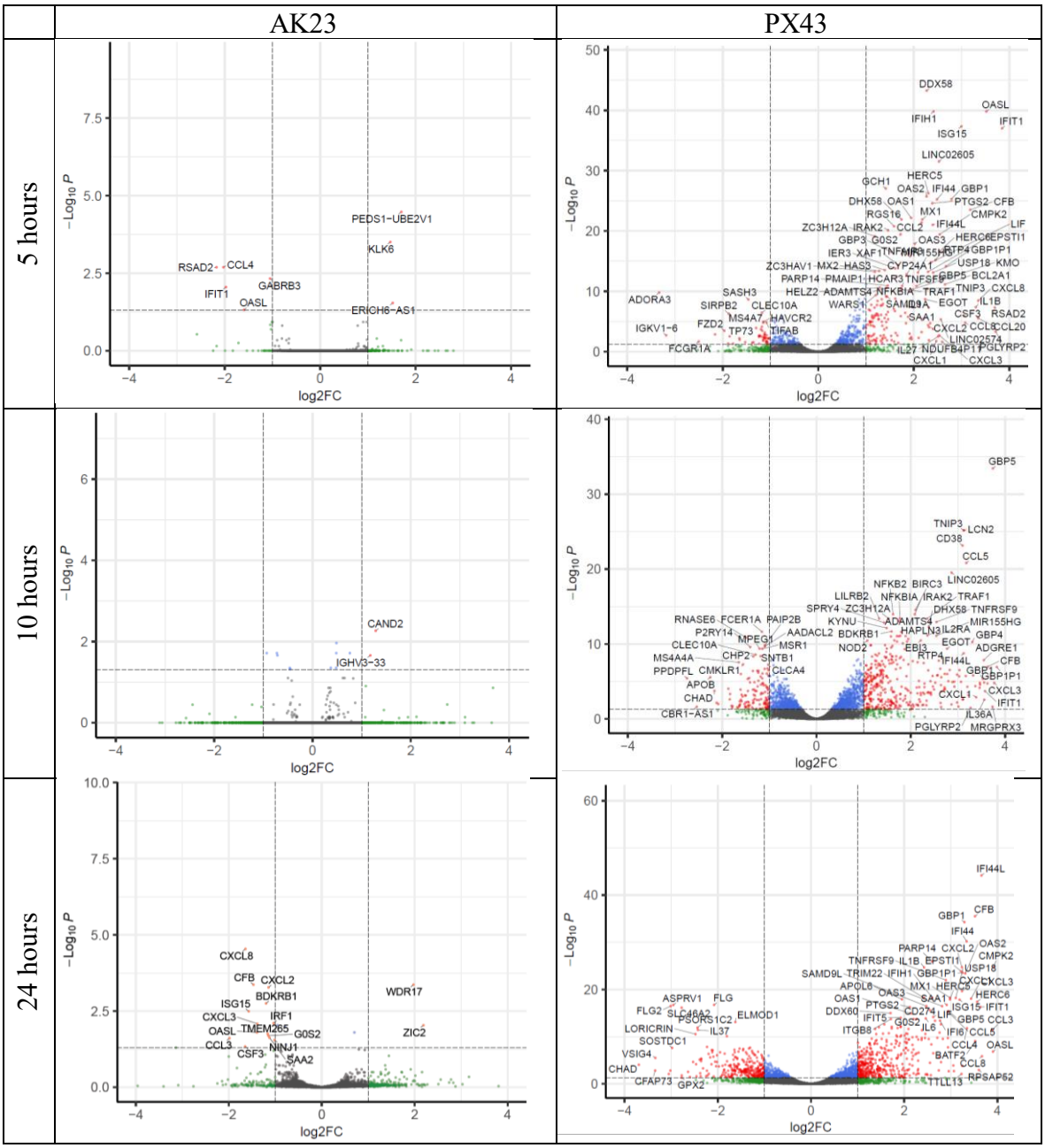

Figure 6.7.: More differentially regulated genes are significantly up- and downregulated after the injection of PX43 than after the injection of AK23. On the left side, volcano plots of human skin organ culture (HSOC) model injected with AK23 compared to murine immunoglobulin G after 5 (total numbers of variables: 17,172), 10 (total number of variables: 23,217), and 24 hours (total number of variables: 22,808) (from top to bottom). On the right side, volcano plots of HSOC model injected with PX43 compared to human immunoglobulin G after 5 (total numbers of variables: 23,489), 10 (total number of variables: 22,988), and 24 hours (total number of variables: 23,013) (from top to bottom). n (biological) = 6. Color code: grey = not significant, green = Log_2 fold change, blue = p value < 0.05, red = p value < 0.05 and Log_2 fold change. Statistical test = Likelihood-ratio test (LRT) from deseq2. n (biological) = 6.

Looking at the heatmaps (**Figure 6.8.**), for all skin samples injected with PX43 the same pathways are upregulated and that there is a clear difference between the injection with the scFv and hIgG. Most notably, chemokines and molecules belonging to the inflammatory pathways are upregulated in PX43 injected skin, while these are downregulated in hIgG injected skin samples. There are also two skin donors which show a higher upregulation in chemokines after 5 and 10 hours compared to the other four skin donors, while a third donor shows a higher upregulation compared to the other five after 24 hours.
Looking at the enrichment plots for AK23 (**Figure 6.9.**), after 5 hours the most enriched pathways include those affecting the ribosome, eukaryotic translation elongation, selenoamino acid metabolism, eukaryotic translation initiation, cellular response to starvation, and DNA methylation. After 10 hours, the negatively enriched pathways are interferon γ and α response, as well as TNFα signaling via NFκB, and the inflammatory response in general; positively enriched pathways are CD22 mediated BCR regulation, FCGR activation, initial triggering of complement, and FCGR3A mediated IL10 synthesis. Looking at 24 hours after AK23 injection, there are only negatively enriched pathways detectable involved in translation, ribosome, selenoamino acid metabolism, and oxidative phosphorylation.

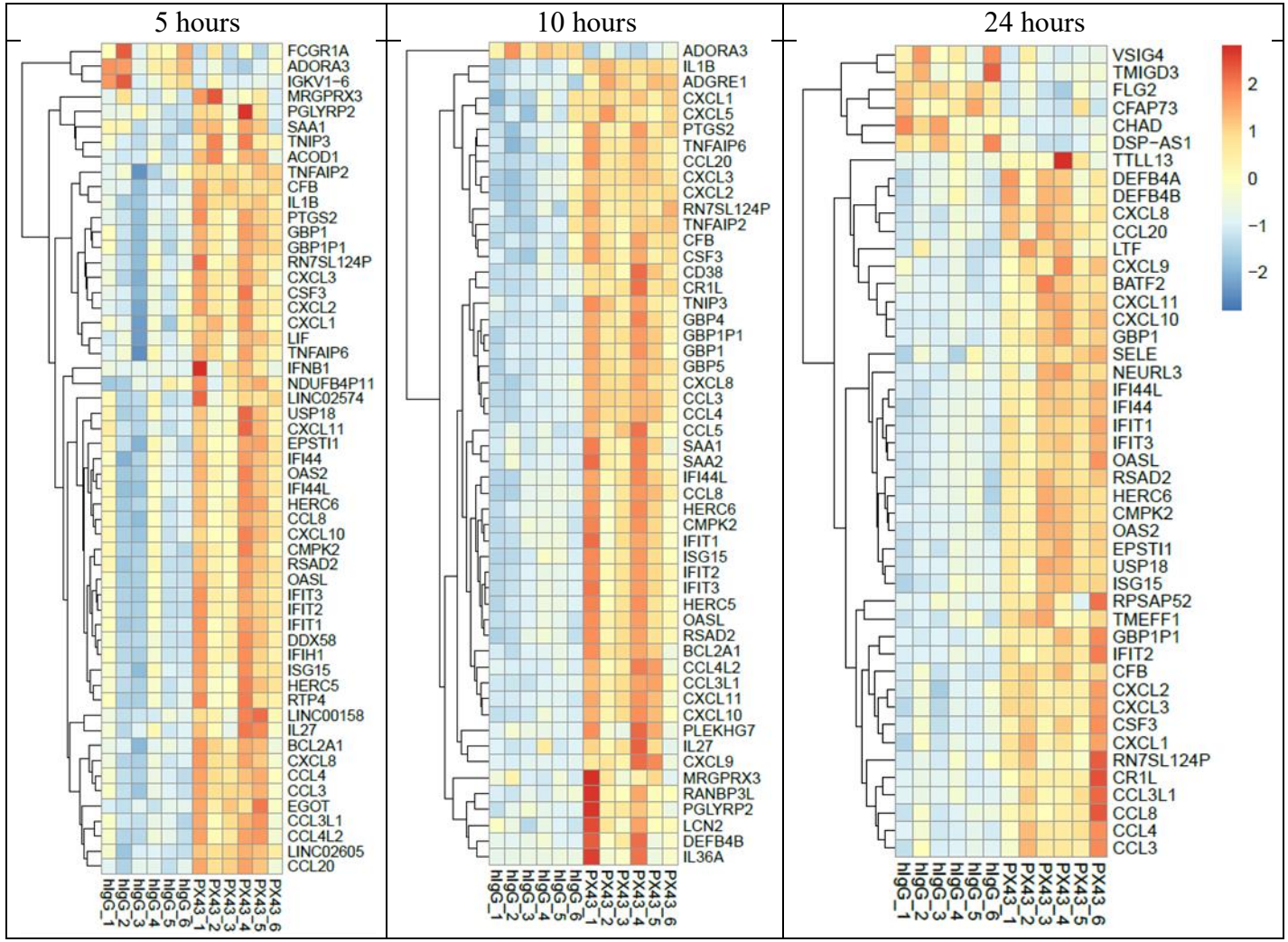

Figure 6.8.: Many chemokines are upregulated in the human skin organ culture model for pemphigus vulgaris after injection of PX43. Heat maps of the human skin organ culture (HSOC) model injected with PX43 and hIgG after 5, 10, and 24 hours showing up- (red) and downregulated (blue) genes. Statistical test = Likelihood-ratio test (LRT) from deseq2. n (biological) = 6.

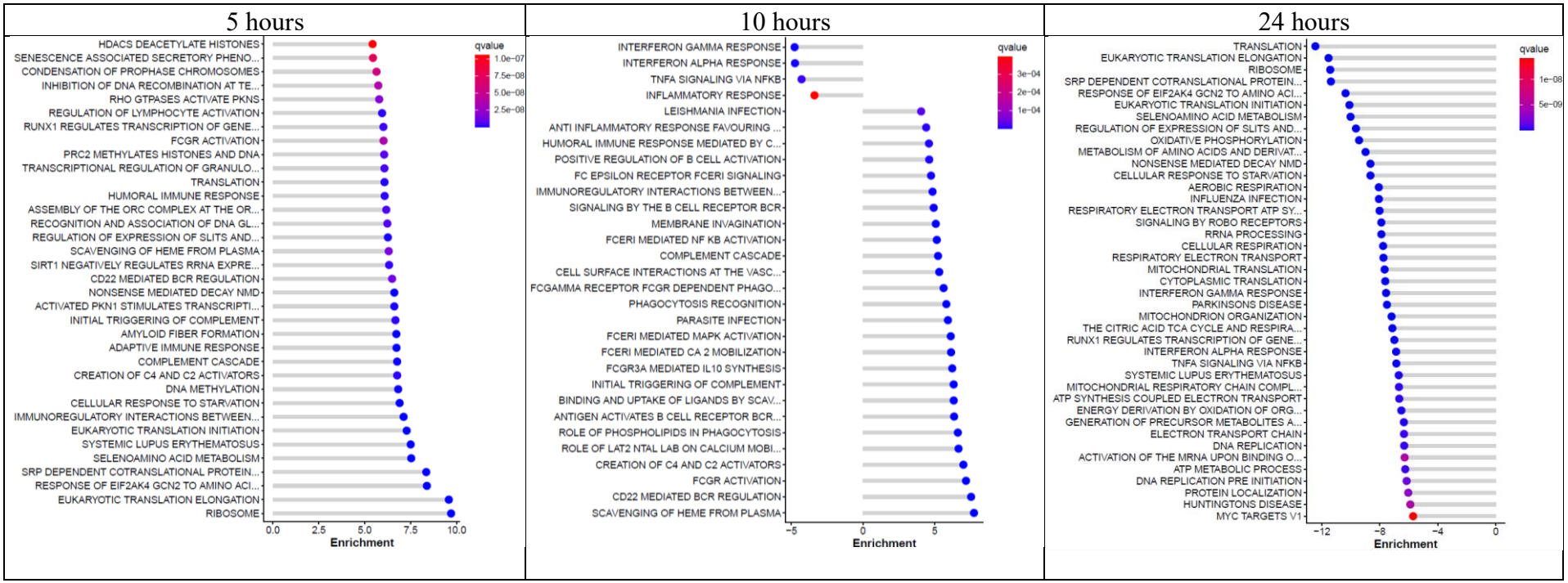

Figure 6.9.: After injection with AK23 in the human skin organ culture model for pemphigus vulgaris, unspecific pathways are initially upregulated but are downregulated after 24 hours. Enrichment plots of the human skin organ culture model injected with AK23 in comparison to murine immunoglobulin G as control. Statistical test = two sample t-test for differentially expressed genes (DEGs), and then summarization meta-test to get the p values for gene sets represented in the enrichment plots. n (biological) = 6.

In contrast to this, the enrichment plots for the HSOC model with PX43 (**Figure 6.10.**), show negatively and positively enriched pathways throughout all incubation times. After 5 hours, negatively enriched pathways include the creation of C4 and C2 activators, CD22 mediated BCR regulation, FCGR activation, and the initial triggering of complement. Looking at the positively enriched pathways, there are TNFα signalling via NFκB, interferon α and γ response, and the signalling by interleukins. After 10 hours, negatively enriched pathways include activated PKN1 simulated transcription, DNA methylation, condensation of prophase chromosomes, and HDACS deacylated histones. Again, positively enriched are TNFα signalling via NFκB, interferon α and γ response, and the signalling by interleukins. Finally, after 24 hours, the enriched pathways have only changed a little and the ones already positively and negatively enriched after 10 hours are enriched here in the same manner.
Looking at the pathway responsive genes for activity interference (PROGENy), it is evident that the injection of AK23 in the HSOC model does not lead to a specific response in the basal keratinocytes throughout all skin samples at all time points (**Figure 6.11.**). After 5 hours incubation with AK23, one sample shows downregulation in the genes involved in androgen, epidermal growth factor (EGFR), estrogen, hypoxia, janus kinase – signal transducers, and activators of transcription (JAK-STAT), mitogen activated protein kinase (MAPK), nuclear factor kappa B (NFκB), p53, transforming growth factor B (TGFb), tumor necrosis factor alpha (TNFα), and Wnt. On the other hand side, there is one skin sample showing an upregulation in these genes, with p53 being the exception, while all other samples give rather mixed results. Same can be seen for the other incubation times of 10 and 24 hours, there is no pathway specifically responsive after AK23 stimulation. In contrast, for basal keratinocytes isolated from skin samples injected with PX43, NFκB and TNFα are upregulated throughout all samples and after all incubation times (**Figure 6.12.**). Except for two samples, PI3K and JAK-STAT are upregulated at all time points. p53 is mostly downregulated or not changed at all in regulation, while the Wnt pathway does not show a specific response to the injection of PX43 as well.
Taken together, the analysis of the transcriptome does not show an up- or downregulation of one specific signalling pathway but rather unspecific inflammatory responses to the binding of PX43 to Dsg1/3 and no specific response at all to the injection with AK23 and its binding to Dsg3.

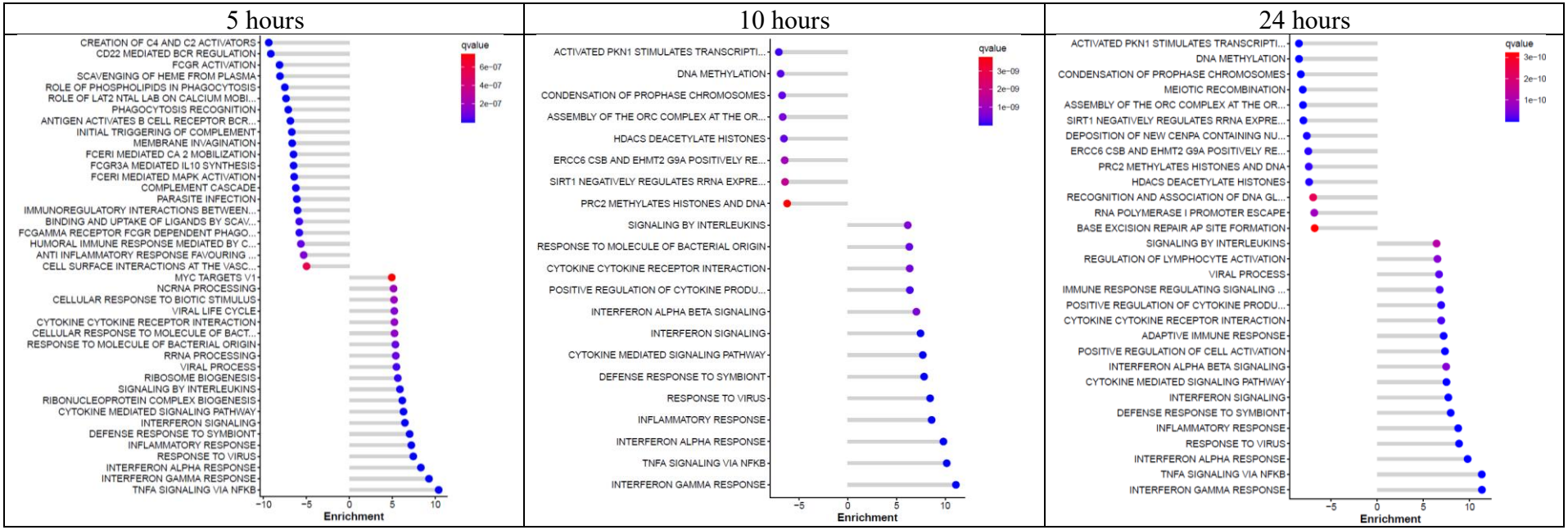

Figure 6.10.: Interferon signalling is upregulated in the human skin organ culture model for pemphigus vulgaris after injection of PX43 after 5, 10, and 24 hours. Enrichment plots of the human skin organ culture model injected with PX43 in comparison to human immunoglobulin G as control. Statistical test = two sample t-test for differentially expressed genes (DEGs), and then summarization meta-test to get the p values for gene sets represented in the enrichment plots. n (biological) = 6.

	PROGENy	Transcription factor activity
5 hours	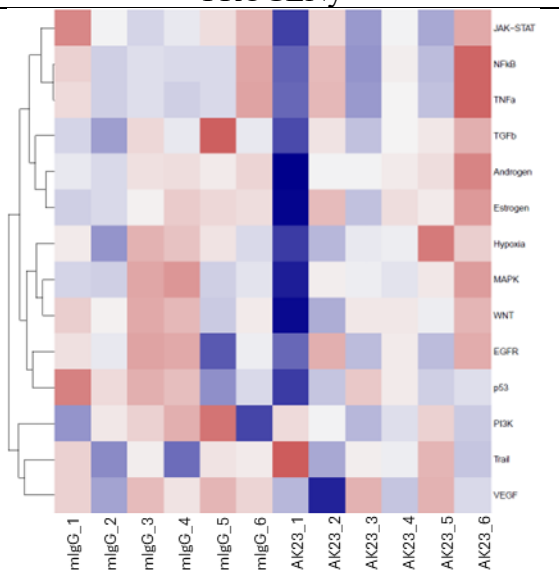	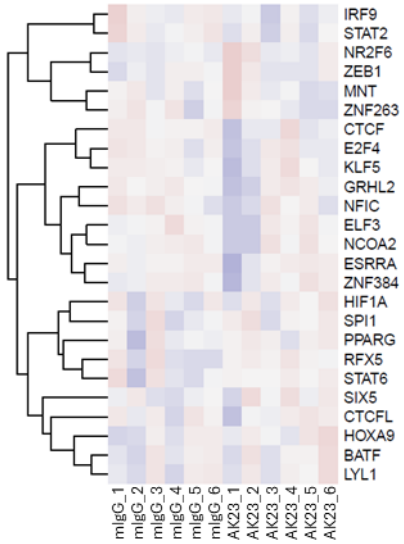
10 hours	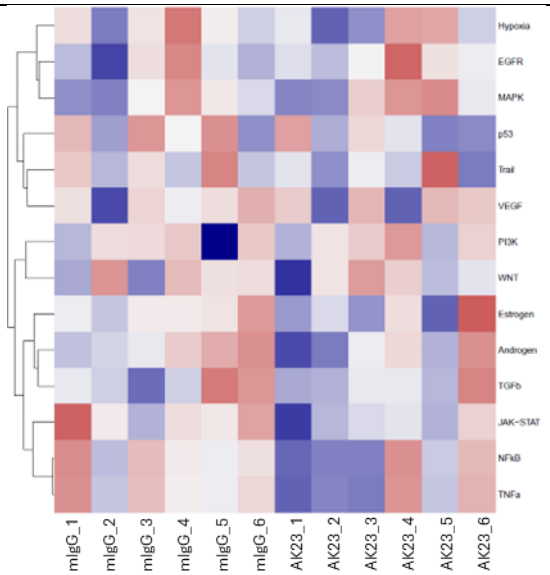	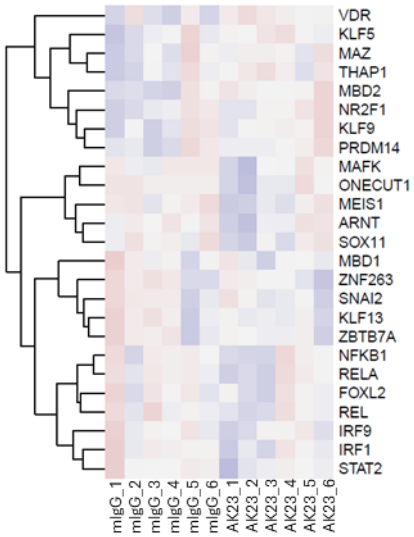
24 hours	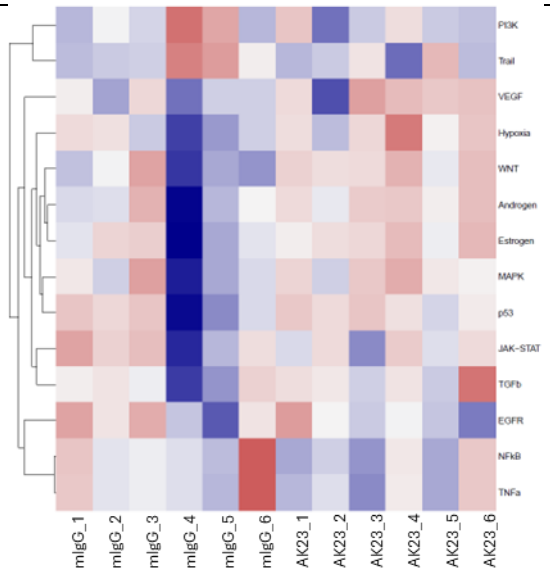	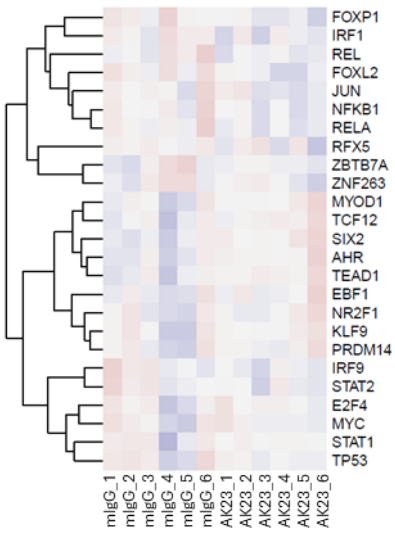

Figure 6.11.: There is no specific pathway up- or downregulated after injection of AK23 into the human skin organ culture model for pemphigus vulgaris. Pathway responsive genes for activity inference (PROGENy) (left column) and transcription factor activities plots (right column) from skin samples from the human skin organ culture (HSOC) model injected with AK23 and murine immunoglobulin G (mIgG) after for 5, 10, and 24 hours incubation. PROGENy plot depicts the up- (red) and downregulation (blue) of the depicted pathways. The transcription factors depicted on the right are part of these pathways, respectively. Statistical test (PROGENy) = linear regression model to fit genes responsive to all pathways simultaneously obtaining the z-coefficients matrix. Statistical test (transcription factor activity) = multivariate linear model. n (biological) = 6.

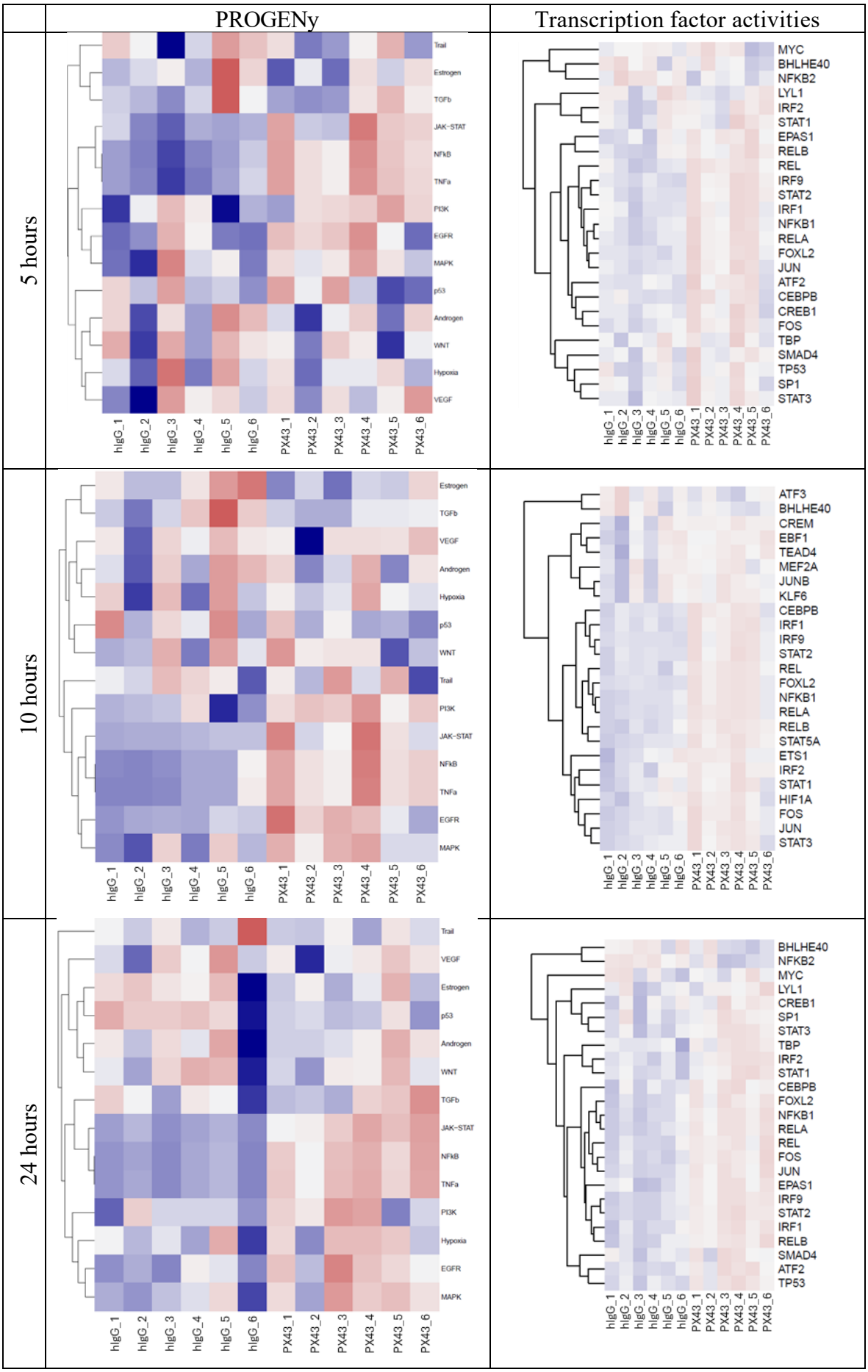
PROGENy
Transcription factor activities
5 hours
10 hours
24 hours
Trail
Estrogen
TGFb
JAK-STAT
NFkB
TNFa
PI3K
EGFR
MAPK
p53
Androgen
WNT
Hypoxia
VEGF
MYC
BHLHE40
NFKB2
LYL1
IRF2
STAT1
EPAS1
RELB
REL
IRF9
STAT2
IRF1
NFKB1
RELA
FOXL2
JUN
ATF2
CEBPB
CREB1
FOS
TBP
SMAD4
TP53
SP1
STAT3
ATF3
CREM
EBF1
TEAD4
MEF2A
JUNB
KLF6
STAT5A
ETS1
HIF1A
hIgG_1
hIgG_2
hIgG_3
hIgG_4
hIgG_5
hIgG_6
PX43_1
PX43_2
PX43_3
PX43_4
PX43_5
PX43_6

Figure 6.12.: NFκB, TNFα, JAK-STAT and PI3K are upregulated in the human skin organ culture model for pemphigus vulgaris after injection of PX43 after 5, 10, and 24 hours of incubation. Pathway responsive genes for activity inference (PROGENy) and transcription factor activities plots from skin samples from the human skin organ culture (HSOC) model injected with PX43 and human immunoglobulin G (hIgG) after for 5, 10, and 24 hours of incubation. PROGENy plot depicts the up- (red) and downregulation (blue) of the depicted pathways. The transcription factors depicted on the right are part of these pathways, respectively. Statistical test (PROGENy) = linear regression model to fit genes responsive to all pathways simultaneously obtaining the z-coefficients matrix. Statistical test (transcription factor activity) = multivariate linear model. n (biological) = 6.

6.3 Shotgun proteome analysis confirms the transcriptome findings of the human skin organ culture model for pemphigus vulgaris

For the analysis of the proteome, skin samples from the HSOC model for PV incubated for 24 hours with either hIgG or PX43 as well as the T0 were used. After the microdissection of the basal keratinocytes, the proteins of the TritonX-soluble fraction were assessed quantitively and qualitatively. As for the transcriptome analysis, the effect of endotoxins was excluded via GSVA-based analysis.
The quality of the isolated proteins was tested by Western blot where β-actin was used as a loading control, while γ-catenin (also known as plakoglobin) was used as a control for protein degradation. As it can be seen in **Figure 6.13.**, plakoglobin is degraded by an estimate of 70 - 80 %, while β-actin is present in all loaded samples.

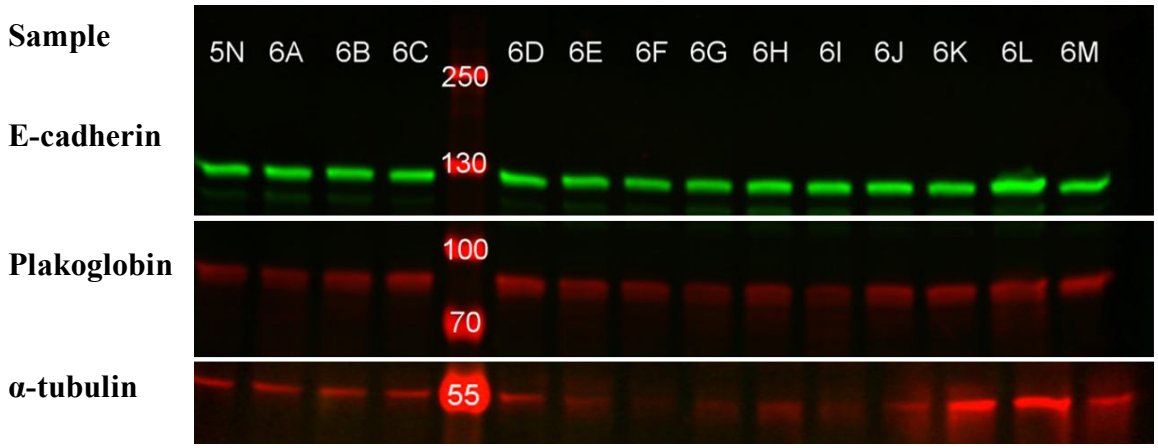

Figure 6.13.: There is only minimal degradation of plakoglobin visible on the Western blot of the TritonX-soluble protein fraction. Western blot of one human skin organ culture model injected with either PX43 / human immunoglobulin G and incubated for 1, 5, 10, and 24 hours (5N, 6A to 6C / 6D to 6G) or AK23 and incubated for 1, 5, 10, and 24 hours (6H to 6K) / murine immunoglobulin G for 1 and 5 hours (6L and 6M). Numbers are representing the molecular weight in kilo Dalton.

For the shotgun proteome analysis, it was decided to analyse the samples from five skin donors those skin was injected with 85 µg of PX43 and 85 µg of hIgG incubated for 24 hours. Additionally, the T0 was also analysed as a baseline to be compared to the other two conditions.
The biological differences of the PX43 and hIgG injected samples are only minimal, same for the difference between the samples incubated for 24 hours compared to T0 (**Figure 6.14.a**). PX43 and hIgG injected samples are clustering together and are distinct from T0, but these differences are only minimal. Although the biological differences are only small according to the PCA plot, phenotypically, the split formation caused by PX43 can be seen in the H&E-stained paraffin sections (**Figure 6.14.b**). Compared to this, hIgG injected skin samples after 24 hours incubation and T0 skin samples show no split formation.

(a)

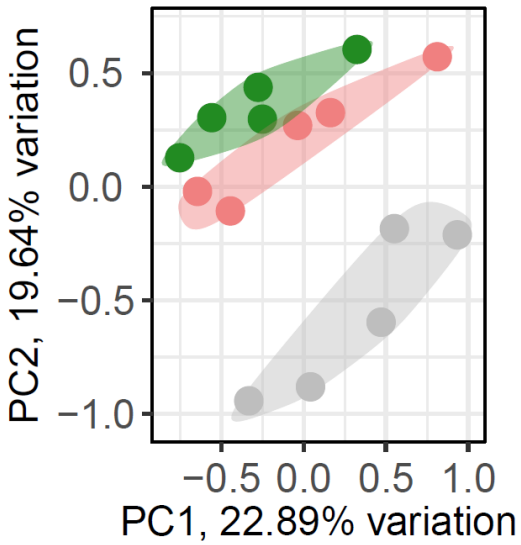

(b)

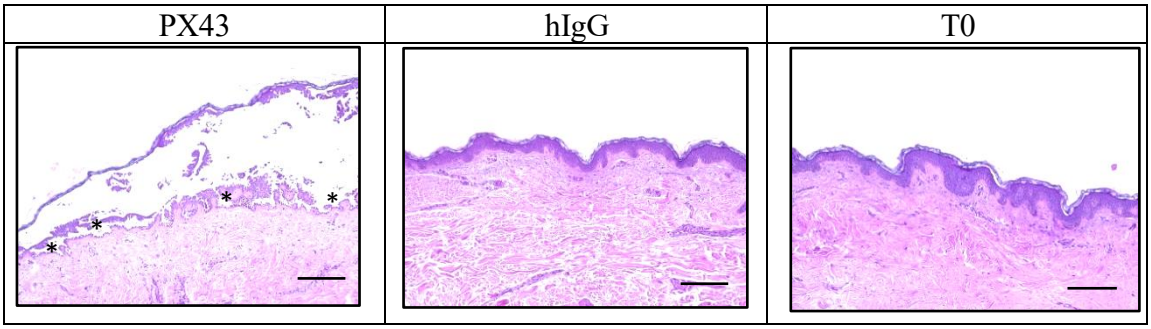

Figure 6.14.: After 24 hours, there are only minimal differences between skin samples injected with PX43 compared to samples injected with human immunoglobulin G and compared to T0. (a) Principal component analysis (PCA) plot of the human skin organ culture (HSOC) model injected with PX43 (green) and human immunoglobulin G (hIgG) (red) after 24 hours of incubation, as well as time point zero (T0) (grey) with corresponding exemplary pictures **(b)** of PX43 injected skin. * = split formation. Scale bars = 100 µm.

Looking at the heat map comparing skin after the injection of PX43 or hIgG after 24 hours incubation, APOA4, DSC1, and DSC3 are downregulated in basal keratinocytes after PX43 injection, while these are upregulated in skin injected with hIgG (**Figure 6.15.a**). Upregulated proteins after the injection of PX43 include NAMPT, S100A8, S100A9, CDH3, CYP51A1, NFκB2, SERPINB4, SOD2, and TNFαIP2, which are all downregulated after hIgG injection. When comparing the enriched pathways, negatively enriched pathways are coagulation and mesenchymal transition, while positively enriched pathways are oxidative phosphorylation, mTORC1 signaling, Myc targets V1, interferon γ response, and TNFα signaling via NFκB (**Figure 6.15.b**). Looking at the scores for up- and downregulated proteins, when comparing PX43 to hIgG treated basal keratinocytes from the HSOC model, SRF, SMAD3, and FLI1 are the most downregulated ones, while HIF1A, ONECUT1, and CEBPE are the most upregulated ones (**Figure 6.15.c**).
When comparing basal keratinocytes from skin injected with PX43 and incubated for 24 hours to skin from T0, APOC3, IL37, F9, SERPINF2, and LGMN are downregulated after PX43 treatment, while those are upregulated in basal keratinocytes from T0 (**Figure 6.16.a**). Most of the proteins which are upregulated when PX43 injected skin is compared to hIgG injected skin, are also upregulated when comparing PX43 to T0; additionally, several keratins (KRT) are upregulated, too. Looking at the enrichment plot (**Figure 6.16.b**), coagulation proteins are negatively enriched, while Myc target V1 and TNFα signalling via NFκB are positively enriched. Scoring the proteins (**Figure 6.16.c**) shows that DBP, TBX21, and NR0B1 are downregulated, while HIF1A, ONECUT1, and CEBPE are upregulated.
Overall, it can be said that the data gathered by the shotgun proteomics is complementing the data gathered by RNA sequencing.

(a)

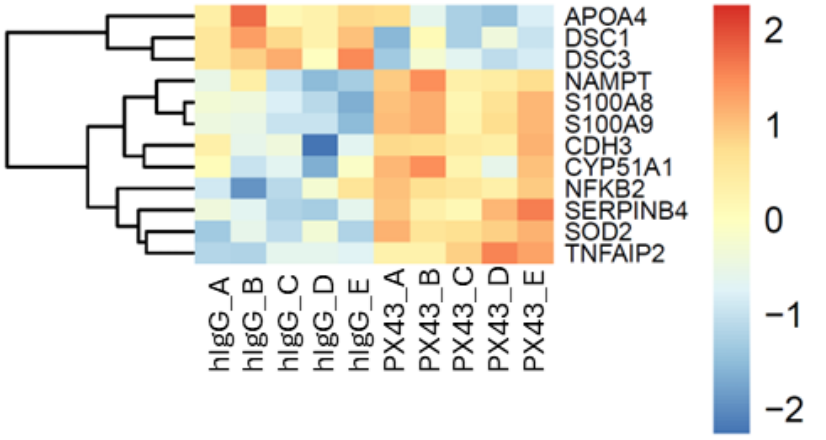
APOA4
DSC1
DSC3
NAMPT
S100A8
S100A9
CDH3
CYP51A1
NFKB2
SERPINB4
SOD2
TNFAIP2
hIgG_A
hIgG_B
hIgG_C
hIgG_D
hIgG_E
PX43_A
PX43_B
PX43_C
PX43_D
PX43_E
2
1
0
−1
−2

(b)

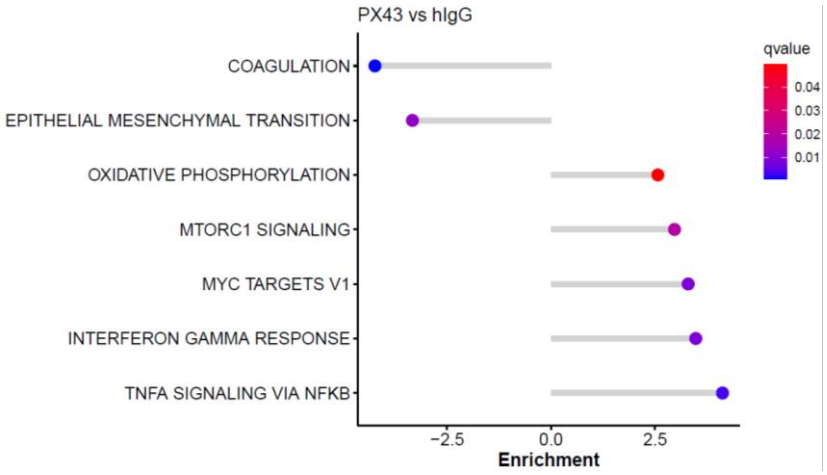
PX43 vs hIgG
COAGULATION
EPITHELIAL MESENCHYMAL TRANSITION
OXIDATIVE PHOSPHORYLATION
MTORC1 SIGNALING
MYC TARGETS V1
INTERFERON GAMMA RESPONSE
TNFA SIGNALING VIA NFKB
−2.5
0.0
2.5
Enrichment
qvalue
0.04
0.03
0.02
0.01

(c)

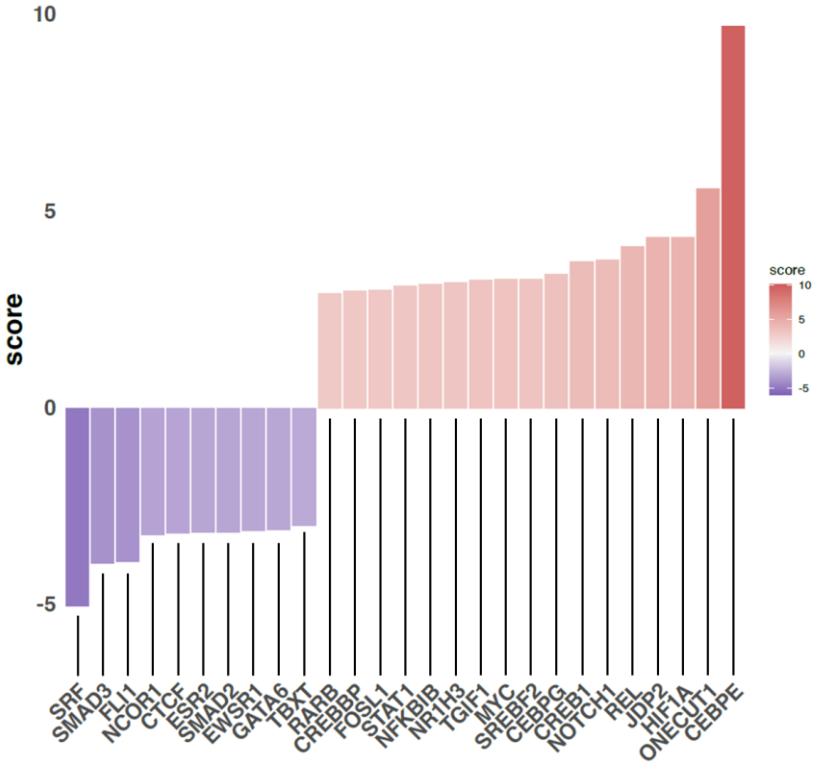
score
10
5
0
-5
SRF
SMAD3
FLI1
NCOR1
CTCF
ESR2
SMAD2
EWSR1
GATA6
TBXT
RARB
CREBBP
FOSL1
STAT1
NFKBIB
NR1H3
TGIF1
MYC
SREBF2
CEBPG
CREB1
NOTCH1
REL
JDP2
HIF1A
ONECUT1
CEBPE

Figure 6.15.: After 24 hours, inflammatory pathways are upregulated in the human skin organ culture model for pemphigus vulgaris. (a) Heat map showing of the up- (red) and downregulated (blue) proteins in the human skin organ culture (HSOC) model 24 hours after injection with PX43 and human immunoglobulin G (hIgG). **(b)** Enrichment plot of significantly up- (to the right) and downregulated (to the left) pathways according to the protein expression in the HSOC model injected with PX43 compared to hIgG. **(c)** Scores for up- (red) and downregulated (violet) proteins in the HSOC model injected with PX43 compared to hIgG. Statistical test = transcription factors inferred by multivariate linear model from decoupleR. n (biological) = 5.

(a)

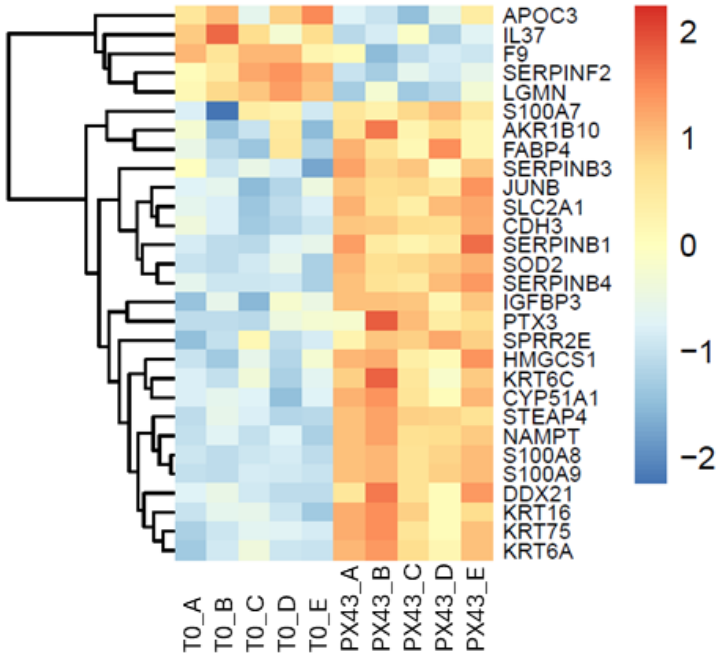
APOC3
IL37
F9
SERPINF2
LGMN
S100A7
AKR1B10
FABP4
SERPINB3
JUNB
SLC2A1
CDH3
SERPINB1
SOD2
SERPINB4
IGFBP3
PTX3
SPRR2E
HMGCS1
KRT6C
CYP51A1
STEAP4
NAMPT
S100A8
S100A9
DDX21
KRT16
KRT75
KRT6A
2
1
0
−1
−2
T0_A
T0_B
T0_C
T0_D
T0_E
PX43_A
PX43_B
PX43_C
PX43_D
PX43_E

(b)

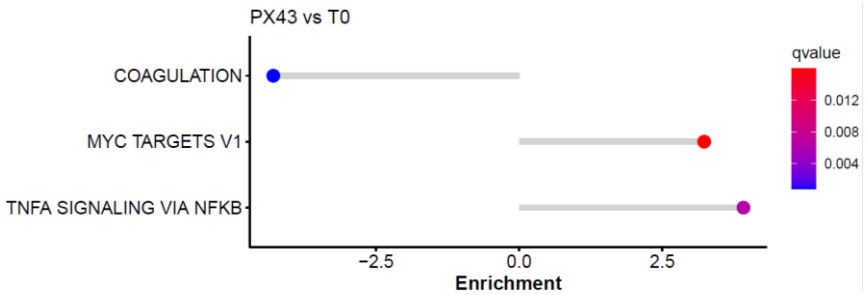
PX43 vs T0
COAGULATION
MYC TARGETS V1
TNFA SIGNALING VIA NFKB
−2.5
0.0
2.5
Enrichment
qvalue
0.012
0.008
0.004

(c)

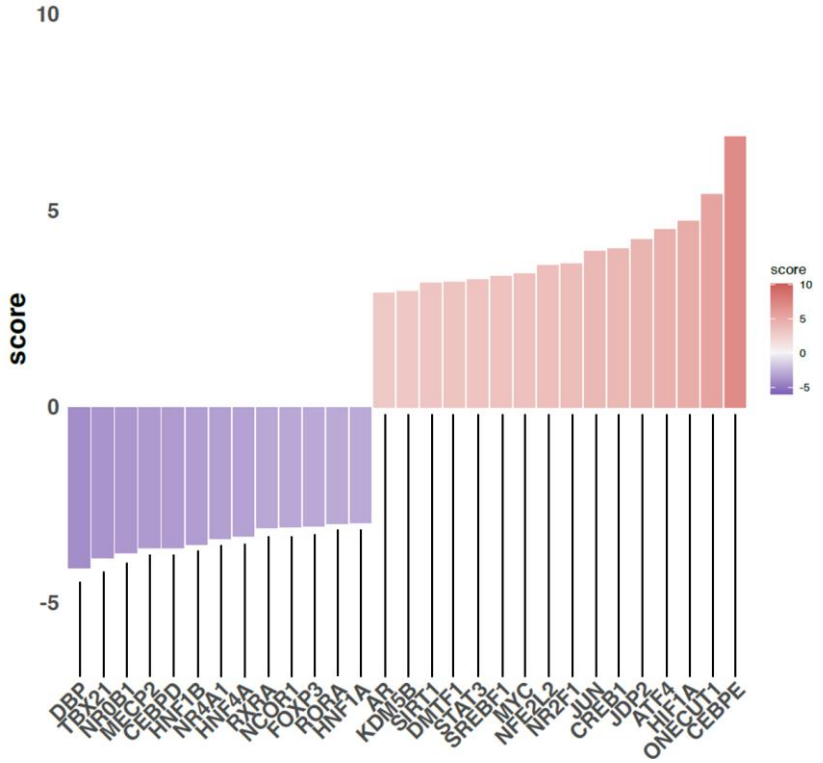
10
5
0
-5
score
score
10
5
0
-5
DBP
TBX21
NR0B1
MECP2
CEBPD
HNF1B
NR4A1
HNF4A
RXRA
NCOR1
FOXO3
RORA
HNF1A
AR
KDM5B
SIRT1
DMTF1
STAT3
SREBF1
MYC
NFE2L2
NR2F1
JUN
CREB1
JDP2
ATF4
HIF1A
ONECUT1
CEBPE

Figure 6.16.: After 24 hours, inflammatory pathways are upregulated in the human skin organ culture model for pemphigus vulgaris compared to T0. (a) Heat map showing of the up- (red) and downregulated (blue) proteins in the human skin organ culture (HSOC) models 24 hours after incubation with PX43 for 24 hours and time point zero (T0). **(b)** Enrichment plot of significantly up- (to the right) and downregulated (to the left) pathways according to the protein expression in the HSOC model incubated with PX43 for 24 hours compared to T0. **(c)** Scores for up- (red) and downregulated (violet) proteins in the HSOC model incubated with PX43 for 24 hours compared to T0. Statistical test = transcription factors inferred by multivariate linear model from decoupleR. n (biological) = 5.

6.4 PX43 binds to desmoglein 1 and desmoglein 3 in the human skin and causes a split in the epidermis

The quality of the HSOC model for PV was checked by staining for three different molecules. The binding of PX43 to Dsg1/3 is visualised with the direct immunofluorescence targeting the HA-tag of the PX43, staining the bound scFv in red (**Figure 6.17.**). PX43 can be seen to be present in the split regions as well as outside of the split, having bound to its target.
Dsg1/3 can be visualized simultaneously on the same tissue cut, showing Dsg1 in red while Dsg3 is stained in green (**Figure 6.18.**). As it can be seen, Dsg3 is present throughout all epidermal layers, while Dsg1 is present in the upper epidermal layers.

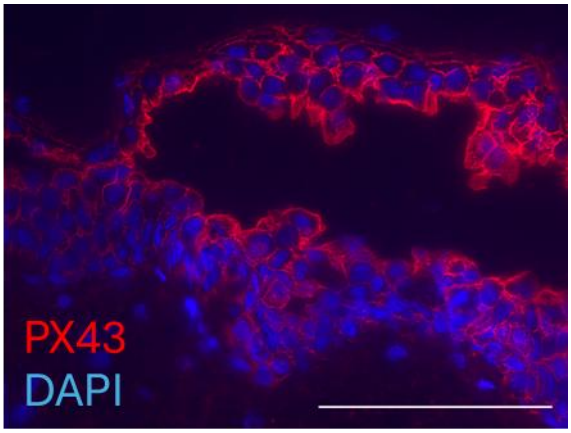

Figure 6.17.: PX43 binds to desmoglein 1 and 3 in the epidermis. Direct immunofluorescence staining of PX43 using a secondary antibody directed against the hemagglutinin-tag attached to single chain variable fragment and final visualization with a tertiary antibody with a red fluorophore directed against the secondary. In blue, the nuclei of the cells are stained with 4′,6-diamidino-2-phenylindole (DAPI). Scale bar = 100 µm.

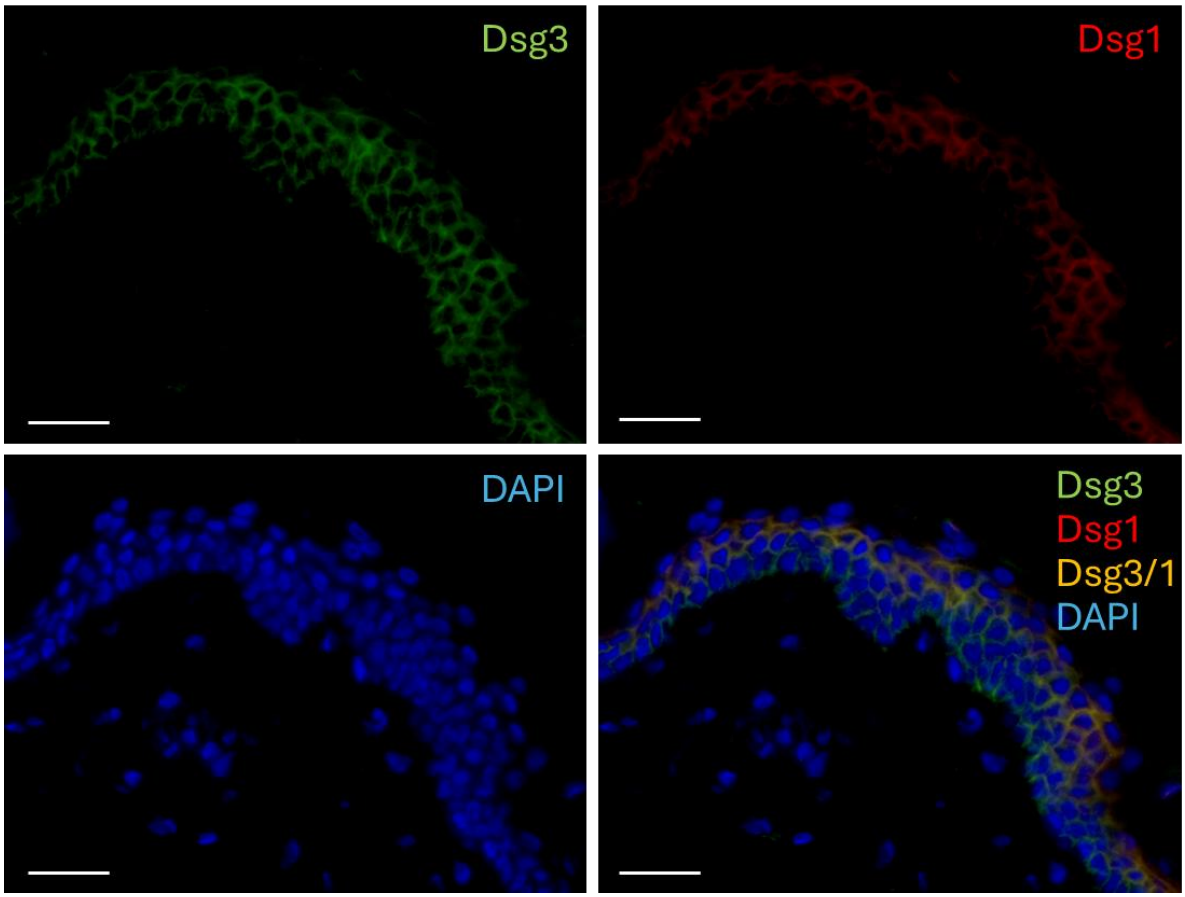

Figure 6.18.: Desmoglein 1 can be found in the upper parts of the epidermis, while desmoglein 3 is expressed throughout all epidermal layers. Immunofluorescence of desmoglein 1 (Dsg1) in red and desmoglein 3 (Dsg3) in green. In blue, the nuclei of the cells are stained with 4′,6-diamidino-2-phenylindole (DAPI). Scale bar = 50 µm.

7 Discussion

7.1 Titration of AK23

PX43 is a well characterized and established scFv for the HSOC model for PV since 2019 (Burmester *et al.* 2019), which allows for high reproducibility of the performed experiments. The pathogenic murine antibody AK23 is well characterized, too, causing blister formation in the mouse model for PV after Dsg3 immunization [Amagai *et al.* 2022]. In the HSOC model for PV, AK23 on its own cannot cause a split due to the compensatory function of Dsg1, while PX43 alone causes a split by binding Dsg3/1. For this reason, after titration of AK23 causing a similar amount of fragmentation compared to PX43 in cell culture, AK23 was injected together with 0.08 µg of ETA, a subclinical dose of ETA preventing Dsg1 to compensate for Dsg3 (Emtenani *et al.* 2021).
The titration of AK23 showed at 20 µg/mL the highest fragmentation in HaCaTs and pHPEKs, while PX43 requires a 2.5 higher concentration (50 µg/mL). This factor was applied to calculate the amount of AK23 for the HSOC model, giving a final amount of 34 µg of AK23 binding to its target in the same manner as 85 µg of PX43. In contrast, in an organ model for PV using mucosa from healthy volunteers, 200 µg of AK23 are injected into the specimens to induce split formation (D. T. Egu *et al.* 2020). Of course, it is important to distinguish between mucosa, skin, and a simple monolayer of keratinocytes in a culture dish. It could be that the mucosa requires a higher amount of AK23 injected than the skin to show split formation. This could be analysed further by quantitative staining of Dsg3 in the mucosa and skin. Additionally, the mucosa organ culture for PV and the HSOC model for PV should be run in parallel to determine more precisely the appropriate amount of AK23 for both organs. This could be done for PX43 as well.
As it is evident by the titration, 20 µg/mL and 50 µg/mL are the highest usable concentrations of AK23 and PX43, respectively, to yield the highest fragmentation rate in keratinocytes. This is explained by the prozone effect describing the observation that an increase in the number of antibodies binding to its antigen does not always result in a higher number of bound antigen (Roy, Rosenmund, and Stefan 2017). This might be the explanation why an increase in the concentration of PX43 and AK23 in the KDA did not result in a higher amount of fragmentation in higher concentrations.
HaCaTs and pHPEKs were both used to titrate AK23 and PX43. Using HaCaTs for the first attempt of titration has several advantages: Since these cells are already immortalized, they are easy to handle and can generate reproducible results. Primary keratinocytes were used to confirm the results of the KDA using HaCaTs. The pHPEKs derive from three pooled donors, allowing an increased comparability and reproducibility of the experiment. The second reason to use pHPEKs is that these cells are due to their primary nature more natural and physiological and therefore closer to the skin organ culture than immortalized keratinocytes (Schmidt *et al.* 2022).

7.2 No increase in number of proliferative cells in the human skin organ culture model for pemphigus vulgaris

It was shown for skin biopsies of PV patients (Williamson *et al.* 2006), canines with PV (Williamson, Suter, *et al.* 2007), and of PV mouse models (Merritt *et al.* 2002, Schulze *et al.* 2012) that there is an increase in the number of proliferative cells compared to healthy biopsies. For this reason, the tissue cuts from three HSOC models were stained for Ki-67+ cells. According to the results, no difference between AK23 and mIgG could be seen 5 h, 10 h, and 24 h after injection, which is also true for PX43 compared to hIgG after 24 hours.
Since the skin of PV patients has to deal with the binding of the autoantibodies for longer than the skin of the HSOC model, it is possible that these proliferative changes in the skin cannot be analysed in a time frame of 24 hours. Further studies for the long term effect (in contrast to the initial events taking place after binding of the autoantibody) could be studied in future experiments, since it is possible to cultivate the skin for up to sixteen days under standard cell culture conditions (Lu *et al*. 2007).
In contrast to proliferation, other studies have focussed on the opposite of proliferation, namely apoptosis. In these studies, it was shown that the incubation of HaCaTs with PV-IgG from patients leads to an increase in apoptosis (Puviani *et al.* 2003, X. Wang *et al*. 2004, Pelacho *et al*. 2004). Future studies and experimental assays for the HSOC model could include analysis of apoptosis and pre-apoptotic stages of the keratinocytes. This staining could be used to assess the spatial arrangement of apoptotic and proliferative cells. The knowledge about the spatial location of these keratinocytes could help in the establishment of therapies supporting proliferative pathways and inhibiting apoptotic pathways.

7.3 Transcriptomic analysis

Until today, transcriptomic analysis in PV research has mainly focused on either the immune cells leading to the disease rather than the keratinocytes which are affected by the production of autoantibodies (Duan *et al.* 2024, Z. Hu *et al.* 2024, Huang *et al.* 2022, Kalantari-Dehaghi *et al.* 2013) or transcriptome analysis of keratinocytes grown in cell culture conditions and then treated with PV-IgG or monoclonal antibodies targeting Dsg3 alone or both Dsg3/1 (Nguyen *et al.* 2004, Mao *et al.* 2017, Alabeedi 2024, Franz *et al.* 2024). In this regard, the experiments performed here aimed to fill this gap in research, revealing the mechanism that leads to acantholysis caused by the binding of autoantibodies to Dsg3/1.

The biological differences between basal keratinocytes treated with AK23 and mIgG are minimal throughout all time points, suggesting that the binding of AK23 to Dsg3 does not induce significant changes on the transcription level of the cells. This can also be seen in the phenotype of the skin sections: AK23 does not cause changes in the epidermal layer on a microscopic level and is essentially indistinguishable from skin injected with mIgG. It was shown that AK23 is able to induce widening between the keratinocytes in human skin (D. T. Egu *et al.* 2017), but there are substantial differences between these two experiments: While the skin utilized in this work comes from plastic surgery within 16 hours, Egu *et al.* used skin from human cadavers within 24 hours after the donor's death. Additionally, the concentration of the AK23 used for the HSOC model from Egu *et al.* is more than 5 times higher and they applied mechanical stress in the from of a rubber head inducing friction onto the skin. Still, even this combination is not inducing a split after AK23 incubation for 24 hours. This is in contrast to the neonatal mouse model using Balb/c mice which were injected with AK23 and shear-stress was induced to their skin (Spindler *et al.* 2013). The combination of antibody and shear-stress resulted in blistering of the murine skin, pointing at species-specific differences between murine and human Dsg3 expression (D. T. Egu *et al.* 2017).

The opposite is true for PX43 and hIgG injected skin. On a microscopic level, the split caused by PX43 binding to Dsg3/1 is a change in the phenotype of the basal cells which lose the contact to their neighbouring cells, leading to a distinct separation in the PCA plot from skin treated with hIgG.

As it is evident for skin injected with AK23 and mIgG, none of the named pathways is responsive in a significant way. This lack of a response on the transcriptomic level can be explained looking at the HE-stained skin sections: There is phenotypically no difference between skin injected with AK23 and its corresponding control. Throughout all time points, AK23 cannot cause a split on its own since in the HSOC model since the epidermal Dsg1 can compensate for the loss of function of Dsg3 (Hammers and Stanley 2020). This results in perfectly intact skin by keratinocytes still holding together and therefore do not have any reason to show any specific response to the malfunction of Dsg3 caused by AK23. The upregulated genes appear to be rather random, being involved in autophagy and metastatis, but other upregulated genes are involved in cytokine signaling and IFN pathways (like OASL, CCLs and CXCLs). This may be an indicator that the keratinocytes do recognize the impaired function of Dsg3 and are indeed reacting to it, but in a rather unspecific way.

On the other hand, PX43 binds both Dsgs, causing cells to lose their contact to their neighbours and sending stress signals, in this case via NFκB, TNFα, and JAK-STAT pathways. More specifically, STAT1, STAT2, and STAT3 are upregulated throughout all time points. STAT1 is usually activated by IFN, but can also be activated by IL-2, -6 and epidermal growth factor (EGF). This results in either an upregulation in the kinase inhibitors P21 and P27 or the inhibition of c-myc (X. Hu *et al.* 2021). Looking at the data from the HSOC model for PV, the upregulation of P21 and P27 was not detected. Myc is detected in the basal keratinocytes but while it is upregulated in one half of the samples, it is downregulated in the other half, making it hard to draw a final conclusion on the influence

of STAT1 on the split formation induced by PX43. STAT1 can also promote apoptosis through p53, which was shown to be activated by PV autoantibodies in experimental studies (Rehman, Huang, and Wan 2021). Interestingly, the p53 pathway itself is overall downregulated in most of the basal keratinocyte samples treated with AK23 and PX43, tp53 is slightly upregulated throughout all time points. p38 MAPK signalling and c-myc are part of the p53 signalling pathways (Y. Chen *et al.* 2005). In the majority of basal keratinocyte samples treated with PX43, p38 MAPK signalling was upregulated throughout all time points, while it was upregulated in only four out of six samples of basal keratinocyte samples treated with AK23 after 24 hours. For the other time points, only in up to three out of six samples this signalling pathway was upregulated, but mostly not regulated or even downregulated. According to literature (Rehman *et al.* 2019), Dsg3 is an anti-stress protein which counterbalances p53. By this, the normal epithelial homeostasis is maintained. Likewise, binding of Dsg3 by autoantibodies and thereby disrupting its function, leads to an imbalance in the anti-stress network and ultimately to deregulation of apoptosis and therefore PV blistering (Rehman, Huang, and Wan 2021). Connecting this with the data from the basal keratinocytes treated with AK23, p53 signalling is upregulated after 24 hours and downregulated before. This could suggest that the binding of AK23 to Dsg3 does not cause immediately a stress response in the basal keratinocytes but rather needs time to cause a change in the p53 network. Interestingly, binding of PX43 to Dsg3/1 does not cause an upregulation in p53, but in PI3K signalling which promotes cell growth and survival. Together with the phenotype of split formation in the skin, this suggests that once the basal keratinocytes are losing their neighbouring cells, they activate pathways ensuring their survival. Simultaneously, they are signalling to the surrounding immune cells and the tissue that there is a disruption in the skin barrier, leading to the upregulation of NFκB and TNFα. The upregulation of interferon regulatory factors (IRFs) is tied to the JAK-STAT pathway, too (X. Hu *et al.* 2021). They play a role in autoimmunity, cell growth, and lymphocyte development.

Recently, Kruppel-like-factor 5 (KLF5) was identified as a protein binding directly to Dsg3 in HaCaT cells (Franz *et al.* 2024). This was achieved by a combination of whole-genome knockout screening and promoter screen of the gene encoding Dsg3. Usually, KLF5 is necessary for Dsg3 transcription as it binds to the Dsg3 promoter region. It is also stated that in PV patients a reduced level of KLF5 is detected and that autoantibodies from PV patients do not only disrupt the intercellular adhesion but also reduce KLF5 in *in vivo* and *in vitro* PV disease models. This is caused by an increased HDAC3 (histone deacetylase 3) activity, binding after its activation by p38 MAPK in front of the KLF5 promoter region, essentially blocking its transcription and by this transcription of Dsg3 (Franz *et al.* 2024). Looking at the data from the HSOC model of PV injected with PX43, no KLF5 is up- or downregulated, but KLF6 is slightly upregulated only at the 10 hours time point. KLF6 is a key transcription factor in basal keratinocytes and its inhibition has been related to decreased proliferation (Zou *et al.* 2021). Consequently, its upregulation here is linked to increased proliferation, most likely due to the cellular loss of neighbouring keratinocytes. Comparing to human skin injected with AK23, after 5 hours of incubation one half of the samples reveals upregulated KLF5, while the other half shows either no regulation or downregulation. After 10 hours only a slight upregulation can be detected and after 24 hours no KLF5 is detected. This difference between the HSOC model and the HaCaT cell experiments from Franz *et al.* could be due to the difference in the used models themselves. While the HSOC model uses whole skin with all layers preserved, HaCaT cells are not only immortalized but also are here used in a cell monolayer. A monolayer is simpler than skin with dermis, epidermis and the corresponding keratinocytes. Nevertheless, further investigation is required to reveal the reason to why some samples of basal keratinocytes isolated from the HSOC model are

showing a downregulation in KLF5, while others do not. The data does not support upregulated p38 MAPK activity which would lead to downregulation of KLF5.
In 2009, the mechanism of apoptolysis was introduced by (Grando *et al.* 2009). This term combines the terms apoptosis and acantholysis. Apoptosis describes the process of controlled, programmed cell death which is initiated by enzymatic reactions (Elmore 2007). It is a crucial process for the development of multicellular organisms, ensuring the maintenance of homeostasis by the elimination of diseased, damaged, and defective cells (Ramani *et al.* 2022). Considering the background of acantholysis in PV, apoptolysis consists of several steps: After the binding of the pathogenic autoantibodies to Dsgs, EGFR and other signalling elements connected to the Dsgs are activated and the intracellular Ca^{2+} concentration is elevated. This leads to the initiation of apoptosis. Early acantholysis is then caused by the collapse and retraction of cleaved tonofilaments and the extradesmosomal Dsgs are internalized. The continued degradation initiated by apoptotic enzymes results in the separation of desmosomes from the cell membrane leading to a separation of the cells from each other and to a production of scavenging antibodies. Finally, following this advanced acantholysis, the basal cells round up and die (Grando *et al.* 2009). So far, an increased expression of EGFR following PV-IgG injection was not reported, but an increase in EGFR autophosphorylation following 30 minutes after injection in the HSOC model (Frušić-Zlotkin *et al.* 2006). In this instance, it was also reported that EGFR is expressed in the perilesional region of the skin from PV patients. The overexpression of EGFR is connected to increased apoptosis via STAT3 signalling (Jackson and Ceresa 2017). On the transcriptomic level, increased expression of EGFR and STAT3 could be detected. As there was no analysis of the autophosphorylation of *EGFR*, it can only be assumed that the upregulation of EGFR is a consequence of phosphorylated *EGFR* which signals via STAT3 as this is upregulated, too. It was shown that STAT3 regulates Dsg3 transcription in primary human keratinocytes: The inhibition of STAT3 significantly increases the expression of Dsg3 on the mRNA and the protein level (Mao *et al.* 2017). Consequently, the upregulation of STAT3 leads to a decreased expression of Dsg3 on both levels. Taken together, this suggests that the binding of PX43 is responsible for the described signalling events leading to the apoptolysis in the epidermis represented in the HE-stained sections as the tombstone pattern of the basal keratinocytes which detached from the suprabasal layer.
The observation of the connection of a visible phenotype with transcriptome alterations align with previous studies (Busch *et al.* 2008, Singh *et al.* 2012, Offermann *et al.* 2016). They also describe that changes on the transcriptome level are linked to secondary responses rather than being the actual cause or driver of the disease mechanism. The lack of long-lasting transcriptome changes in the HSOC model treated with AK23 without a visible phenotype as it is in human skin treated with PX43 is a good example of the connection of phenotype to transcriptome. From this perspective, split formation in the HSOC model and correlating changes on the transcriptome level are resembling a gene expression profile of wounding and cell detachment rather than a specific response to autoantibody binding. The data presented here supports the theory that PV is a desmosome remodelling disease where autoantibodies are weakening the adhesion of Dsg3/1 (within and outside of the desmosome), but do not disrupt the cell-cell adhesion completely (Desalegn Tadesse Egu *et al.* 2024, Radine *et al.* 2022).
Taken together, the transcriptome changes reported before do not support a signalling dependent mechanism activated by the binding of either AK23 to Dsg3 or PX43 to Dsg3/1 in the HSOC model for PV. Although several factors in favour for p38 MAPK signalling are represented in the transcriptome data, there is no conclusive evidence on the consistency of this signalling pathway in response to the binding of Dsg3 or Dsg3/1. The inconsistency of a singular activated pathway but the consistency of upregulation in the immune response as a reaction to the split formation suggests that the basal keratinocytes react in a signalling

independent way to the binding of PX43 to Dsg3/1. In combination with the split formation caused by PX43, the transcriptome changes are most likely a reaction to early wounding and the start of wound healing reactions.

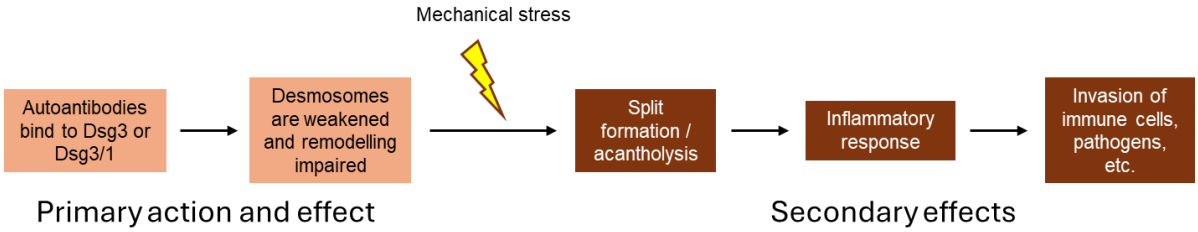

Figure 7.1.: Split formation / acantholytic events happening after autoantibody binding are secondary effects. The binding of autoantibodies to either Dsg3 or Dsg 3/1 (primary action) lead to the weakening of desmosomes and an impaired remodelling mechanism of them (primary effect). Once mechanical stress is applied, split formation in the human skin organ culture model for pemphigus vulgaris or acantholysis in the mucosa and/or skin of the patients take place. This triggers inflammatory response genes leading to an invasion of immune cells, while the broken barrier provided originally by the keratinocytes cannot prevent pathogens (like bacteria, viruses, etc.) from entering the epithelial layers.

7.4 Proteomic data

As for the transcriptome data, the proteome profile for immune cells and antibodies from PV patients has been established comprising of those from blood (Kalantari-Dehaghi *et al.* 2013, J. Chen *et al.* 2017, Luo *et al.* 2024). This has been done just recently for the keratinocytes in patients (Cheng *et al.* 2024), but has not been done for the keratinocytes from the HSOC model for PV.
Here, the focus was set to the 24 hours incubation of human skin with PX43 to see how the proteome reflects the transcriptome data acquired so far.
As it is evident by the PCA plots and the corresponding histological pictures, the biological differences are only minimal despite the split caused by PX43. This suggests that there is no long lasting effect on the proteome level induced by PX43 binding to Dsg3/1 compared to hIgG. The difference between T0 and the other two conditions after 24 hours incubation are very likely due to the "age" of the skin. T0 is a sample taken less than 16 hours after the plastic surgery has taken place, while the additional 24 hours incubation under standard cell culture conditions leads to changes in the protein levels in the skin reacting to the culturing conditions.
mTOR plays a vital role in proliferation, adhesion, and migration (Cheng *et al.* 2024). In the context of the HSOC model for PV, mTOR proteins are likely upregulated due to the keratinocytes losing contacts to each other (adhesion), and trying to stabilize the epidermal layer by means of cellular division (proliferation) and recruitment of neighbouring keratinocytes (migration).
It was reported by Williamson *et al.* (Williamson, Hunziker, *et al.* 2007) that there is an increased c-myc expression in PV patients and also the passive transfer mouse model for PV. C-myc is a molecule which induces proliferation in stem cells and differentiation in keratinocytes (Williamson *et al.* 2006). In the data shown here, MYC protein is elevated but according to the Ki-67-staining, no increased proliferation could be reported. Further investigation would be needed to clarify if this is difference is due to the characteristics of the passive transfer mouse model for PV, PV patients, and the HSOC model for PV.
When comparing the proteome of PX43 treated basal keratinocytes from the HSOC model to whole skin lysates from lesional and non-lesional skin from PV patients (Cheng *et al.* 2024), both show an enrichment in the oxidative phosphorylation. According to the authors, this upregulation in proteins involved in the oxidative phosphorylation may be a step happening before blister formation. It might be possible that the release of interferons, which is detected on the transcriptome level, is initiated by the oxidative phosphorylation (Cheng *et al.* 2024), which in turn activates the JAK/STAT pathway. STAT3, which is present in the mitochondrion, too, in turn promotes oxidative phosphorylation leading to an interconnected loop which ultimately results in an activation of the NFκB pathway.
Concluding on this data, it is likely that the binding of autoantibodies to either Dsg3 or Dsg3/1 is a primary action and the weakening and impaired remodelling of the desmosomes a primary effect of the binding (see **Figure 7.1.**). As long as no mechanical stress is applied to the effect mucosa or skin, respectively, the keratinocytes will not have any significant signalling pathway activated. Once mechanical stress leads to split formation in the skin samples form the HSOC model for PV or to acantholysis in the mucosa or skin from PV patients (secondary effect), the keratinocytes react by the activation of inflammatory response genes and immune cells will invade the affected areas. Since the mucosal or skin barrier are impaired, pathogens like bacteria and viruses can enter the epithelia leading to an amplified immune reaction to them.

7.5 Method limitations

Although a variety of experimental assays and standardized models were used for this work, a few words to their limitations need to be said.
The KDA relies on the formation of a cell monolayer using either primary keratinocytes (here pHPEKs) or immortalized keratinocytes (here HaCaTs). Primary keratinocytes have the advantage that they are very close to the actual natural state of the cells, but they cannot be kept in culture for very long as they are going to lose their primary properties after each passage (Shay and Wright 2000). This can be omitted using immortalized cell lines, but these are not as close to the natural cell state in the human body as primary ones (Voloshin *et al.* 2023). Nevertheless, the cell monolayer required for the KDA is not close to the human skin and cannot represent the natural state of the cells. Another crucial point for the KDA to work properly, is the confluence of the monolayer. Although confluency is very well defined, it is a subjective concept (Topman, Sharabani-Yosef, and Gefen 2011): A confluency of 80 %, for example, could appear to a different experimenter as 60 % confluency.
The HSOC model for PV can eliminate several limitations of the classical cell culture: The use of human skin allows the study of the keratinocytes in their natural environment and the interaction with other cell types in the skin (Varani 2012). This allows for a nearly complete picture of the interplay of the skin under different conditions. Factors that still need to be taken into consideration is the absence of a complete immune system and blood flow. There are still residual immune cells in the cells, but there is no communication with lymph nodes (Zhou *et al*. 2018). Although the experiments used skin mainly from the abdomen (with one exception being skin from the breast), the age of the skin donors varies from 30 years to 55 years. The difference in 20 years could also lead to the differences in donor specific responses to the injection of PX43 and AK23.
Accounting for both, cell culture and human skin organ culture, the cells are in an artificial environment providing as many nutrients as possible. But must be kept in mind that cell culture conditions are never as perfect for cells and organ cultures as their natural environment, the body they are originated from.
During the production of PX43, AK23, and mIgG, the contamination with endotoxins occurred. The effect was excluded by re-analysis of the transcriptome data after hypergeometric testing (Hartmann et al. 2025). The genes influenced by endotoxins were identified after the injection of endotoxin-free mIgG and hIgG and incubation for 5,10, and 24 hours. The basal keratinocytes were isolated and prepared for RNA-seq. It could be verified that the effect of the endotoxin does not change the gene response qualitatively when the skin was injected with the contaminated PX43 and AK23.

7.6 Outlook

The above claimed signalling independent mechanism of split formation in the HSOC model for PV is currently under investigation. Inhibitors targeting various molecules in the keratinocytes are tested to validate the findings of this study and will shed light on the steps which are required make the basal keratinocytes lose contact with neighbouring cells.
During the production of PX43, endotoxins were not removed from the scFv preparation. Although the effect of endotoxin was omitted in these data by means of bioinformatics, the validation experiments are done with endotoxin free preparations. This will biologically confirm the results from the previous experiments.
In this project, a variety of different tools were used to understand the mechanism of PV, a disorder caused by autoantibodies directed against Dsg3/1. The set up for the HSOC model for PV had to be adjusted for the use of AK23 which does not cause a split formation in the skin as it is caused by PX43. Figuring out the amount of AK23 binding to Dsg3 corresponding to the same amount of PX43 binding to Dsg3/1 was determined by the KDA on HaCaTs and on pHPEKs. Using the determined concentration in the HSOC model did not meet the expectation of split formation of the same length: Since AK23 cannot cause a split in human skin on its own, ETA was added to cut Dsg1 which would have hold the epidermis together even if Dsg3 was inhibited by AK23. The split formation in AK23 with ETA treated skin was significantly smaller compared to the split caused by PX43.
On the transcriptome level, PX43 injected skin showed upregulation in inflammatory pathways mediated by NFkB and TNF. On the other hand, there was no such pathway upregulated upon injection with AK23.
The proteome analysis 24 hours after the injection with PX43 could confirm what was already visible on the transcriptomic level, namely the upregulation of inflammatory pathways probably as a response of the keratinocytes losing their neighbours and signalling this to the immune system and other cells present in the epidermis and dermis.

8 Thanks to…

"A dissertation is like chess boxing."
This sentence was born just a few weeks before I handed in the dissertation. We had one of our happy lunch breaks and talked about everything. Somehow, we came up with the topic of interesting sport events. My MD student Lennart brought up the topic of chess boxing, where the participants play one round of chess, do one boxing round, and then come back to the chess board. It just hit me that this is actually a very nice comparison: Playing the round of chess is when a PhD student has time to plan everything, does literature research, or just anything that is not critical until a certain deadline. The boxing part consists of affirmed mentioned deadlines, experiments, data analysis, posters, talks, and all the little emergency things that happen around the more relaxed part of the PhD life.
I have to thank a lot of people. They all helped me to get this far in my life and to evolve in the person I am now. Without further ado, I want to say thank you:
Jenny, thank you so much for this rollercoaster of a journey! You gave me a chance to do science and work on a very cool project, which will always be one of my favourites. I could not have asked for a better supervisor, "Doktormutter", and group leader. Despite all the highs and lows, you always supported me and taught me to manage the bigger and smaller problems in science and whatever else happening in life.
I would also like to thank the examination committee Prof. Dr. rer. nat. **Rudi Manz** and Prof. Dr. rer. nat. **Norbert Tautz** for assuming the role of second referee and head of examination committee.
I also want to thank the managing director of the LIED, Prof. Dr. med. **Ralf Ludwig**, his working group and their technician **Claudia Kauderer**, for the cooperation in my dissertation project and their support.
One very big thank you is for Prof. Dr. phil. nat. **Eliane Müller** and the cooperation partners in our project. Without them this dissertation would not have existed in the first place! Thank you, Eliane, for the stay at your lab but also for your input, insights, and ideas! I am very happy to be part of this great consortium that you assembled and for the nice meetings we had. **William**, **Siavash**, and **Patrizia**, thank you for your support during the whole time and the great team work to get the parcels safe and sound to your laboratory. It was fun working with you together and I felt very welcome during my stay in your laboratory. **Rene**, thank you for taking all organizational issues into your hand and managing so well.
To **Hauke Busch** and **Antje Müller**, thank you for supporting me as my thesis advisory committee together with Jenny. A very special thanks to Hauke, for all your analysis and bioinformatics insights! Without your and **Sen Guo**'s analysis skills, I would have not been able to analyse any of this transcriptome and proteome data.
To Dr. med. Dr. rer. nat. **Christoph Hammers**, thank you for providing us with a great amount of the scFv for this project and thank you for your cooperation during the last years. Thank you to **Laura Tomaschewski** to produce the scFv in the first place in cooperation with **Dagmar Willkomm** from the Technische Hochschule Lübeck. Your fermenter was a real game changer for this project!
Nadine, thank you for your support when figuring out how to do things that are officially not in our job description and make it work. Thank you for your help when I was struggling with new protocols and whenever I needed someone to talk to.
Sylva, thank you for cutting all the samples at the cryostat!
Skadi, **Sina**, and **Laura**, thank you for your work in organizing the RTG 2633 which I am part of and the beautiful retreats, poster walks, and seminars.
Sarah, **Caren**, **Tasja,** and **Maja**, thank you so, so much for being my "Doktor-Schwestern". I'm glad to be or have been with you in one office and happy that we can support each other in such a great way!

I also want to thank the students I had along the way! Thank you for your help and work and your patience while I was figuring out how to supervise you. **Max** and **Luca**, thank you for being the first two medical students for me to supervise. It was not easy for me to handle the two projects of you, but I think the three of us handled it quite well. **Nora** and **Julia Wimmer-Groß**, thank you for your support and input. With you, we could close one project and got some valuable insights on the other. **Danial**, thank you for continuing Max's project. It has been a joy to have you around. **Lennart** and **Marie**, thank you for bringing my project to a closure. Your work is incredibly important and I am happy to have you as a third generation of medical students that I supervise.
Clara, thank you! Nadine and I are still so happy that you helped us to get the production and purification of the scFv back on the tracks! **Mikko**, thank you for your support not only for Luca in the cell culture, but also for my own project. **Julia Meyer**, you did a big part of my own experiments during my first two years. Thank you so much for your work!
Thank you to my student assistances! **Bety**, **Linus**, and **Katja**, without your help, I would be sitting until today at the microtome cutting my paraffin blocks!
I also want to thank all the skin donors and plastic surgeons I work together! Thank you for your cooperation!
Thanks to the Routine laboratory from the LIED that you helped to proceed all of these skin samples!

The second big thank you goes to the family and friends who supported me since I started this "science stuff":
Mama and **Papa**, thank you so much for always being there for me and supporting me during the highs and lows not only during the dissertation, but also when I started my Bachelor studies. You mean the world to me and I do not know if I would have come this far without your unconditional support and love. Of course, I want to thank my brothers, **Jonathan** and **Lars**: The three of us took quite different carrier options but we never let each other down. Thank you!
To **my grandparents**, thank you for your support during school, Bachelor's and Master's studies, and during my time as a PhD student.
Mario, I cannot stress enough how thankful I am to have met you and to have your support. The last 2.5 years have not been the easiest for the two of us, but we made the best of all the chaos that hit us, and you lifted me up whenever I was down. Thank you so much for being there, being my partner, and being you.
Tine, I do not know where to start: Thank you for your mentorship for over a decade! You guided me through the research field and shared your own experiences with me. I cannot stress enough how grateful I am to have met you and your husband **Tom**. Thank you for all your support and your friendship.
I also want to thank **Theresa**, **Max**, and **Sven** for their friendship and understanding whenever I was not really responding to messages because I was stressed out about science. Thank you for your understanding and always supporting me.
Chrissi, thank you for your support for the last years. I enjoyed studying with you in Rheinbach and I am so, so happy that we are still friends and seeing each other despite living so far away. You are one of my best friends and I am thankful to always discuss with you not only matters of life but also matters of laboratory work.

I want to thank everyone I have met along this way for their support!

Thank you to all my friends, family, and working group for staying with and join me during this match of chess boxing!

9 References

Abdo, Joseph M., Nikolai A. Sopko, and Stephen M. Milner. 2020. 'The Applied Anatomy of Human Skin: A Model for Regeneration'. *Wound Medicine* 28 (March):100179. https://doi.org/10.1016/j.wndm.2020.100179.

Ahmad, Zuhaida Asra, Swee Keong Yeap, Abdul Manaf Ali, Wan Yong Ho, Noorjahan Banu Mohamed Alitheen, and Muhajir Hamid. 2012. 'scFv Antibody: Principles and Clinical Application'. *Clinical and Developmental Immunology* 2012:1–15. https://doi.org/10.1155/2012/980250.

Ahsan, Haseeb. 2023. 'Origins and History of Autoimmunity—A Brief Review'. *Rheumatology & Autoimmunity* 3 (1): 9–14. https://doi.org/10.1002/rai2.12049.

Alabeedi, Faris Mohsin Ali. 2024. 'Alteration of Reactive Oxygen Species Master Transcription Factor Nrf2 in Keratinocytes Exposed to Monoclonal Pathogenic Antibody AK23 against Desmoglein-3 in Pemphigus Vulgaris'. *Autoimmunity* 57 (1): 2377138. https://doi.org/10.1080/08916934.2024.2377138.

Amagai, M., N. Matsuyoshi, Z. H. Wang, C. Andl, and J. R. Stanley. 2000. 'Toxin in Bullous Impetigo and Staphylococcal Scalded-Skin Syndrome Targets Desmoglein 1'. *Nature Medicine* 6 (11): 1275–77. https://doi.org/10.1038/81385.

Aoyama, Yurni, and Yasuo Kitajima. 1999. 'Pemphigus Vulgaris-IgG Causes a Rapid Depletion of Desmoglein 3 (Dsg3) from the Triton X-100 Soluble Pools, Leading to the Formation of Dsg3-Depleted Desmosomes in a Human Squamous Carcinoma Cell Line, DJM-1 Cells'. *Journal of Investigative Dermatology* 112 (1): 67–71. https://doi.org/10.1046/j.1523-1747.1999.00463.x.

Avrameas, Stratis, and Carlo Selmi. 2013. 'Natural Autoantibodies in the Physiology and Pathophysiology of the Immune System'. *Journal of Autoimmunity* 41 (March):46–49. https://doi.org/10.1016/j.jaut.2013.01.006.

Barrandon, Y., and H. Green. 1987. 'Three Clonal Types of Keratinocyte with Different Capacities for Multiplication'. *Proceedings of the National Academy of Sciences of the United States of America* 84 (8): 2302–6. https://doi.org/10.1073/pnas.84.8.2302.

Berkowitz, Paula, Peiqi Hu, Simon Warren, Zhi Liu, Luis A Diaz, and David S Rubenstein. 2006. 'p38MAPK Inhibition Prevents Disease in Pemphigus Vulgaris Mice'. *MEDICAL SCIENCES*.

Blattner, F. R., G. Plunkett, C. A. Bloch, N. T. Perna, V. Burland, M. Riley, J. Collado-Vides, et al. 1997. 'The Complete Genome Sequence of Escherichia Coli K-12'. *Science (New York, N.Y.)* 277 (5331): 1453–62. https://doi.org/10.1126/science.277.5331.1453.

Bonné, Stefan, Barbara Gilbert, Mechthild Hatzfeld, Xinyu Chen, Kathleen J. Green, and Frans Van Roy. 2003. 'Defining Desmosomal Plakophilin-3 Interactions'. *The Journal of Cell Biology* 161 (2): 403–16. https://doi.org/10.1083/jcb.200303036.

Braga-Lagache, Sophie, Natasha Buchs, Mircea-Ioan Iacovache, Benoît Zuber, Christopher Benjamin Jackson, and Manfred Heller. 2016. 'Robust Label-Free, Quantitative Profiling of Circulating Plasma Microparticle (MP) Associated Proteins'. *Molecular & Cellular Proteomics* 15 (12): 3640–52. https://doi.org/10.1074/mcp.M116.060491.

Breitkreutz, Dirk, Nicolae Mirancea, and Roswitha Nischt. 2009. 'Basement Membranes in Skin: Unique Matrix Structures with Diverse Functions?' *Histochemistry and Cell Biology* 132 (1): 1–10. https://doi.org/10.1007/s00418-009-0586-0.

Bruin, Alain de, Reto Caldelari, Lina Williamson, Maja M. Suter, Thomas Hunziker, Marianne Wyder, and Eliane J. Müller. 2007. 'Plakoglobin-Dependent Disruption of the Desmosomal Plaque in Pemphigus Vulgaris'. *Experimental Dermatology* 16 (6): 468–75. https://doi.org/10.1111/j.1600-0625.2007.00557.x.

Burmester, Imke A. K., Shirin Emtenani, Jan-Gerrit Johns, Ralf J. Ludwig, Christoph M. Hammers, and Jennifer E. Hundt. 2019. 'Translational Use of a Standardized Full Human Skin Organ Culture Model in Autoimmune Blistering Diseases'. *Current Protocols in Pharmacology* 85 (1): e56. https://doi.org/10.1002/cpph.56.

Burmester, Imke A. K., Sarah Flaswinkel, Clara-Sophie Thies, Anika Kasprick, Mayumi Kamaguchi, Valéria Bumiller-Bini, Shirin Emtenani, et al. 2020. 'Identification of Novel Therapeutic Targets for Blocking Acantholysis in Pemphigus'. *British Journal of Pharmacology* 177 (22): 5114–30. https://doi.org/10.1111/bph.15233.

Busch, Hauke, David Camacho-Trullio, Zbigniew Rogon, Kai Breuhahn, Peter Angel, Roland Eils, and Axel Szabowski. 2008. 'Gene Network Dynamics Controlling Keratinocyte Migration'. *Molecular Systems Biology* 4 (1): 199. https://doi.org/10.1038/msb.2008.36.

Bystryn, Jean-Claude, and Jennifer L Rudolph. 2005. 'Pemphigus'. *The Lancet* 366 (9479): 61–73. https://doi.org/10.1016/S0140-6736(05)66829-8.

Caldelari, R., A. de Bruin, D. Baumann, M. M. Suter, C. Bierkamp, V. Balmer, and E. Müller. 2001. 'A Central Role for the Armadillo Protein Plakoglobin in the Autoimmune Disease Pemphigus Vulgaris'. *The Journal of Cell Biology* 153 (4): 823–34. https://doi.org/10.1083/jcb.153.4.823.

Calkins, Cathárine C., Shannon V. Setzer, Jean Marie Jennings, Susan Summers, Kazuyuki Tsunoda, Masayuki Amagai, and Andrew P. Kowalczyk. 2006. 'Desmoglein Endocytosis and Desmosome Disassembly Are Coordinated Responses to Pemphigus Autoantibodies'. *The Journal of Biological Chemistry* 281 (11): 7623–34. https://doi.org/10.1074/jbc.M512447200.

Chen, Jing, Qi Zheng, Christoph M. Hammers, Christoph T. Ellebrecht, Eric M. Mukherjee, Hsin-Yao Tang, Chenyan Lin, et al. 2017. 'Proteomic Analysis of Pemphigus Autoantibodies Indicates a Larger, More Diverse, and More Dynamic Repertoire than Determined by B Cell Genetics'. *Cell Reports* 18 (1): 237–47. https://doi.org/10.1016/j.celrep.2016.12.013.

Chen, Yi, Ze-Hong Miao, Wei-Min Zhao, and Jian Ding. 2005. 'The P53 Pathway Is Synergized by P38 MAPK Signaling to Mediate 11,11′-dideoxyverticillin-induced G_2 /M Arrest'. *FEBS Letters* 579 (17): 3683–90. https://doi.org/10.1016/j.febslet.2005.05.053.

Cheng, Yuqi, Mingming Zhao, CaiHong Zhu, Xianfa Tang, Wenjun Wang, Huayang Tang, Xiaodong Zheng, et al. 2024. 'Proteomic Analysis Reveals Oxidative Phosphorylation and JAK - STAT Pathways Mediated Pathogenesis of Pemphigus Vulgaris'. *Experimental Dermatology* 33 (10): e15184. https://doi.org/10.1111/exd.15184.

Chernyavsky, Alex, Kyle T. Amber, Arianna F. Agnoletti, Candice Wang, and Sergei A. Grando. 2019. 'Synergy among Non-Desmoglein Antibodies Contributes to the Immunopathology of Desmoglein Antibody-Negative Pemphigus Vulgaris'. *The Journal of Biological Chemistry* 294 (12): 4520–28. https://doi.org/10.1074/jbc.RA118.006743.

Colombo, Irma, Enrico Sangiovanni, Roberta Maggio, Carlo Mattozzi, Stefania Zava, Yolanda Corbett, Marco Fumagalli, et al. 2017. 'HaCaT Cells as a Reliable In Vitro Differentiation Model to Dissect the Inflammatory/Repair Response of Human Keratinocytes'. *Mediators of Inflammation* 2017:7435621. https://doi.org/10.1155/2017/7435621.

Costenbader, Karen H., Steffen Gay, Marta E. Alarcón-Riquelme, Luca Iaccarino, and Andrea Doria. 2012. 'Genes, Epigenetic Regulation and Environmental Factors: Which Is the Most Relevant in Developing Autoimmune Diseases?' *Autoimmunity Reviews* 11 (8): 604–9. https://doi.org/10.1016/j.autrev.2011.10.022.

Di Zenzo, Giovanni, Kyle T. Amber, Beyza S. Sayar, Eliane J. Müller, and Luca Borradori. 2016. 'Immune Response in Pemphigus and beyond: Progresses and Emerging Concepts'. *Seminars in Immunopathology* 38 (1): 57–74. https://doi.org/10.1007/s00281-015-0541-1.

Didona, Dario, Roberto Maglie, Rüdiger Eming, and Michael Hertl. 2019. 'Pemphigus: Current and Future Therapeutic Strategies'. *Frontiers in Immunology* 10:1418. https://doi.org/10.3389/fimmu.2019.01418.

Duan, Shumin, Qionghua Li, Fei Wang, Wenjing Kuang, Yunmei Dong, Dan Liu, Jiongke Wang, et al. 2024. 'Single-Cell Transcriptomes and Immune Repertoires Reveal the Cell State and Molecular Changes in Pemphigus Vulgaris'. *The Journal of Immunology* 212 (3): 375–88. https://doi.org/10.4049/jimmunol.2300312.

Egu, D. T., A. M. Sigmund, E. Schmidt, V. Spindler, E. Walter, and J. Waschke. 2020. 'A New Ex Vivo Human Oral Mucosa Model Reveals That p38MAPK Inhibition Is Not Effective in Preventing Autoantibody-Induced Mucosal Blistering in Pemphigus'. *The British Journal of Dermatology* 182 (4): 987–94. https://doi.org/10.1111/bjd.18237.

Egu, D. T., E. Walter, V. Spindler, and J. Waschke. 2017. 'Inhibition of p38MAPK Signalling Prevents Epidermal Blistering and Alterations of Desmosome Structure Induced by Pemphigus Autoantibodies in Human Epidermis'. *The British Journal of Dermatology* 177 (6): 1612–18. https://doi.org/10.1111/bjd.15721.

Egu, Desalegn Tadesse, Thomas Schmitt, Nancy Ernst, Ralf Joachim Ludwig, Michael Fuchs, Matthias Hiermaier, Sina Moztarzadeh, et al. 2024. 'EGFR Inhibition by Erlotinib Rescues Desmosome Ultrastructure and Keratin Anchorage and Protects against Pemphigus Vulgaris IgG–Induced Acantholysis in Human Epidermis'. *Journal of Investigative Dermatology* 144 (11): 2440–52. https://doi.org/10.1016/j.jid.2024.03.040.

Elmore, Susan. 2007. 'Apoptosis: A Review of Programmed Cell Death'. *Toxicologic Pathology* 35 (4): 495–516. https://doi.org/10.1080/01926230701320337.

Emtenani, Shirin, Saeedeh Ghorbanalipoor, Sarah Mayer-Hain, Khalaf Kridin, Lars Komorowski, Christian Probst, Takashi Hashimoto, et al. 2021. 'Pathogenic Activation and Therapeutic Blockage of FcαR-Expressing Polymorphonuclear Leukocytes in IgA Pemphigus'. *The Journal of Investigative Dermatology* 141 (12): 2820–28. https://doi.org/10.1016/j.jid.2021.06.007.

Franz, Henriette, Maitreyi Rathod, Aude Zimmermann, Chiara Stüdle, Vivien Beyersdorfer, Karen Leal-Fischer, Pauline Hanns, et al. 2024. 'Unbiased Screening Identifies Regulators of Cell-Cell Adhesion and Treatment Options in Pemphigus'. *Nature Communications* 15 (1): 8044. https://doi.org/10.1038/s41467-024-51747-2.

Frušić-Zlotkin, Marina, Dorin Raichenberg, Xin Wang, Marina Frušić-Zlotkin, Dorin Raichenberg, Xin Wang, Michael David, Beno Michel, and Yoram Milner. 2006. 'Apoptotic Mechanism in Pemphigus Autoimmunoglobulins-Induced Acantholysis—Possible Involvement of the EGF Receptor'. *Autoimmunity* 39 (7): 563–75. https://doi.org/10.1080/08916930600971836.

Fuchs, Elaine, and Srikala Raghavan. 2002. 'Getting under the Skin of Epidermal Morphogenesis'. *Nature Reviews Genetics* 3 (3): 199–209. https://doi.org/10.1038/nrg758.

Garrod, David, and Martyn Chidgey. 2008. 'Desmosome Structure, Composition and Function'. *Biochimica et Biophysica Acta (BBA) - Biomembranes* 1778 (3): 572–87. https://doi.org/10.1016/j.bbamem.2007.07.014.

Garrod, David R., Mohamed Y. Berika, William F. Bardsley, David Holmes, and Lydia Tabernero. 2005. 'Hyper-Adhesion in Desmosomes: Its Regulation in Wound

Healing and Possible Relationship to Cadherin Crystal Structure'. *Journal of Cell Science* 118 (Pt 24): 5743–54. https://doi.org/10.1242/jcs.02700.

Grando, Sergei A., Jean-Claude Bystryn, Alexander I. Chernyavsky, Marina Frušić-Zlotkin, Robert Gniadecki, Roberta Lotti, Yoram Milner, Mark R. Pittelkow, and Carlo Pincelli. 2009. 'Apoptolysis: A Novel Mechanism of Skin Blistering in Pemphigus Vulgaris Linking the Apoptotic Pathways to Basal Cell Shrinkage and Suprabasal Acantholysis'. *Experimental Dermatology* 18 (9): 764–70. https://doi.org/10.1111/j.1600-0625.2009.00934.x.

Green, Kathleen J., Avinash Jaiganesh, and Joshua A. Broussard. 2019. 'Desmosomes: Essential Contributors to an Integrated Intercellular Junction Network'. *F1000Research* 8:F1000 Faculty Rev-2150. https://doi.org/10.12688/f1000research.20942.1.

Hammers, Christoph M., Jing Chen, Chenyan Lin, Stephen Kacir, Don L. Siegel, Aimee S. Payne, and John R. Stanley. 2015. 'Persistence of Anti-Desmoglein 3 IgG(+) B-Cell Clones in Pemphigus Patients over Years'. *The Journal of Investigative Dermatology* 135 (3): 742–49. https://doi.org/10.1038/jid.2014.291.

Hammers, Christoph M., and John R. Stanley. 2014. 'Antibody Phage Display: Technique and Applications'. *The Journal of Investigative Dermatology* 134 (2): 1–5. https://doi.org/10.1038/jid.2013.521.

Hammers, Christoph M., and John R. Stanley. 2016. 'Mechanisms of Disease: Pemphigus and Bullous Pemphigoid'. *Annual Review of Pathology* 11 (May):175–97. https://doi.org/10.1146/annurev-pathol-012615-044313.

Hammers, Christoph M., and John R. Stanley. 2020. 'Recent Advances in Understanding Pemphigus and Bullous Pemphigoid'. *Journal of Investigative Dermatology* 140 (4): 733–41. https://doi.org/10.1016/j.jid.2019.11.005.

Hartmann, Veronika, Sen Guo, Siavash Rahimi, Uta Radine, Danielle Malheiros, Amanda Salviano-Silva, Valeria Bumiller-Bini Hoch, et al. 2025. 'In Pemphigus, Cell Detachment, but Not Autoantibody Binding, Induces Cell-Wide, Long-Lasting Transcriptomic and Proteomic Changes'. https://doi.org/10.1101/2025.02.10.637416.

Hatzfeld, Mechthild. 2007. 'Plakophilins: Multifunctional Proteins or Just Regulators of Desmosomal Adhesion?' *Biochimica et Biophysica Acta (BBA) - Molecular Cell Research* 1773 (1): 69–77. https://doi.org/10.1016/j.bbamcr.2006.04.009.

Hertl, M. 2006. 'T Cell Control in Autoimmune Bullous Skin Disorders'. *Journal of Clinical Investigation* 116 (5): 1159–66. https://doi.org/10.1172/JCI28547.

Hu, Chung-Hong, Beno Michel, and John R Schiltz. 1978. 'Epidermal Acantholysis Induced In Vitro by Pemphigus Autoantibody' 90 (2): 18.

Hu, Xiaoyi, Jing Li, Maorong Fu, Xia Zhao, and Wei Wang. 2021. 'The JAK/STAT Signaling Pathway: From Bench to Clinic'. *Signal Transduction and Targeted Therapy* 6 (1): 402. https://doi.org/10.1038/s41392-021-00791-1.

Hu, Zhi, Meiling Zheng, Ziyu Guo, Wenhui Zhou, Wenyu Zhou, Nan Yao, Guiying Zhang, Qianjin Lu, and Ming Zhao. 2024. 'Single-Cell Sequencing Reveals Distinct Immune Cell Features in Cutaneous Lesions of Pemphigus Vulgaris and Bullous Pemphigoid'. *Clinical Immunology* 263 (June):110219. https://doi.org/10.1016/j.clim.2024.110219.

Huang, Zi-xuan, Peng Qu, Kan-kan Wang, Jie Zheng, Meng Pan, and Hai-qin Zhu. 2022. 'Transcriptomic Profiling of Pemphigus Lesion Infiltrating Mononuclear Cells Reveals a Distinct Local Immune Microenvironment and Novel lncRNA Regulators'. *Journal of Translational Medicine* 20 (1): 182. https://doi.org/10.1186/s12967-022-03387-7.

Ishii, Ken, Chenyan Lin, Don L. Siegel, and John R. Stanley. 2008. 'Isolation of Pathogenic Monoclonal Anti-Desmoglein 1 Human Antibodies by Phage Display of Pemphigus Foliaceus Autoantibodies'. *Journal of Investigative Dermatology* 128 (4): 939–48. https://doi.org/10.1038/sj.jid.5701132.

Ishii, Ken, Kenji Yoshida, John R. Stanley, Jun Yamagami, Masayuki Amagai, and Akira Ishiko. 2020. 'Pemphigus Vulgaris and Foliaceus IgG Autoantibodies Directly Block Heterophilic Transinteraction between Desmoglein and Desmocollin'. *The Journal of Investigative Dermatology* 140 (10): 1919-1926.e7. https://doi.org/10.1016/j.jid.2020.02.010.

Jackson, Nicole M., and Brian P. Ceresa. 2017. 'EGFR-Mediated Apoptosis via STAT3'. *Experimental Cell Research* 356 (1): 93–103. https://doi.org/10.1016/j.yexcr.2017.04.016.

Jeffes, E. W., R. P. Kaplan, and A. R. Ahmed. 1984. 'Acantholysis Produced in Vitro with Pemphigus Serum: Hydrocortisone Inhibits Acantholysis, While Dapsone and 6-Mercaptopurine Do Not Inhibit Acantholysis'. *Journal of Clinical Immunology* 4 (5): 359–63. https://doi.org/10.1007/BF00917138.

Jennings, Jean M., Dana K. Tucker, Margaret D. Kottke, Masataka Saito, Emmanuella Delva, Yasushi Hanakawa, Masayuki Amagai, and Andrew P. Kowalczyk. 2011. 'Desmosome Disassembly in Response to Pemphigus Vulgaris IgG Occurs in Distinct Phases and Can Be Reversed by Expression of Exogenous Dsg3'. *Journal of Investigative Dermatology* 131 (3): 706–18. https://doi.org/10.1038/jid.2010.389.

Jones, J. C., J. Arnn, L. A. Staehelin, and R. D. Goldman. 1984. 'Human Autoantibodies against Desmosomes: Possible Causative Factors in Pemphigus'. *Proceedings of the National Academy of Sciences of the United States of America* 81 (9): 2781–85. https://doi.org/10.1073/pnas.81.9.2781.

Jones, J. C., K. M. Yokoo, and R. D. Goldman. 1986. 'A Cell Surface Desmosome-Associated Component: Identification of Tissue-Specific Cell Adhesion Molecule'. *Proceedings of the National Academy of Sciences of the United States of America* 83 (19): 7282–86. https://doi.org/10.1073/pnas.83.19.7282.

Kalantari-Dehaghi, Mina, Grant J. Anhalt, Michael J. Camilleri, Alex I. Chernyavsky, Sookhee Chun, Philip L. Felgner, Algis Jasinskas, et al. 2013. 'Pemphigus Vulgaris Autoantibody Profiling by Proteomic Technique'. *PloS One* 8 (3): e57587. https://doi.org/10.1371/journal.pone.0057587.

Kammers, Kai, Robert N. Cole, Calvin Tiengwe, and Ingo Ruczinski. 2015. 'Detecting Significant Changes in Protein Abundance'. *EuPA Open Proteomics* 7 (June):11–19. https://doi.org/10.1016/j.euprot.2015.02.002.

Kasperkiewicz, Michael, Christoph T. Ellebrecht, Hayato Takahashi, Jun Yamagami, Detlef Zillikens, Aimee S. Payne, and Masayuki Amagai. 2017. 'Pemphigus'. *Nature Reviews. Disease Primers* 3 (May):17026. https://doi.org/10.1038/nrdp.2017.26.

Kitajima, Y., S. Inoue, and H. Yaoita. 1986. 'Effects of Pemphigus Antibody on the Organization of Microtubules and Keratin-Intermediate Filaments in Cultured Human Keratinocytes'. *The British Journal of Dermatology* 114 (2): 171–79. https://doi.org/10.1111/j.1365-2133.1986.tb02795.x.

Kowalczyk, Andrew P., and Kathleen J. Green. 2013. 'Structure, Function, and Regulation of Desmosomes'. In *Progress in Molecular Biology and Translational Science*, 116:95–118. Elsevier. https://doi.org/10.1016/B978-0-12-394311-8.00005-4.

Lotti, Roberta, Claudio Giacinto Atene, Alessandra Marconi, Giulia Di Rocco, L. Reggiani Bonetti, Tommaso Zanocco Marani, and Carlo Pincelli. 2019. 'Development of a Desmocollin-3 Active Mouse Model Recapitulating Human Atypical Pemphigus'. *Frontiers in Immunology* 10:1387. https://doi.org/10.3389/fimmu.2019.01387.

Lotti, Roberta, Claudio Giacinto Atene, Emma Dorotea Zanfi, Matteo Bertesi, and Tommaso Zanocco-Marani. 2022. 'In Vitro, Ex Vivo, and In Vivo Models for the Study of Pemphigus'. *International Journal of Molecular Sciences* 23 (13): 7044. https://doi.org/10.3390/ijms23137044.

Lu, Zhongfa, Sybille Hasse, Eniko Bodo, Christian Rose, Wolfgang Funk, and Ralf Paus. 2007. 'Towards the Development of a Simplified Long-Term Organ Culture Method for Human Scalp Skin and Its Appendages under Serum-Free Conditions'. *Experimental Dermatology* 16 (1): 37–44. https://doi.org/10.1111/j.1600-0625.2006.00510.x.

Luo, Xiaojia, Jianting Ouyang, Fuqiong Jiang, Yaozhong Zhang, Yuan Wang, Yongzhuo Wu, and Lingyu Hu. 2024. 'Conjoint Analysis of Methylation, Transcriptomic, and Proteomic Profiles in Pemphigus Vulgaris'. *Orphanet Journal of Rare Diseases* 19 (1): 437. https://doi.org/10.1186/s13023-024-03458-6.

Mahoney, M. G., Z. Wang, K. Rothenberger, P. J. Koch, M. Amagai, and J. R. Stanley. 1999. 'Explanations for the Clinical and Microscopic Localization of Lesions in Pemphigus Foliaceus and Vulgaris'. *The Journal of Clinical Investigation* 103 (4): 461–68. https://doi.org/10.1172/JCI5252.

Mao, Xuming, Michael Jeffrey T. Cho, Christoph T. Ellebrecht, Eric M. Mukherjee, and Aimee S. Payne. 2017. 'Stat3 Regulates Desmoglein 3 Transcription in Epithelial Keratinocytes'. *JCI Insight* 2 (9): e92253. https://doi.org/10.1172/jci.insight.92253.

Mavropoulos, Athanasios, Timoklia Orfanidou, Christos Liaskos, Daniel S. Smyk, Vassiliki Spyrou, Lazaros I. Sakkas, Eirini I. Rigopoulou, and Dimitrios P. Bogdanos. 2013. 'P38 MAPK Signaling in Pemphigus: Implications for Skin Autoimmunity'. *Autoimmune Diseases* 2013:1–11. https://doi.org/10.1155/2013/728529.

Merritt, Anita J., Mohamed Y. Berika, Wenwu Zhai, Sarah E. Kirk, Baijing Ji, Matthew J. Hardman, and David R. Garrod. 2002. 'Suprabasal Desmoglein 3 Expression in the Epidermis of Transgenic Mice Results in Hyperproliferation and Abnormal Differentiation'. *Molecular and Cellular Biology* 22 (16): 5846–58. https://doi.org/10.1128/MCB.22.16.5846-5858.2002.

Mestrallet, Guillaume, Nathalie Rouas-Freiss, Joel LeMaoult, Nicolas O. Fortunel, and Michele T. Martin. 2021. 'Skin Immunity and Tolerance: Focus on Epidermal Keratinocytes Expressing HLA-G'. *Frontiers in Immunology* 12:772516. https://doi.org/10.3389/fimmu.2021.772516.

Michel, B., and C. S. Ko. 1977. 'An Organ Culture Model for the Study of Pemphigus Acantholysis'. *The British Journal of Dermatology* 96 (3): 295–302. https://doi.org/10.1111/j.1365-2133.1977.tb06141.x.

Miller, Phillip W., Donald N. Clarke, William I. Weis, Christopher J. Lowe, and W. James Nelson. 2013. 'The Evolutionary Origin of Epithelial Cell–Cell Adhesion Mechanisms'. In *Current Topics in Membranes*, 72:267–311. Elsevier. https://doi.org/10.1016/B978-0-12-417027-8.00008-8.

Morioka, S., K. Naito, and H. Ogawa. 1981. 'The Pathogenic Role of Pemphigus Antibodies and Proteinase in Epidermal Acantholysis'. *The Journal of Investigative Dermatology* 76 (5): 337–41. https://doi.org/10.1111/1523-1747.ep12519988.

Muñoz-López, Paola, Rosa María Ribas-Aparicio, Elayne Irene Becerra-Báez, Karla Fraga-Pérez, Luis Fernando Flores-Martínez, Armando Alfredo Mateos-Chávez, and Rosendo Luria-Pérez. 2022. 'Single-Chain Fragment Variable: Recent Progress in Cancer Diagnosis and Therapy'. *Cancers* 14 (17): 4206. https://doi.org/10.3390/cancers14174206.

Murrell, Dedee F., Sandra Peña, Pascal Joly, Branka Marinovic, Takashi Hashimoto, Luis A. Diaz, Animesh A. Sinha, et al. 2020. 'Diagnosis and Management of Pemphigus: Recommendations of an International Panel of Experts'. *Journal of the American*

Academy of Dermatology 82 (3): 575-585.e1. https://doi.org/10.1016/j.jaad.2018.02.021.

Neil, Jessica E., Marc B. Brown, and Adrian C. Williams. 2020. 'Human Skin Explant Model for the Investigation of Topical Therapeutics'. *Scientific Reports* 10 (1): 21192. https://doi.org/10.1038/s41598-020-78292-4.

Nguyen, Vu Thuong, Juan Arredondo, Alexander I. Chernyavsky, Yasuo Kitajima, Mark Pittelkow, and Sergei A. Grando. 2004. 'Pemphigus Vulgaris IgG and Methylprednisolone Exhibit Reciprocal Effects on Keratinocytes'. *The Journal of Biological Chemistry* 279 (3): 2135–46. https://doi.org/10.1074/jbc.M309000200.

Offermann, Barbara, Steffen Knauer, Amit Singh, María L. Fernández-Cachón, Martin Klose, Silke Kowar, Hauke Busch, and Melanie Boerries. 2016. 'Boolean Modeling Reveals the Necessity of Transcriptional Regulation for Bistability in PC12 Cell Differentiation'. *Frontiers in Genetics* 7 (April). https://doi.org/10.3389/fgene.2016.00044.

Oktarina, D.A.M., G. Van Der Wier, G.F.H. Diercks, M.F. Jonkman, and H.H. Pas. 2011. 'IgG-Induced Clustering of Desmogleins 1 and 3 in Skin of Patients with Pemphigus Fits with the Desmoglein Nonassembly Depletion Hypothesis: Pemphigus Deposition Patterns'. *British Journal of Dermatology* 165 (3): 552–62. https://doi.org/10.1111/j.1365-2133.2011.10463.x.

Patel, H. P., L. A. Diaz, G. J. Anhalt, R. S. Labib, and Y. Takahashi. 1984. 'Demonstration of Pemphigus Antibodies on the Cell Surface of Murine Epidermal Cell Monolayers and Their Internalization'. *The Journal of Investigative Dermatology* 83 (6): 409–15. https://doi.org/10.1111/1523-1747.ep12273480.

Payne, Aimee S., Ken Ishii, Stephen Kacir, Chenyan Lin, Hong Li, Yasushi Hanakawa, Kazuyuki Tsunoda, Masayuki Amagai, John R. Stanley, and Don L. Siegel. 2005. 'Genetic and Functional Characterization of Human Pemphigus Vulgaris Monoclonal Autoantibodies Isolated by Phage Display'. *The Journal of Clinical Investigation* 115 (4): 888–99. https://doi.org/10.1172/JCI24185.

Pelacho, B., C. Natal, A. España, I. Sánchez-Carpintero, M.J. Iraburu, and M.J. López-Zabalza. 2004. 'Pemphigus Vulgaris Autoantibodies Induce Apoptosis in HaCaT Keratinocytes'. *FEBS Letters* 566 (1–3): 6–10. https://doi.org/10.1016/j.febslet.2004.03.107.

Pollmann, Robert, Thomas Schmidt, Rüdiger Eming, and Michael Hertl. 2018. 'Pemphigus: A Comprehensive Review on Pathogenesis, Clinical Presentation and Novel Therapeutic Approaches'. *Clinical Reviews in Allergy & Immunology* 54 (1): 1–25. https://doi.org/10.1007/s12016-017-8662-z.

Puviani, Mario, Alessandra Marconi, Carlo Pincelli, and Emanuele Cozzani. 2003. 'Fas Ligand in Pemphigus Sera Induces Keratinocyte Apoptosis through the Activation of Caspase-8'. *Journal of Investigative Dermatology* 120 (1): 164–67. https://doi.org/10.1046/j.1523-1747.2003.12014.x.

Radine, Uta Katharina, Valéria Bumiller-Bini Hoch, Angelica B. Winter Boldt, Detlef Zillikens, Ralf J. Ludwig, Christoph M. Hammers, Matthias Klinger, and Jennifer E. Hundt. 2022. 'Electron Microscopy of Desmosomal Structures in the Pemphigus Human Skin Organ Culture Model'. *Frontiers in Medicine* 9 (November):997387. https://doi.org/10.3389/fmed.2022.997387.

Ramadon, Delly, Maeliosa T. C. McCrudden, Aaron J. Courtenay, and Ryan F. Donnelly. 2022. 'Enhancement Strategies for Transdermal Drug Delivery Systems: Current Trends and Applications'. *Drug Delivery and Translational Research* 12 (4): 758–91. https://doi.org/10.1007/s13346-021-00909-6.

Ramani, Pratibha, Renu Ravikumar, Deepak Pandiar, K. Monica, Reshma Poothakulath Krishnan, Abilasha Ramasubramanian, and Gheena Sukumaran. 2022. 'Apoptolysis:

A Less Understood Concept in the Pathogenesis of Pemphigus Vulgaris'. *Apoptosis* 27 (5–6): 322–28. https://doi.org/10.1007/s10495-022-01726-z.

Rehman, Ambreen, Yang Cai, Christian Hünefeld, Hana Jedličková, Yunying Huang, Muy Teck Teh, Usama Sharif Ahmad, et al. 2019. 'The Desmosomal Cadherin Desmoglein-3 Acts as a Keratinocyte Anti-Stress Protein via Suppression of P53'. *Cell Death & Disease* 10 (10): 750. https://doi.org/10.1038/s41419-019-1988-0.

Rehman, Ambreen, Yunying Huang, and Hong Wan. 2021. 'Evolving Mechanisms in the Pathophysiology of Pemphigus Vulgaris: A Review Emphasizing the Role of Desmoglein 3 in Regulating P53 and the Yes-Associated Protein'. *Life (Basel, Switzerland)* 11 (7): 621. https://doi.org/10.3390/life11070621.

Roy, Ranjita Dutta, Christian Rosenmund, and Melanie I. Stefan. 2017. 'Cooperative Binding Mitigates the High-Dose Hook Effect'. *BMC Systems Biology* 11 (1): 74. https://doi.org/10.1186/s12918-017-0447-8.

Russo, Michael V. 2003. 'The Emergence of Sustainable Industries: Building on Natural Capital'. *Strategic Management Journal* 24 (4): 317–31. https://doi.org/10.1002/smj.298.

Saito, Masataka, Sara N. Stahley, Christopher Y. Caughman, Xuming Mao, Dana K. Tucker, Aimee S. Payne, Masayuki Amagai, and Andrew P. Kowalczyk. 2012. 'Signaling Dependent and Independent Mechanisms in Pemphigus Vulgaris Blister Formation'. *PloS One* 7 (12): e50696. https://doi.org/10.1371/journal.pone.0050696.

Salinas, Gabriela Franco, Faouzi Braza, Sophie Brouard, Paul-Peter Tak, and Dominique Baeten. 2013. 'The Role of B Lymphocytes in the Progression from Autoimmunity to Autoimmune Disease'. *Clinical Immunology* 146 (1): 34–45. https://doi.org/10.1016/j.clim.2012.10.005.

Schiltz, J. R., B. Michel, and R. Papay. 1979. 'Appearance of "Pemphigus Acantholysis Factor" in Human Skin Cultured with Pemphigus Antibody'. *The Journal of Investigative Dermatology* 73 (6): 575–81. https://doi.org/10.1111/1523-1747.ep12541618.

Schmidt, Morna F., Maria Feoktistova, Diana Panayotova-Dimitrova, Ramona A. Eichkorn, and Amir S. Yazdi. 2022. 'Pitfalls in the Application of Dispase-Based Keratinocyte Dissociation Assay for In Vitro Analysis of Pemphigus Vulgaris'. *Vaccines* 10 (2): 208. https://doi.org/10.3390/vaccines10020208.

Schroeder, Harry W., and Lisa Cavacini. 2010. 'Structure and Function of Immunoglobulins'. *Journal of Allergy and Clinical Immunology* 125 (2): S41–52. https://doi.org/10.1016/j.jaci.2009.09.046.

Schuh, Theda, Robert Besch, Evelyn Braungart, Michael J. Flaig, Kathrin Douwes, Christian A. Sander, Viktor Magdolen, Christopher Probst, Katja Wosikowski, and Klaus Degitz. 2003. 'Protease Inhibitors Prevent Plasminogen-Mediated, but Not Pemphigus Vulgaris-Induced, Acantholysis in Human Epidermis'. *Biological Chemistry* 384 (2): 311–15. https://doi.org/10.1515/BC.2003.035.

Schulze, Katja, Arnaud Galichet, Beyza S. Sayar, Anthea Scothern, Denise Howald, Hillard Zymann, Myriam Siffert, et al. 2012. 'An Adult Passive Transfer Mouse Model to Study Desmoglein 3 Signaling in Pemphigus Vulgaris'. *The Journal of Investigative Dermatology* 132 (2): 346–55. https://doi.org/10.1038/jid.2011.299.

Sekiguchi, Maiko, Yuko Futei, Yoshiko Fujii, Toshiro Iwasaki, Takeji Nishikawa, and Masayuki Amagai. 2001. 'Dominant Autoimmune Epitopes Recognized by Pemphigus Antibodies Map to the N-Terminal Adhesive Region of Desmogleins'. *The Journal of Immunology* 167 (9): 5439–48. https://doi.org/10.4049/jimmunol.167.9.5439.

Shay, Jerry W., and Woodring E. Wright. 2000. 'Hayflick, His Limit, and Cellular Ageing'. *Nature Reviews Molecular Cell Biology* 1 (1): 72–76. https://doi.org/10.1038/35036093.

Shigetomi, Kenta, and Junichi Ikenouchi. 2019. 'Cell Adhesion Structures in Epithelial Cells Are Formed in Dynamic and Cooperative Ways'. *BioEssays* 41 (7): 1800227. https://doi.org/10.1002/bies.201800227.

Shimanovich, I., T. Baumann, E. Schmidt, D. Zillikens, and C. M. Hammers. 2020. 'Long-Term Outcomes of Rituximab Therapy in Pemphigus'. *Journal of the European Academy of Dermatology and Venereology: JEADV* 34 (12): 2884–89. https://doi.org/10.1111/jdv.16561.

Silver, J. D., M. E. Ritchie, and G. K. Smyth. 2009. 'Microarray Background Correction: Maximum Likelihood Estimation for the Normal-Exponential Convolution'. *Biostatistics* 10 (2): 352–63. https://doi.org/10.1093/biostatistics/kxn042.

Singh, Amit, Juliana M. Nascimento, Silke Kowar, Hauke Busch, and Melanie Boerries. 2012. 'Boolean Approach to Signalling Pathway Modelling in HGF-Induced Keratinocyte Migration'. *Bioinformatics* 28 (18): i495–501. https://doi.org/10.1093/bioinformatics/bts410.

Spindler, Volker, Vera Rötzer, Carina Dehner, Bettina Kempf, Martin Gliem, Mariya Radeva, Eva Hartlieb, Gregory S. Harms, Enno Schmidt, and Jens Waschke. 2013. 'Peptide-Mediated Desmoglein 3 Crosslinking Prevents Pemphigus Vulgaris Autoantibody-Induced Skin Blistering'. *The Journal of Clinical Investigation* 123 (2): 800–811. https://doi.org/10.1172/JCI60139.

Strimmer, Korbinian. 2008. 'A Unified Approach to False Discovery Rate Estimation'. *BMC Bioinformatics* 9 (July):303. https://doi.org/10.1186/1471-2105-9-303.

Suter, M. M., J. E. Wilkinson, E. P. Dougherty, and R. M. Lewis. 1990. 'Ultrastructural Localization of Pemphigus Vulgaris Antigen on Canine Keratinocytes in Vivo and in Vitro'. *American Journal of Veterinary Research* 51 (4): 507–11.

Suter, Maja M., Katja Schulze, Wilhelmina Bergman, Monika Welle, Petra Roosje, and Eliane J. Müller. 2009. 'The Keratinocyte in Epidermal Renewal and Defence'. *Veterinary Dermatology* 20 (5–6): 515–32. https://doi.org/10.1111/j.1365-3164.2009.00819.x.

Swanson, D. L., and M. V. Dahl. 1983. 'Methylprednisolone Inhibits Pemphigus Acantholysis in Skin Cultures'. *The Journal of Investigative Dermatology* 81 (3): 258–60. https://doi.org/10.1111/1523-1747.ep12518278.

Thomason, Helen A., Anthea Scothern, Selina McHarg, and David R. Garrod. 2010. 'Desmosomes: Adhesive Strength and Signalling in Health and Disease'. *Biochemical Journal* 429 (3): 419–33. https://doi.org/10.1042/BJ20100567.

Topman, Gil, Orna Sharabani-Yosef, and Amit Gefen. 2011. 'A Method for Quick, Low-Cost Automated Confluency Measurements'. *Microscopy and Microanalysis* 17 (6): 915–22. https://doi.org/10.1017/S1431927611012153.

Tovanabutra, Napatra, Christina E. Bax, Rui Feng, Carolyn J. Kushner, and Aimee S. Payne. 2022. 'Temporal Outcomes after Rituximab Therapy for Pemphigus Vulgaris'. *The Journal of Investigative Dermatology* 142 (4): 1058-1064.e7. https://doi.org/10.1016/j.jid.2021.09.013.

Tsunoda, Kazuyuki, Takayuki Ota, Miyo Aoki, Taketo Yamada, Tetsuo Nagai, Taneaki Nakagawa, Shigeo Koyasu, Takeji Nishikawa, and Masayuki Amagai. 2003. 'Induction of Pemphigus Phenotype by a Mouse Monoclonal Antibody against the Amino-Terminal Adhesive Interface of Desmoglein 3'. *Journal of Immunology (Baltimore, Md.: 1950)* 170 (4): 2170–78. https://doi.org/10.4049/jimmunol.170.4.2170.

Udey, Mark C. 1999. 'Pemphigus—Diseases of Antidesmosomal Autoimmunity'. *JAMA* 282 (6): 572. https://doi.org/10.1001/jama.282.6.572.

Uldry, Anne-Christine, Anabel Maciel-Dominguez, Maïwenn Jornod, Natasha Buchs, Sophie Braga-Lagache, Justine Brodard, Jovana Jankovic, Nicolas Bonadies, and Manfred Heller. 2022. 'Effect of Sample Transportation on the Proteome of Human Circulating Blood Extracellular Vesicles'. *International Journal of Molecular Sciences* 23 (9): 4515. https://doi.org/10.3390/ijms23094515.

Van Der Wier, Gerda, Hendri H. Pas, Duco Kramer, Gilles F.H. Diercks, and Marcel F. Jonkman. 2014. 'Smaller Desmosomes Are Seen in the Skin of Pemphigus Patients with Anti-Desmoglein 1 Antibodies but Not in Patients with Anti-Desmoglein 3 Antibodies'. *Journal of Investigative Dermatology* 134 (8): 2287–90. https://doi.org/10.1038/jid.2014.140.

Varani, James. 2012. 'Human Skin Organ Culture for Assessment of Chemically Induced Skin Damage'. *Expert Review of Dermatology* 7 (3): 295–303. https://doi.org/10.1586/edm.12.24.

Voloshin, Nikita, Pyotr Tyurin-Kuzmin, Maxim Karagyaur, Zhanna Akopyan, and Konstantin Kulebyakin. 2023. 'Practical Use of Immortalized Cells in Medicine: Current Advances and Future Perspectives'. *International Journal of Molecular Sciences* 24 (16): 12716. https://doi.org/10.3390/ijms241612716.

Wang, Lifeng, Fu-Sheng Wang, and M. Eric Gershwin. 2015. 'Human Autoimmune Diseases: A Comprehensive Update'. *Journal of Internal Medicine* 278 (4): 369–95. https://doi.org/10.1111/joim.12395.

Wang, X., F. Brégégère, M. Frušić-Zlotkin, M. Feinmesser, B. Michel, and Y. Milner. 2004. 'Possible Apoptotic Mechanism in Epidermal Cell Acantholysis Induced by Pemphigus Vulgaris Autoimmunoglobulins'. *Apoptosis* 9 (2): 131–43. https://doi.org/10.1023/B:APPT.0000018795.05766.1f.

Waschke, Jens, Volker Spindler, Paola Bruggeman, Detlef Zillikens, Gudula Schmidt, and Detlev Drenckhahn. 2006. 'Inhibition of Rho A Activity Causes Pemphigus Skin Blistering'. *The Journal of Cell Biology* 175 (5): 721–27. https://doi.org/10.1083/jcb.200605125.

Watt, F. M., and H. Green. 1982. 'Stratification and Terminal Differentiation of Cultured Epidermal Cells'. *Nature* 295 (5848): 434–36. https://doi.org/10.1038/295434a0.

Wei, Qi, and Hayden Huang. 2013. 'Insights into the Role of Cell–Cell Junctions in Physiology and Disease'. In *International Review of Cell and Molecular Biology*, 306:187–221. Elsevier. https://doi.org/10.1016/B978-0-12-407694-5.00005-5.

Wier, Gerda van der, Hendri H. Pas, and Marcel F. Jonkman. 2010. 'Experimental Human Cell and Tissue Models of Pemphigus'. *Dermatology Research and Practice* 2010:143871. https://doi.org/10.1155/2010/143871.

Wierzbicka, Justyna M., Michał A. Żmijewski, Jakub Antoniewicz, Michal Sobjanek, and Andrzej T. Slominski. 2017. 'Differentiation of Keratinocytes Modulates Skin HPA Analog'. *Journal of Cellular Physiology* 232 (1): 154–66. https://doi.org/10.1002/jcp.25400.

Wilgram, G. F., J. B. Caulfield, and W. F. Lever. 1961. 'An Electron Microscopic Study of Acantholysis in Pemphigus Vulgaris'. *The Journal of Investigative Dermatology* 36 (May):373–82. https://doi.org/10.1038/jid.1961.58.

Williamson, Lina, Thomas Hunziker, Maja M. Suter, and Eliane J. Müller. 2007. 'Nuclear C-Myc: A Molecular Marker for Early Stage Pemphigus Vulgaris'. *The Journal of Investigative Dermatology* 127 (6): 1549–55. https://doi.org/10.1038/sj.jid.5700735.

Williamson, Lina, Natalia A. Raess, Reto Caldelari, Anthony Zakher, Alain de Bruin, Horst Posthaus, Reinhard Bolli, Thomas Hunziker, Maja M. Suter, and Eliane J. Müller. 2006. 'Pemphigus Vulgaris Identifies Plakoglobin as Key Suppressor of C-Myc in

the Skin'. *The EMBO Journal* 25 (14): 3298–3309. https://doi.org/10.1038/sj.emboj.7601224.

Williamson, Lina, Maja M. Suter, Thierry Olivry, Marianne Wyder, and Eliane J. Müller. 2007. 'Upregulation of C-Myc May Contribute to the Pathogenesis of Canine Pemphigus Vulgaris'. *Veterinary Dermatology* 18 (1): 12–17. https://doi.org/10.1111/j.1365-3164.2007.00561.x.

Woo, T. Y., V. A. Hogan, H. Patel, G. J. Anhalt, R. S. Labib, J. J. Voorhees, and L. A. Diaz. 1983. 'Specificity and Inhibition of the Epidermal Cell Detachment Induced by Pemphigus IgG in Vitro'. *The Journal of Investigative Dermatology* 81 (1 Suppl): 115s–21. https://doi.org/10.1111/1523-1747.ep12540871.

Yannas, Ioannis V. 2015. 'Regeneration of Skin'. In *Tissue and Organ Regeneration in Adults*, by Ioannis V. Yannas, 89–136. New York, NY: Springer New York. https://doi.org/10.1007/978-1-4939-1865-2_5.

Yokouchi, Mariko, Marwah Adly Saleh, Keiko Kuroda, Takahisa Hachiya, John R. Stanley, Masayuki Amagai, and Ken Ishii. 2009. 'Pathogenic Epitopes of Autoantibodies in Pemphigus Reside in the Amino-Terminal Adhesive Region of Desmogleins Which Are Unmasked by Proteolytic Processing of Prosequence'. *Journal of Investigative Dermatology* 129 (9): 2156–66. https://doi.org/10.1038/jid.2009.61.

Yu, Fengchao, Sarah E. Haynes, Guo Ci Teo, Dmitry M. Avtonomov, Daniel A. Polasky, and Alexey I. Nesvizhskii. 2020. 'Fast Quantitative Analysis of timsTOF PASEF Data with MSFragger and IonQuant'. *Molecular & Cellular Proteomics: MCP* 19 (9): 1575–85. https://doi.org/10.1074/mcp.TIR120.002048.

Yuan, Qiuyun, Wanchun Yang, and Xuefeng Zhang. 2023. 'Immune Cells in Pemphigus Vulgaris and Bullous Pemphigoid: From Pathogenic Roles to Targeting Therapies'. *International Immunopharmacology* 123 (October):110694. https://doi.org/10.1016/j.intimp.2023.110694.

Zhou, Lijuan, Xianqi Zhang, Ralf Paus, and Zhongfa Lu. 2018. 'The Renaissance of Human Skin Organ Culture: A Critical Reappraisal'. *Differentiation* 104 (November):22–35. https://doi.org/10.1016/j.diff.2018.10.002.

Zou, Zhiran, Xiao Long, Qian Zhao, Yandong Zheng, Moshi Song, Shuai Ma, Yaobin Jing, et al. 2021. 'A Single-Cell Transcriptomic Atlas of Human Skin Aging'. *Developmental Cell* 56 (3): 383-397.e8. https://doi.org/10.1016/j.devcel.2020.11.002.

10 Appendix

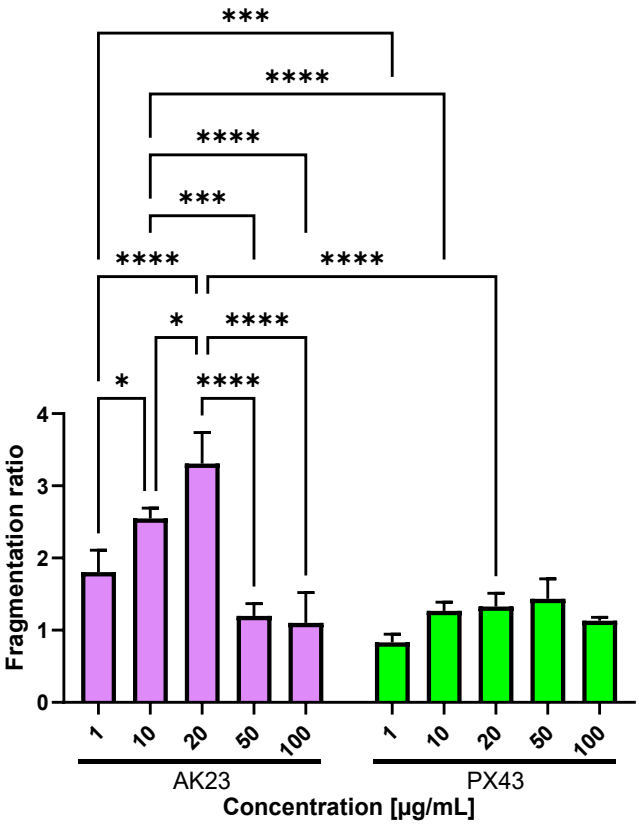

Figure 10.1.: In the keratinocyte dissociation assay performed on HaCaT cells, 20 µg/mL of AK23 and 50 µg/mL of PX43 cause the highest fragmentation. Graphical representation of the fragmentation ratio of human high calcium immortalized epidermal keratinocytes (HaCaT cells) incubated with 1, 10, 20, 50 and 100 µg/mL AK23 (violet) and PX43 (green) for 24 hours in comparison to murine immunoglobulin G (mIgG) and human immunoglobulin G (hIgG), respectively. Two-way ANOVA was performed and p value < 0.05 [*], p value < 0.0004 [***] and p value < 0.0001 [****] are shown.

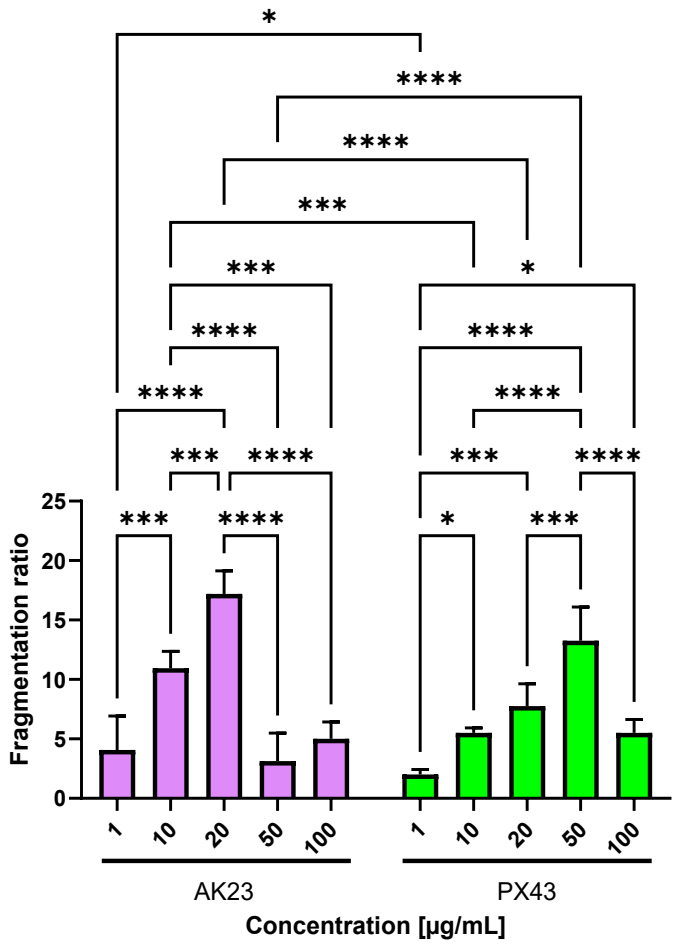

Figure 10.2.: In the keratinocyte dissociation assay performed on pooled human primary epidermal keratinocytes, 20 µg/mL of AK23 and 50 µg/mL of PX43 cause the highest fragmentation. Graphical representation of the fragmentation ratio of pooled human primary epidermal keratinocytes (pHPEK), incubated with 1, 10, 20, 50 and 100 µg/mL AK23 (violet) and PX43 (green) for 24 hours in comparison to murine immunoglobulin G (mIgG) and human immunoglobulin G (hIgG), respectively. Two-way ANOVA was performed and p value < 0.05 [*], p value < 0.0004 [***] and p value < 0.0001 [****] are shown.